26-236

NASA

Technical Memorandum 83824

OAO-3 End of Mission Tests Report

SEPTEMBER 1981

National Aeronautics and
Space Administration

Goddard Space Flight Center
Greenbelt, Maryland 20771

OAO-3 END OF MISSION TESTS REPORT

September 1, 1981

Preface

The Orbiting Astronomical Observatory-Copernicus (OAO-C) was redesignated OAO-3 after it was launched and became operational; however, some authors still refer to it as OAO-C, as will be seen in this text, while others more correctly refer to it as OAO-3.

The End-of-Mission (EOM) Tests on OAO-3 were performed in response to a request from NASA Headquarters (see text for further details). Pursuant to the request, test proposals were solicited from the technical community (GSFC engineers, NASA centers, universities, and industry). For the selected/approved tests, the proposers (test engineers) prepared detailed test Plans with procedures which were carried out by the Orbiting Satellites Project/Science with support from the project's contractors (Grumman and Westinghouse), and under the direction of the EOM Test Manager, Dr. Ford Kalil. The test engineers were responsible for analysing their data and preparing their reports. This text is a consolidation of those reports into this final report, "OAO-3 End-of-Mission Tests Report."

TABLE OF CONTENTS

TABLE OF CONTENTS (Continued)

TABLE OF CONTENTS (Continued)

TABLE OF CONTENTS (Continued)

LIST OF TABLES

LIST OF ILLUSTRATIONS

LIST OF ILLUSTRATIONS (Continued)

SECTION 1
INTRODUCTION

1.1 SUMMARY

A total of 16 proposals were received for the OAO-3 End of Mission Test by the Orbiting Satellite Project/Science (OSP/S) office. Three of these tests were not accomplished primarily due to scheduling conflicts in network support. Some of the experiments were combined leaving a total of 12 tests that were performed. These tests are summarized in Table 1-1. Some very interesting and unusual results were obtained from these tests over the 8 1/2 year lifetime of the OAO-3.

The glitch (high voltage shutdown) test No. 1 was performed to determine the cause of the high voltage shutdown in the Princeton Experiment Package (PEP). Data showed no evidence that arcing occurred which could cause the shutdown of the high voltage. The exact cause of the glitches could not be isolated.

The purpose of performing the PEP sensitivity test (No. 2) was to complete the documentation of the instrument degradation and to make the final instrument calibration. Two of the four phototubes indicated an appreciable amount of degradation while the second two phototubes retained 60% of their launch period sensitivity.

The sensitivity degradation of PEP test (No. 3) consisted of three separate tests, one of which was the measurement of possible outgassed contamination on the wide and narrow entrance slits. A small change occurred in the measured ratio of the two slit openings and was considered insufficient to cause the large instrument degradation. The second test pertained to the measurement of changes that occurred in the image size or shape which would reduce the amount of light entering the PEP. Data from the fine error sensor indicated that the image encountered a small change since launch, but was not sufficient to cause the large sensitivity degradation of the PEP. The third test was an investigation of contamination on the optical surfaces in the PEP. Heating of the

TABLE 1-1

OAO-3 END-OF-MISSION TESTS

Test No.	Principle Investigatc	Test Name	Test Description & Comments
1.	R. Polidan Princeton	Glitch Testing of Princeton Experimental Package(PEP)	Scoop up atmosphere until high voltage arc-over occurs.
2.	R. Polidan Princeton	Final Sensitivity Measurements of PEP	Photometric test to complete history of degradation.
3.	R. Polidan Princeton	Sensitivity Degradation of PEP	Measure slit ratio with light passage. Solar heat to evaporate contamination. Check for change of signal level.
4.	R. Polidan Princeton	PEP Fine Error System Guidance Test	A thorough test of PEP fine error guidance system.
5.	R. Polidan Princeton	Test of Failed Units	With a block of known passes over a 3 day period, with properly designed test sequence evaluate causes of failur present performance of: 1. Sequence controller "A" and "B" 2. Focus motor 3. Calibration lamps 4. Guidance channel "A"
6.	R. Polidan Princeton	Test of Redundant Units	Most electronic units are 3 fold redundant. Check how many redundant units are switchable and operable.
7.	F.J. Kull GSFC/408	Inertial Reference Unit (IRU) Calibration	Continue normal calibrations until end of mission.
8.	F.J. Kull GSFC/408	Star Tracker Sensitivity	Measure sensitivity of all four gimballed star trackers.

TABLE 1-1

OAO-3 END-OF-MISSION TESTS (Continued)

Test No.	Principle Investigator	Test Name	Test Description & Comments
9.	R. McIntosh GSFC/732	Heat Pipe Performance Test	Measure performance of the four heat pipe experiments, using different level of heating.
10.	S. Ollendorf GSFC/732	Thermal Control Coating Degradation	Measure degradation of the two types of thermal control coatings - Silver, Teflon and ALZAK.
11.	D. Margolies GSFC/710.2	Command & Data Handling (C&DH) Subsystem Checks	Check performance of redundant elements of C&DH subsystems. Check elements and functions of C&DH subsystem that have been used infrequently or not at all.
12.	M. Tasevoli GSFC/711	Power Subsystem Solar Array, Nickel-Cadmium Batteries, OPB Power Boost	Collect solar array temperature, volts current vs. solar angle & compare with beginning-of-life values. Carefully monitor and discharge fully charged batteries to a deep discharge and then recharge them. This will provide both an accurate end-of-life capacity of individual battery difference. Note: The past charge-discharge methodology used on OAO-3 has been so successful for the 8-year life of the spacecraft, that the batteries are essentially like new. Check operation of OBP for proper regulation of array power at 900 W.

optical surfaces to remove contamination could not be performed, because no heaters were provided in the PEP. To resolve this deficiency, the heating was obtained by pointing the OAO-3 towards the sun. Unexpected results showed that the signal level was reduced by a maximum factor of 7. Further tests revealed the image size or shape was greatly altered. It thus appeared the greatly altered stellar image was the principle cause of the reduction of the PEP sensitivity.

The fine error sensor test (No. 4) was performed to evaluate the performance of the sensor after a long time span of operation. Results of this test showed the quality of operation was at or above the pre-launce specifications.

The purpose of the failed units test (No. 5) was to check the status of five units in the PEP that failed and consisted of: Focus motors, calibration lamps, sequence controllers A and B, and guidance channel A. Attempts to operate the above first four units failed at the end of OAO-3 mission. The guidance channel A operated properly when it was actuated and its early mission failure was due to the use of a wrong turn-on sequence. A good operational record was obtained from the OAO-3 since only four units failed out of sixty over a period of 8 1/2 years.

The check for redundant units test (No. 6) was not performed. However, all channel A units were turned on when the guidance channel A was switched on. All of the channel A units performed to expectations and the spacecraft was left in this mode.

The operational performance of the inertial reference unit test (No. 7) was flawless during the entire mission of the spacecraft. This test demonstrated that properly designed gyros with ball bearings can meet stringent performance requirements for long life mission applications.

Results obtained from the star tracker sensitivity test (No. 8) indicated that there were no significant changes in the star trackers sensitivities.

The heat pipe test (No. 9) consisted of 3 fixed conductance heat pipes which performed within the design limits and showed no degradation over the spacecraft life period.

Results of the thermal control coatings test (No. 10) indicated that the A-1 alzak and A-5 silver teflon skins degraded significantly over the life period of the OAO-3. Their solar absorptivity increased by a factor of about 2.5. The high degree of degradation was contributed to more than 30,000 hours of exposure to the sun's radiation.

The communication and data handling subsystem test (No. 11) performed very well, with a few exceptions, throughout the life of OAO-3. No degradation was experienced in either the command receiver or the transmitters.

The power subsystem test (No. 12) consisted of a solar array, nickel-cadmium batteries and the on-board processor power boost tests. A very successful performance of the entire power subsystem was obtained from this test including the expected amount of solar array degradation due to radiation. The power subsystem had performed exceptionally well for the entire life of the mission. Much can be learned from the charge-discharge cycle(s) used in the mission operations.

It appears that battery life can be significantly prolonged by carefully monitoring the charge-discharge cycle with particular care not to overcharge.

1.2 GENERAL

Goddard's Orbiting Astronomical Observatory-C (OAO-3) was the heaviest and most complex U.S. unmanned space observatory and was designed to seek answers to some of the fundamental questions concerning stars and interstellar matter. The spacecraft was launched from the Kennedy Space Center, Florida, on board an Atlas-Centaur rocket on August 21, 1972.

Its orbit was 460 miles above earth and the huge 4,900-pound automated spacecraft viewed the starts with a precision and clarity never before possible. It was capable of pointing its sensitive ultraviolet telescope, the largest ever orbited, at an object about the size of a volleyball seen from a distance of 400 statute miles, for periods up to one hour.

After orbit was achieved, the OAO-3 was renamed Copernicus in honor of the Polish Astronomer Nicholaus Copernicus who lived from 1473 to 1543. He is called the founder of modern astronomy. The year 1973 marked the 500th anniversary of his birth.

The principal viewing device of OAO-3 was a 32-inch (0.81 M) diameter reflecting telescope housed in the central tube of the 10-foot (3.1 M) long cylinder shaped spacecraft. It provided, via a radio signal, data in the form of ultraviolet spectral readings. This region of the electromagnetic spectrum is invisible to ground-based observatories because of the obscuring effect of the Earth's atmosphere. The instrument was provided by Princeton University, with Professor Lyman Spitzer, Jr. as principal investigator.

The second instrument carried by OAO-3 was provided by England's University College, London, under the sponsorship of the U.K. Science Research Council. It consisted of three small telescopes and a collimated proportional counter to study X-ray sources in space, at various wavelengths up to 70 Angstroms.

One of the major discoveries of space exploration was the finding that many objects in the universe emit X-rays. It had long been known that the sun emitted low intensity X-rays, and astronomers assumed that other stars emitted proportional amounts that could not be detected from Earth. However, sounding rockets and Goddard's Uhuru satellite program have discovered more than 200 X-ray sources in the universe. These sources give off enormous amounts of energy. They exist in such diverse regions as the Magellanic Clouds, the Crab Nebula, gallaxies and even in some areas of the sky where no visible object can be found. The enormous energy they emit suggest energy processes heretofore thought impossible.

The OAO-3 carried a newly-developed gyro inertial reference unit as its primary attitude sensor, augmented with four star trackers. In addition, three more new instruments were used on board the OAO-3 and consisted of: (1) A newly-developed electrically scanned star tracker, (2) a precision digital solar aspect sensor to help assure precision pointing, and (3) a new and unique on board computer, to improve and simplify orbital operations, was used as an experiment. Its stored command memory was able to handle 16,000 18-bit words and store up to 1,024 ground commands. This allowed automatic operation of OAO-3 between its daily contacts with the Goddard operated STDN station at Rosman, N.C..

The primary objectives in performing the OAO-3 experiments was to study the interstellar absorption of hydrogen, oxygen, carbon, silicon, and other common elements in the interstellar gas; to investigate ultraviolet radiation emitted from so-called young hot stars (early type stars) in wavelength regions between 930 and 3,000 Angstroms; and to locate and map new X-ray sources.

1.3 BACKGROUND AND PURPOSE OF EOM TESTS

NASA's Chief Engineer requested that each project develop a terminal test program for acquiring engineering information prior to shutdown or reentry of an operational satellite (Ref. 1). NASA's Director, Astrophysics Division, concluded that engineering test for end-of-mission satellites could be useful, if properly planned and executed, and the data disseminated to those who will use the results for future spacecraft development. Primarily, contractors, their subcontractors, and in-house engineers involved in the original spacecraft

development and who will be involved in future projects would derive the most benefit from the end-of-mission tests (Ref. 2). As a preliminary step in responding to the requirements (Ref. 1), GSFC was requested to prepare engineering test plans for OAO-3. These test plans were approved by NASA Headquarters.

1. Letter from Walter C. Williams, Code D, NASA HQ to Associate Administrators of Codes E, M, R, S, and T, NASA HQ, Subject: "Engineering Uses of Satellites at End of Mission", 17 Nov. 1978.
2. Letter from T.B. Norris, Code SC-7, NASA HQ to Director, GSFC, Subject: Same as Ref. 1, March 28, 1979.

The purpose of this report is to present the tests that were conducted, their results, and conclusions, so that contractors, subcontractors, and in-house engineers who were involved in spacecraft development could derive benefit from the tests.

OAO-C End of Mission Heat Pipe Tests

by
W. Harwell
Grumman Aerospace Corporation
Bethpage, New York 11714

February 9, 1981

TABLE OF CONTENTS

SECTION 2
OAC-C END OF MISSION HEAT PIPE TESTS

2.1 SUMMARY

End of mission tests were performed on the three fixed conductance heat pipes mounted to the structure tube and the variable conductance heat pipe mounted to the On-Board Processor. Testing consisted of systematically enabling commandable heaters directly mounted to the heat pipes and using flight telementry to monitor temperature responses. This test data was then compared to preflight and early flight data. There were no detectable differences between the data sets. It can be concluded that after 8 1/2 years in orbit the pipes are operating within design limits with no degradation in performance. From the consistent sets of data it can be inferred that there has been little or no leakage of the working fluids out of the pipes, neither has there been any significant gas generation within the pipes.

2.2 INTRODUCTION

The OAO-C spacecraft is the first recorded instance of heat pipes being included as part of a space vehicle's thermal design (Ref. 1). Fixed conductance heat pipes (FCHP) are mounted to the structure tube at each of Levels 4, 5 and 6 and a variable conductance heat pipe (VCHP) couples the On-Board Processor (OBP) heat sink to a heat rejection radiator. The FCHP's were designed to reduce the circumferential temperature difference around the structure tube, thereby, decreasing distortion of the tube. The VCHP was designed to minimize temperature excursions of the OBP. The heat pipes were flown primarily to gain zero gravity experience with a number of different heat pipe wicking geometries and manufacturing techniques. The thermal design of the vehicle assumed that failure of one or all of the heat pipes would not result in failure of the spacecraft to meet its mission objectives.

Operation of the OAO-C heat pipes can be inferred from two operational modes:

a) Mode 1 - Normal vehicle operation. For example if one circumferential GCHP failed, then circumferential temperature differences in the structure tube would reach 40°F compared to 9°F with the pipe operating.

b) Mode 2 - Heat pipe test mode. Ground commandable heaters directly bonded to the heat pipes can be selectively enabled and the temperature response monitored.

Comparative data for the first mode were available from component level testing up through vehicle acceptance thermal vacuum testing (ATV) and the 8 1/2 years of flight. Data for the second mode were available from component level testing up through vehicle ATV and the first few months of flight (Ref. 2, 3 and 6). The end-of-mission (EOM) testing covered by this report consisted of systematically enabling the commandable heat pipe heaters and monitoring their temperature responses.

2.3 OBJECTIVE OF TEST

The objective of the end-of-mission (EOM) tests was to compare the performance of the OAO-C heat pipes under comparable pre-flight, early flight and end-of-mission conditions. The end result was to determine whether or not any performance degradation had occurred due to leakage of fluid or generation of gas.

2.4 METHODOLOGY

The performance of the OAO-C heat pipes at low heat through-put levels can be readily verified from temperature distributions during normal spacecraft operational modes (Mode 1). Although the heat pipes were included in a failsafe thermal design they, never-the-less, significantly contribute to a reduction in circumferential temperature distributions in the case of the fixed conductance heat pipes (FCHP) and On-Board Processor (OBP) operating temperature in the case of the variable conductance heat pipe (VCHP). Verification of heat pipe performance in this mode involves a systematic comparison of data recorded during component level testing, vehicle acceptance thermal vacuum testing and the 8 1/2 years of flight.

Heat pipe performance at high heat transport levels can be verified by commanding on heaters directly bonded to the heat pipes and monitoring their temperature response via flight telemetry (Mode 2). Performance verification is, simply, a comparison of data taken during vechicle ATV and the first few months of flight with EOM data. It should be noted that analysis and ground tests have shown that the pedestal and spiral artery heat pipes can handle the Mode 1 heat loads with unprimed arteries. Mode 2 heat loads require the arteries to be primed.

2.5 DESCRIPTION OF HARDWARE AND INSTRUMENTATION

As shown in Figure 2-1, each of the three FCHP's have different wicking systems; an internally axially groved heat pipe at level 4, a pedestal artery heat pipe at level 5, and a spiral artery at level 6. All three heat pipes were formed into 48 inch diameter open hoops and mounted to the inner surface of the structure tube with either seven (level 4) or eight saddles (levels 5 and 6). The locations of the discontinuities in the hoops can be seen in Figure 2-2. All three are charged with ammonia and were designed to gain comprehensive flight experience (2, 4). The levels 4 and 6 heat pipes were fabricated by Grumman Aerospace Corporation and the level 5 heat pipe by Dynatherm Corporation.

The flight test instrumentation on the FCHP's consists of ground commandable heaters and thermistors (Figure 2-2). Input power to each of the three pipes was achieved by using strip heaters wrapped around the pipes between saddles. The level 4 pipe has two heaters, each of which provided approximately 20 watts input power. The power sources for the level 5 heat pipe consisted of a 25 watt heater wrapped around the pipe, and a 50 watt heater bonded to a pipe saddle. The level 6 heat pipe heater layout was similar to the level 5 layout. Absolute temperature sensors were installed on the levels 5 and 6 heat pipe, wheras differential thermistors were used on the level 4 heat pipe. All heaters were wired into the spacecraft's unregulated voltage line. Each heater can be ground commanded.

The fourth pipe, Figure 2-3, being flown on the spacecraft is the Variable Conductance Heat Pipe developed by the NASA Ames Research Center and fabricated by TRW (Ref. 3). The VCHP has a hot, non-wicked reservoir with a hybrid wick, methanol working fluid and helium as the non-condensible gas. The major role of this experiment was to determine how well a variable conductance heat pipe would operate in zero-g while maintaining the temperature of an electronic package, the On-Board-Processor, within a narrow temperature range 58°F to 68°F. For experimental purposes, commandable heaters rated at 10 and 20 watts

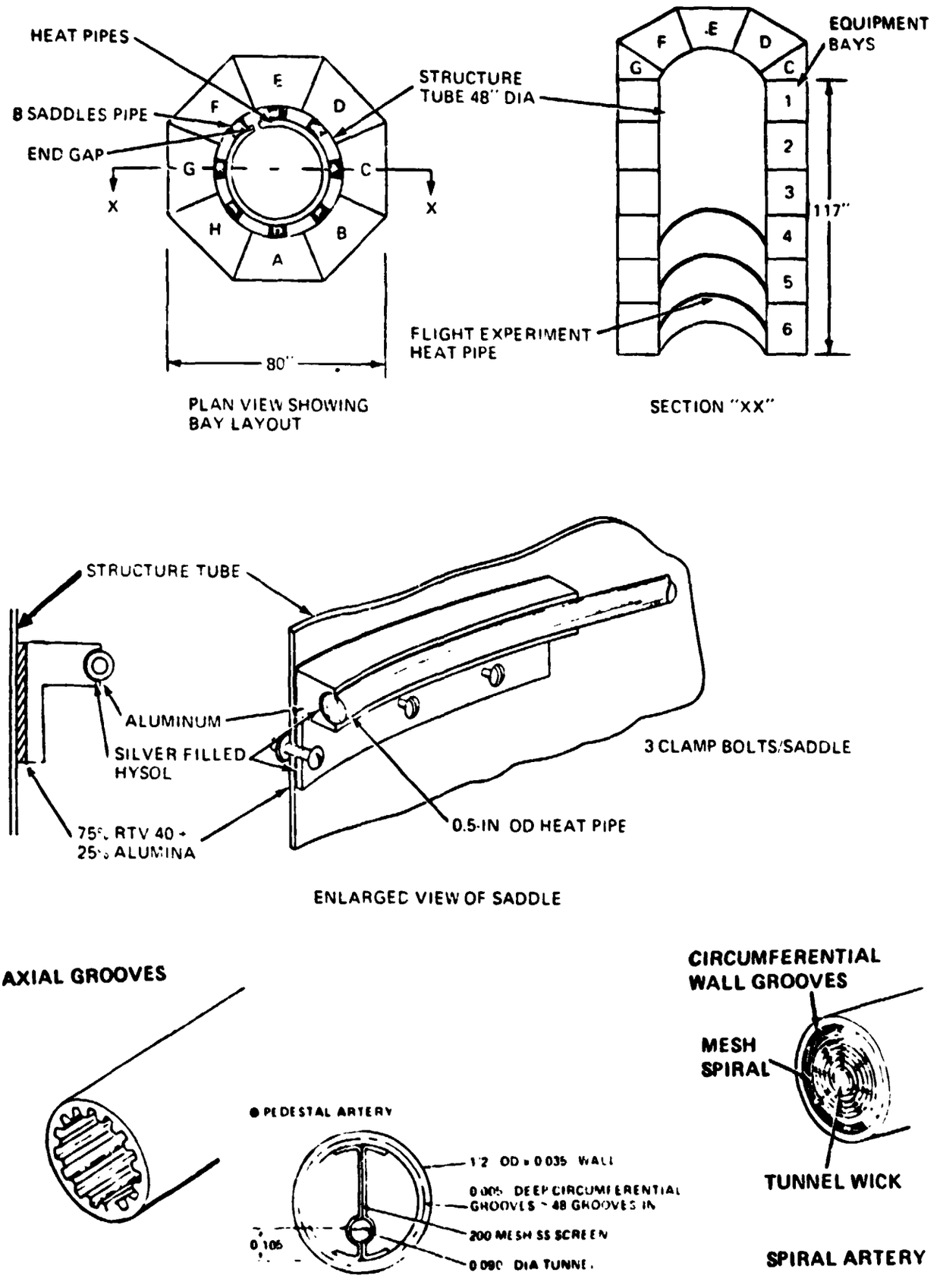

Figure 2-1. OAO-C Isothermalizer Heat Pipe Configuration.

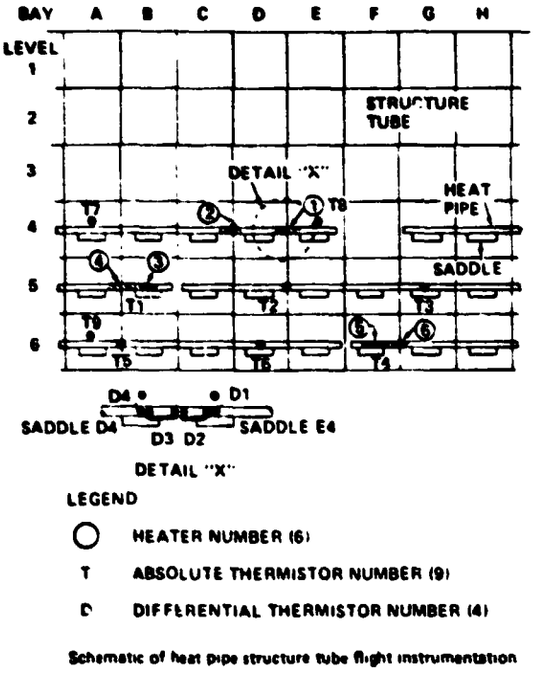

Schematic of heat pipe structure tube flight instrumentation

Figure 2-2. OAO-C Isothermalizer Instrumentation.

ORIGINAL PAGE
COLOR PHOTOGRAPH

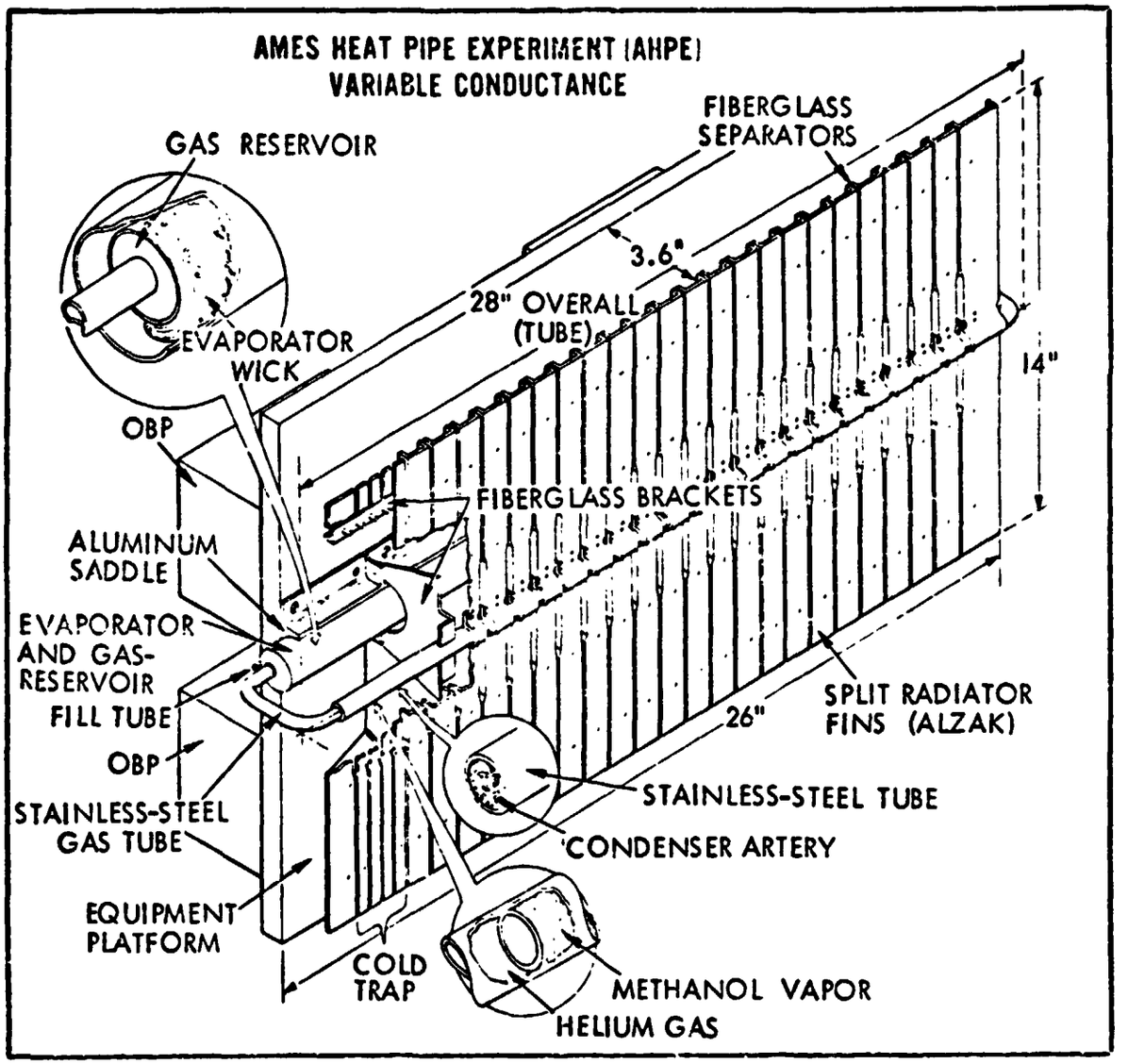

Figure 2-3. AHPE Hardware Configuration.
(Variable Conductance Heat Pipe Experiment)

(at 28V) were mounted on the evaporator section. Flight telemetry consisted of five thermistors, two located on the evaporator and one each on the condensor (radiator) the cold trap, and the equipment mounting plate (equipment heat sink).

2.6 DISCUSSION OF RESULTS

2.6.1 NORMAL SPACECRAFT OPERATING MODE 1

The FCHP's were configured into the OAO late in the spacecraft design stage, hence only a limited number of telemetry channels could be dedicated to the three heat pipes. The flight checkout philosophy developed was, therefore, that the pipes would be extensively checked out during ground test (ATV) using both ground test and flight instrumentation, and then in orbit with the flight instrumentation to obtain comparative performance data. The spacecraft ATV test was described by Caruso, et al (Ref. 5).

A 380-node computer thermal model of the spacecraft was built up in support of the vehicle thermal design. This model was run to give steady-state predictions corresponding to the ATV hot and cold case conditions. The model was also run with the heat pipe subroutine disabled. A comparison of these computer runs and the ATV thermocouple test data are given in Figure 2-4 for the spacecraft Level 6 structure tube. The test data indicated that the three heat pipes were operating as predicted, and decreased the structure circumferential temperature differences from 40 to 9°F while carrying spacecraft loads. The difference in temperature level between the predictions and the measured data is due to an overestimation of the thermal bay couplings in the computer model. As most of the thermal bays are located at the aft end of the spacecraft, the aft structure would run warm.

The structure tube acts as the heat sink for many of the electronic boxes, therefore, the reduction in structure tube circumferential temperature difference also results in a change in operating temperature of up to $\pm$ 20°F in some of the electronic boxes. The flight performance of the structure tube/electronic boxes in the normal spacecraft operating mode was, within the limits of the instrumentation, the same as recorded during the ATV test:

a) The temperature difference of 1.5 to 3°F between the A-4 and E-4 structure recorded during the 8 1/2 years of flight verifies that the axial groove heat pipe was operating as predicted.

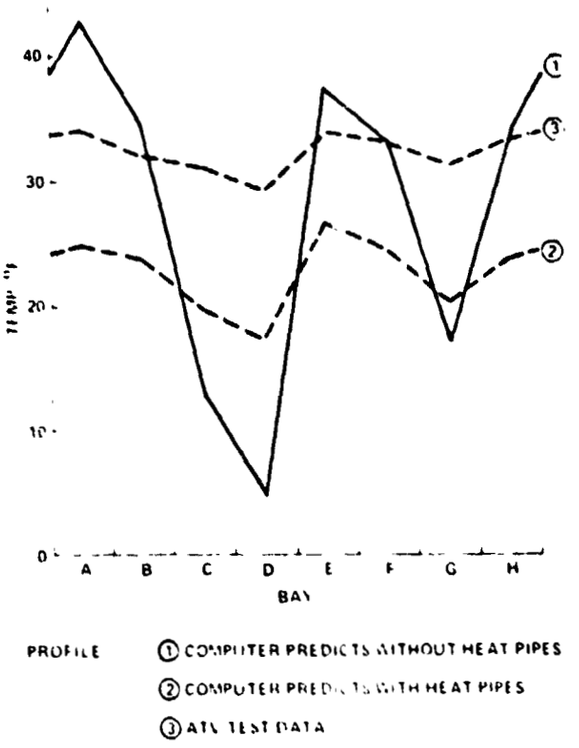

Figure 2-4. Level 6 Structure Tube Temperature.

b) The diode box in bay F-5 was designed to reject heat to the structure. If the pedestal artery heat pipe had not operated the equipment in bay F-5, it would have run some 15 to 20°F warmer. The box operated within 3°F of predictions and, therefore, it can be concluded that the pedestal artery heat pipe was operating.

c) The inertial reference unit (IRU) located in bay F-6 was designed to dump 15 watts to the structure tube. If the heat pipe had not operated the box would have run 20°F warmer than predictions. The box ran a maximum of 4°F warmer throughout the mission, therefore, the spiral artery heat pipe must have been operating under normal spacecraft loads.

All three FCHP's were, therefore, operating in the normal spacecraft operating mode.

Temperature histories for the VCHP thermistors recorded during Janurary 1981 with the spacecraft in the normal operating mode are shown in Figure 2-5. These data are in excellent agreement with data reported for the early phases of the mission, Figure 2-6. The VCHP is exhibiting variable conductance and controlling, although the turn-on and turn-off are triggered by variations in cold trap temperature rather than variations in source temperature or source dissipation. This is predictable from variations in methanol vapor pressure in the condenser. The cold trap temperature is running some 10 to 20°F warmer than predicted, but is in agreement with ATV data. This is most likely due to heat leak from the inboard components. The net result of the hotter than predicted cold trap was to force the control temperature range up by approximately 4°F.

2.6.2 HEAT PIPE CHECK-OUT MODE 2

The flight data recorded during the heater checks are summarized in Tables 2-1, 2-2 and 2-3. Where possible, the flight data are compared with applicable ATV test data. At all levels of comparison there is extremely good agreement between the flight and ATV data sets, and there are no indications of dry-out. The OAO steady-state comprehensive thermal model was run to simulate the flight condition where both heaters at each level were on (at 30.8 V) and the thermal work term evaluated as 1930, 4900 and 6000 watt inches for the Levels 4, 5 and 6 FCHP's respectively.

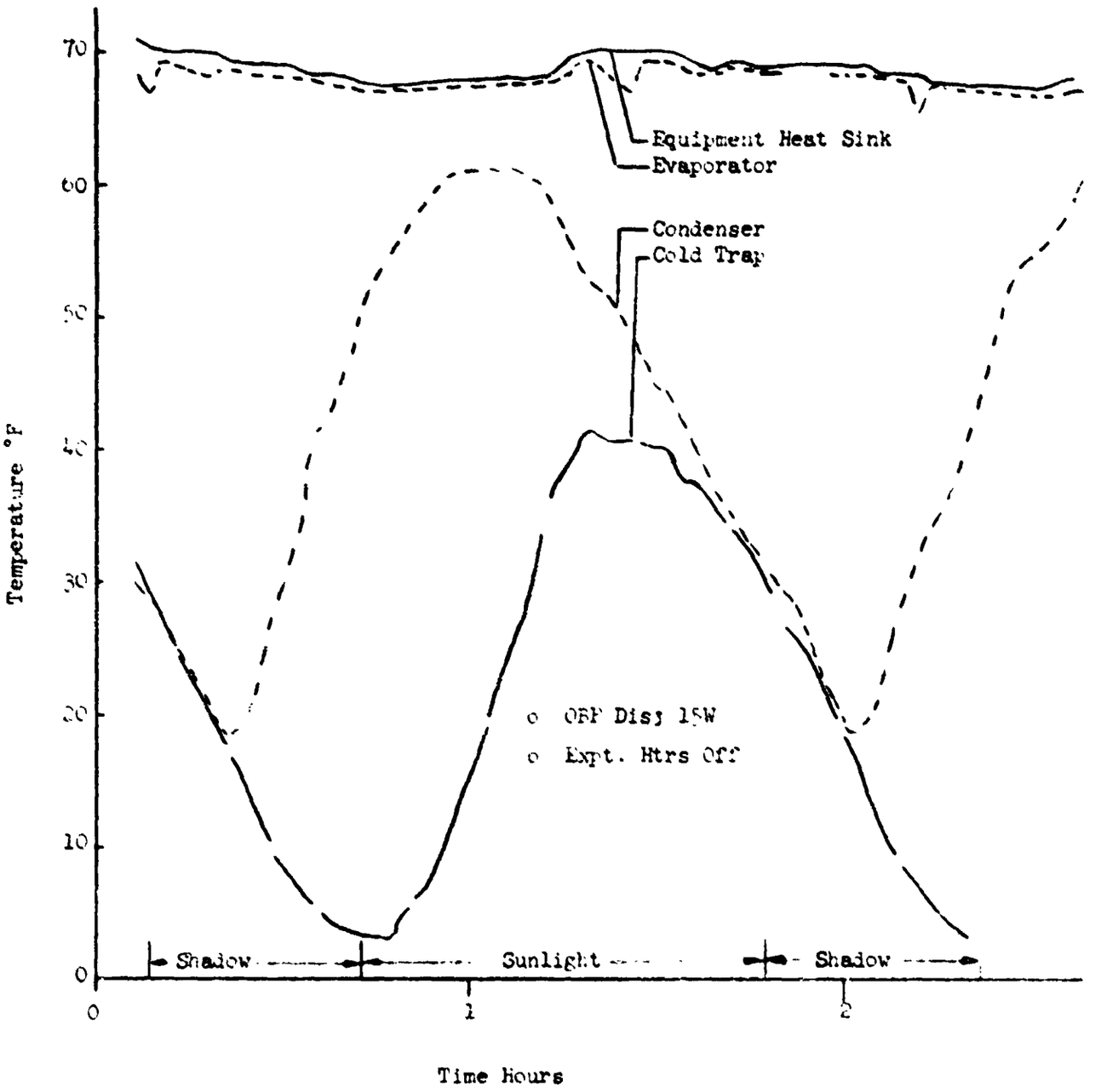

Figure 2-5. OBP VCHP Temperature History - Mode 1.

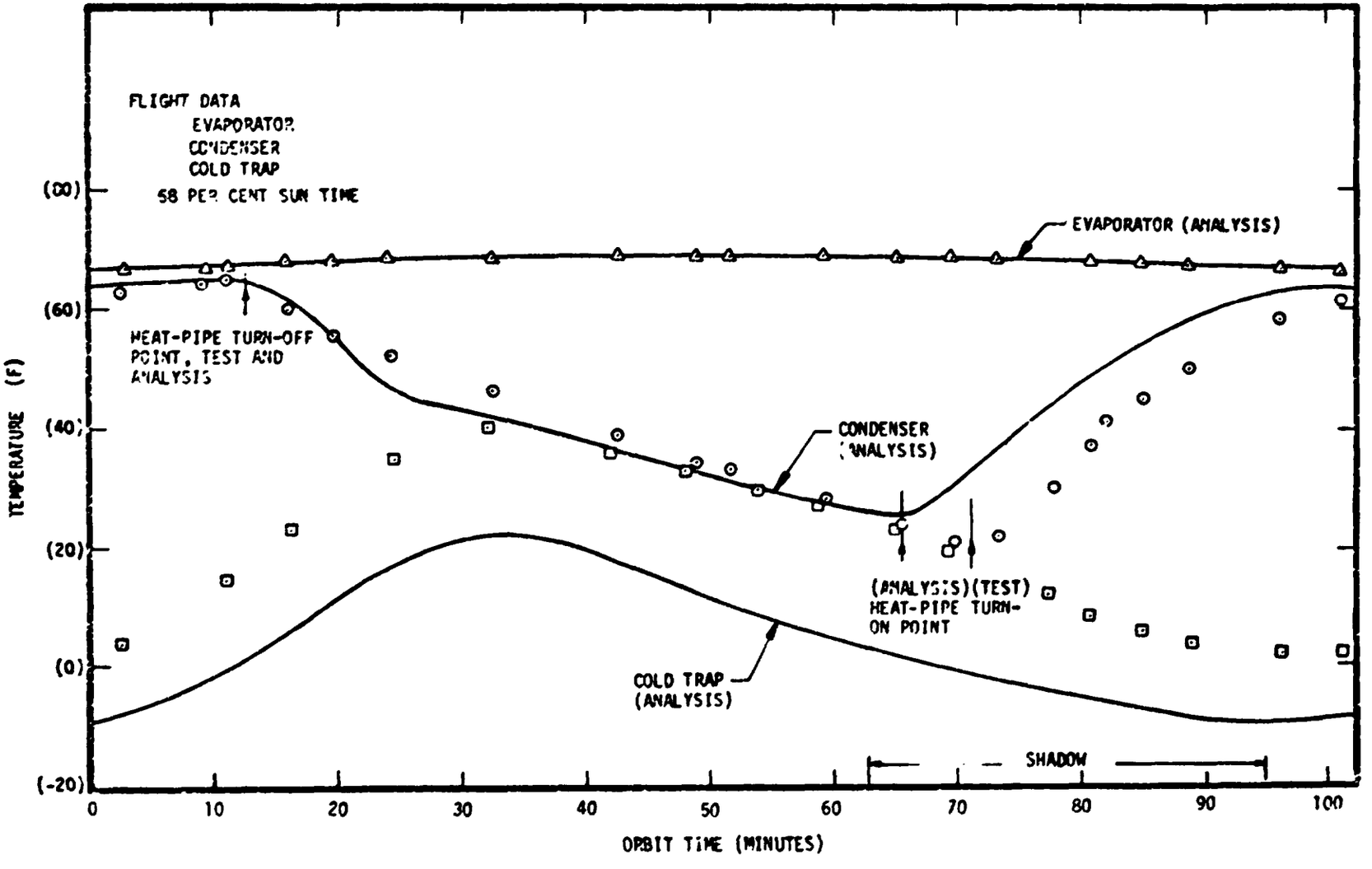

Figure 2-6. Correlation of Flight and Analysis Data, Orbit 1592. (Ref. 6).

2.6.2.1 Level 4 FCHP

One of the differential temperature sensors on the level 4 heat pipe began to drift negatively during the fifth year of flight The sensor is not an open circuit and does change with time indicating that one of the sensor beads (probably the heat pipe bead) has lifted. The loss of this sensor does not impact the validity of the heat pipe test and analysis.

The main conclusions to be drawn from the available data (Table 2 1) is that the pipe will handle approximately 2,000 watt-inches without dryout in a zero gravity environment. There are no significant differences in performance between flight test and ATV test. No degradation in flight performance has been detected. The heat input corresponds to approximately 2.2 w/in^2.

2.6.2.2 Level 5 FCHP

The pedestal artrery heat pipe dried out during ATV "Heater-on" periods. Analysis has shown that although screen pumping in the pedestal artery pipe could handle spacecraft loads, the artery would have to be primed to handle the heater loads. It was subsequently demonstrated that the spacecraft was not level in the thermal vacuum chamber and the three heat pipes were in fact tilted by 0.22 inch. This would be a sufficient tilt to prevent priming of the pedestal artery but, due to the relative locations of the heaters, would assist pumping in the other two levels. On re-leveling, the pedestal artery heat pipe operated (i.e., primed) with full heater power without dryout.

High circumferential temperature differences were also measured on the pedestal artery pipe during the early thermal vacuum test (ETV). The indications are that the high ΔT's were due to incipient wall groove dryout; that is, the grooves could not pump the full pipe diameter in one g.

The test data recorded during "heater on" events are summarized in Table 2-2. The ground test data shown correspond to thermocouple data recorded in the GAC clean room. For comparison, the ETV incipient dryout data are also shown. The high temperature reported at T-3 was matched by a high local structure temperature. Not withstanding the problems associated with ground testing of this pipe, the flight performance is excellent:

- The pipe pumped 4877 watt-inches with a heater power density of up to 12 w/in. without dryout indicating that the artery was primed.
- The circumferential temperature differences were very low.

The low ΔT's and the fact that they did not increase with heat input, would tend to indicate that the pipe was not operating near its hydrodynamic limit.

TABLE 2-1

Grooved Heat Pipe Testing - Summary Sheet

Heater Number	Channel	Test Series					
		ATV	Sept 72		Oct 72	March 73	EOM
2	D-1, °F		-3.4		-3.1	-3.4	-3.3
	D-2, °F		-1.8		-1.5	-1.5	-1.4
	D-3, °F		-2.1		-1.9	-1.8	-1.8
	D-4, °F		-1.4		-0.9	-0.9	----
	T-8, °F		36.9		42.5	45.7	48.9
	T-7, °F		39.4		44.1	47.4	50.8
	(T-7)-(T-8) °F		2.5		1.6	1.7	1.9
	Power, W		18		24	24	23
1	D-1, °F	-3.0	-3.5		-3.5	-4.0	-3.6
	D-2, °F	-7.8	-5.8		-6.8	-7.4	-6.8
	D-3, °F	3.4	1.5		3.0	3.2	3.2
	D-4, °F	-1.0	-1.5		-0.8	-1.0	----
	T-8, °F	37.7	37.7		45.7	49.1	49.1
	T-7, °F	39.5	39.4		47.4	49.9	50.8
	(T-7)-(T-8) °F	1.8	1.4		1.7	0.8	1.7
	Power, W	27	18		27	25	25
1 & 2	D-1, °F	-4.8	-4.3	-4.6	-4.2	-4.6	-4.3
	D-2, °F	-9.1	-5.9	-9.2	-8.2	-9.3	-8.4
	D-3, °F	5.6	1.8	6.1	5.1	6.0	4.9
	D-4, °F	0 4	-1.0	0.2	0.0	0.1	----
	T-8, °F	68.0	44.9	52.4	55.0	59.4	58.5
	T-7, °F	69.1	46.5	54.4	56.3	61.2	59.2
	(T-7)-(T-8) °F	1.1	1.6	2.0	1.3	1.8	0.7
	Power, W	55	36	55	54	54	52

TABLE 2-2

Pedestal Artery Heat Pipe Testing - Summary Sheet

Heater	Channel	Test Series						
		ETV	ATV*	Sept 72		Oct 72	March 73	EOM
4	T-1, °F	-7.5	78.5	33.5		40.9	42.5	49.8
	T-2, °F	-7.0	77.5	30.0		37.7	38.9	45.2
	T-3, °F	-8.5	76.8	27.1		35.3	37.7	44.1
	(T-1)-(T-3)°F	1.0	1.7	6.4		5.6	4.8	5.7
	Power, W	25	25	19		26	25	25
3	T-1, °F	5.0	82.5	36.6		45.7	47.4	49.9
	T-2, °F	2.0	80.7	34.6		44.9	47.4	47.1
	T-3, °F	1.9	79.4	32.3		41.7	41.7	46.3
	(T-1)-(T-3)°F	3.1	3.1	4.1		4.0	5.7	3.6
	Power, W	50	50	33		50	45	45
3 & 4	T-1, °F	18.5	85.5	41.7	50.8	56.3	57.2	61.2
	T-2, °F	8.0	83.7	40.0	49.9	54.2	52.4	58.5
	T-3, °F	7.0	82.0	37.7	46.6	52.4	52.4	57.4
	(T-1)-(T-3)°F	11.5**	3.5	4.0	4.2	3.9	4.8	3.8
	Power, W	75	75	52	79	79	76	72

*Post ATV Thermocouple data taken in OAO clean room.

**Data taken during ETV indicates incipient wall groove dryout.

TABLE 2-3

Spiral Artery Heat Pipe Testing - Summary Sheet

Heater	Channel	Test Series					
		ATV	Sept 72		Oct 72	March 73	ECN
6	T-4, °F	25.1	26.4		35.3	32.3	45.7
	T-5, °F	22.6	23.0		32.3	32.3	42.5
	T-6, °F	24.7	26.6		33.5	33.5	43.5
	(T-4)-(T-5)°F	2.5	3.4		3.0	0.0	3.2
	Power, W	26	19		26	25	25
5	T-4, °F	68.5	40.0		55.9	58.5	62.1
	T-5, °F	48.4	30.0		44.1	46.6	50.7
	T-6, °F	51.0	32.8		46.5	48.2	52.6
	(T-4)-(T-5)°F	20.1*	10.0		11.8	11.9	11.4
	Power, W	55	40		59	59	55
Both 5 & 6	T-4, °F	59.5	48.2	62.1	73.2	72.1	75.1
	T-5, °F	36.9	33.8	45.7	56.8	56.8	62.1
	T-6, °F	39.5	37.9	49.0	60.2	60.2	65.6
	(T-4)-(T-5)°F	22.6*	14.4	16.4	16.4	15.3	13.0
	Power, W	90	59	90	90	87	87

*ATV data taken prior to slitting tape around thermistor. The high ΔT effect only seen when saddle heater was energized. Air test showed a decrease of 5.7° in ΔT on slitting.

2.6.2.3 Level 6 FCHP

The flight test data for the spiral artery heat pipe as reported in Table 2-3, is in very good agreement with ATV test data. The high circumferential temperature differences reported for the spiral artery heat pipe is due to some aluminum tape which acts as a heat bridge between the test heater and thermistor bead, (Ref. 2).

Computer runs on the multinode thermal model showed that the spiral artery heat pipe operated at 6,000 watt-inches. This is well within the hydrodynamic limit of the primed pipe, but greater than the screen pumping limit. Also, the pipe decreases the level 6 circumferential structure temperature difference from 39°F (without pipes) to 9°F (with pipes). The decrease in circumferential temperature difference due to heat pipes is much more pronounced at Level 6 than either Level 4 or Level 5. This is due to the unique configuration at Level 6 which has three thermal control bays plus a high-dissipation bay which is strongly tied to structure.

2.6.2.4 OBP VCHP

Temperature histories for the OBP VCHP during periods when the experiment heaters were enabled are shown on Figures 2-7a, b, and c. During this time, the OBP was dissipating 15 watts. The data shows that at the start of the test when the 20 watt heater was enabled the pipe quickly opened-up and the system temperature increased. For comparison, data reported by Eninger (Ref. 6) are shown in Figure 2-8. Both sets of data show the VCHP to be open and the orbital cycling of the evaporator and condenser temperatures. The transport limit of the heat pipe was not exceeded, but the limited radiator area forced the system temperature above the control range. The difference in operating temperature between the two test conditions is due to small differences in OBP dissipation plus difference in external thermal environments.

2.7 CONCLUSIONS

A span of 8 1/2 years of zero gravity flight experience has been accumulated with three fixed conductance heat pipes and one variable conductance heat pipe. The heat pipes had four different wicking geometries and were fabricated by three different manufacturers. Analysis of flight thermal data

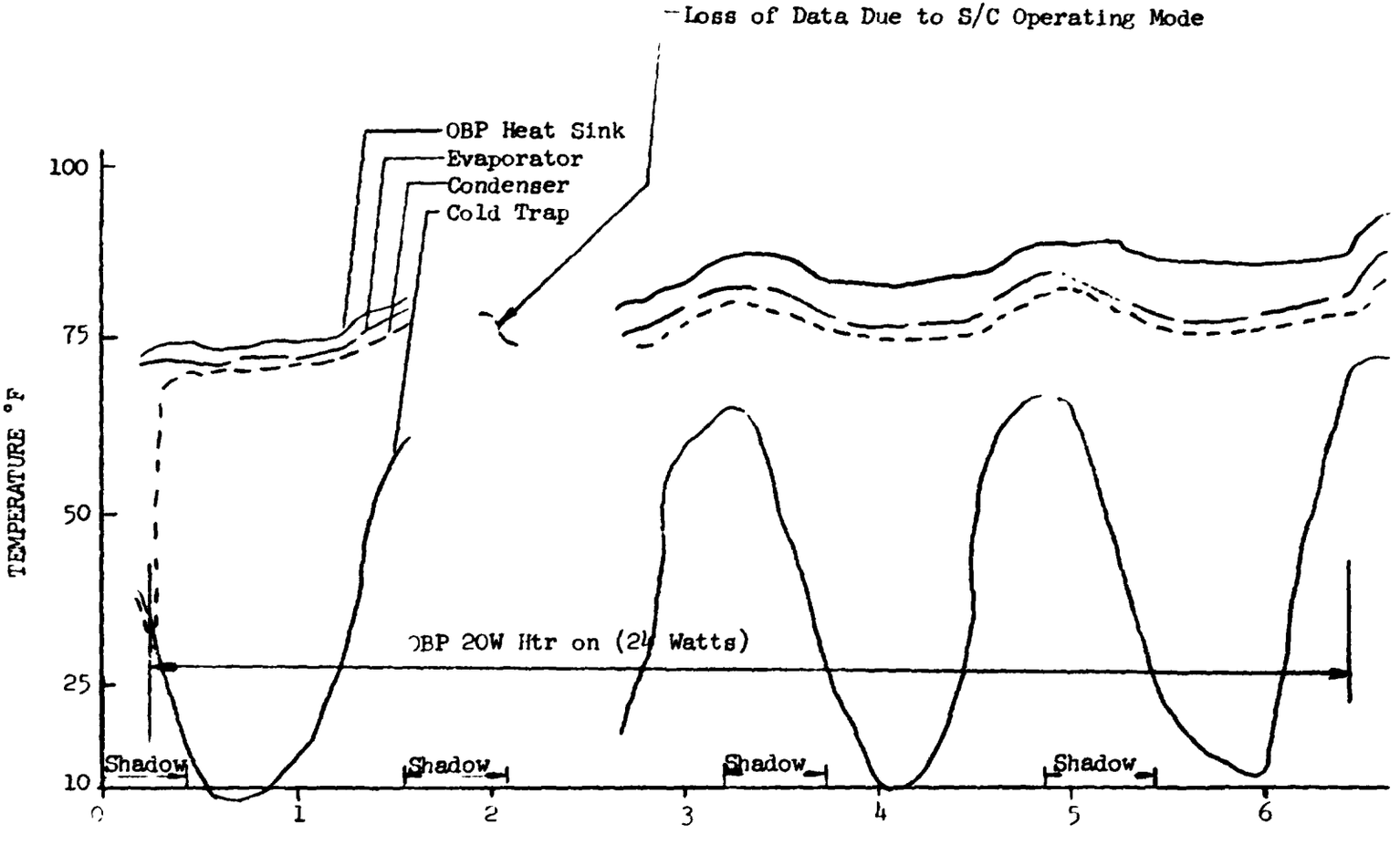

Figure 2-7a. OBP VCHP Temperature History - Mode 2.

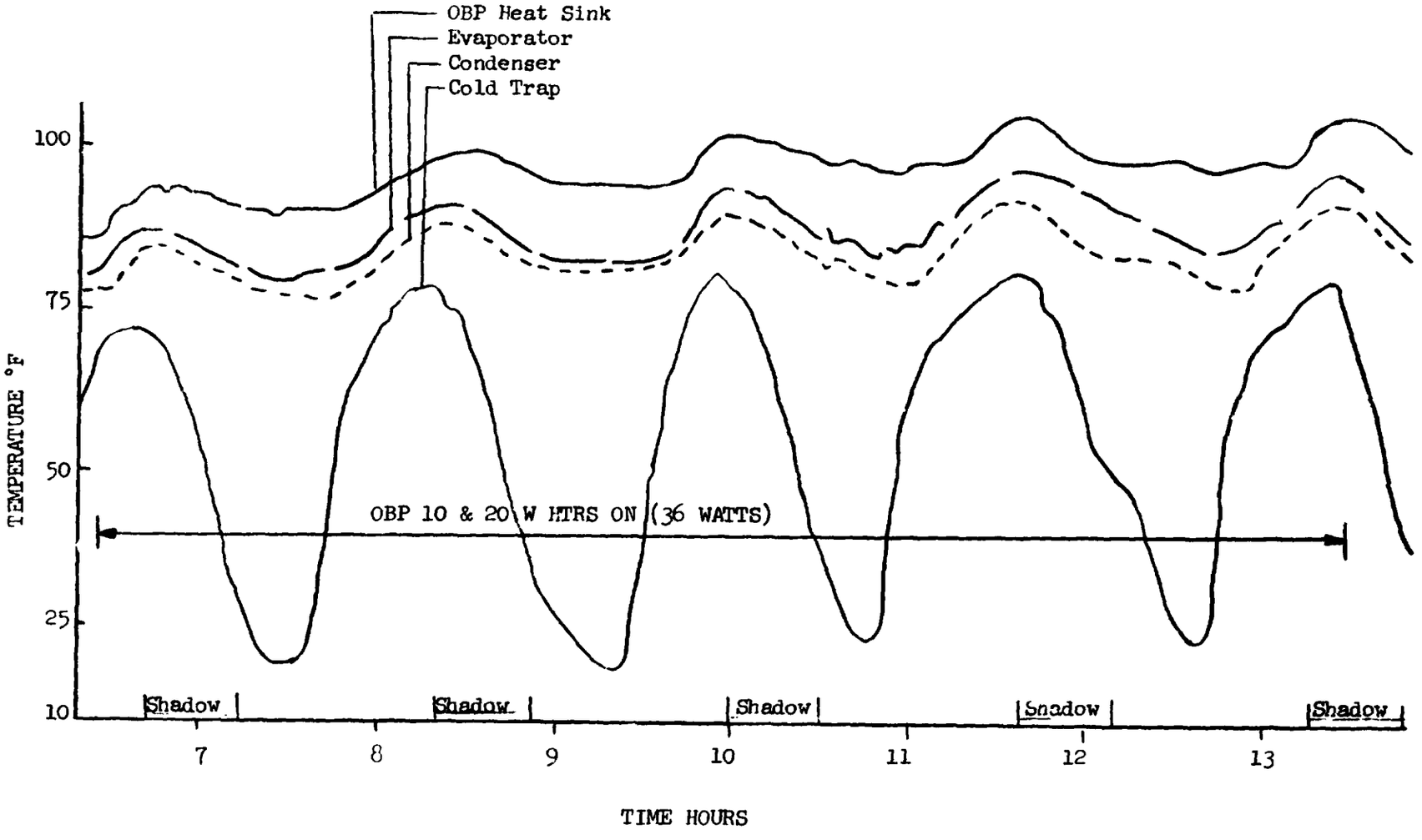

Figure 2-7b. OBP VCHP Temperature History - Mode 2.

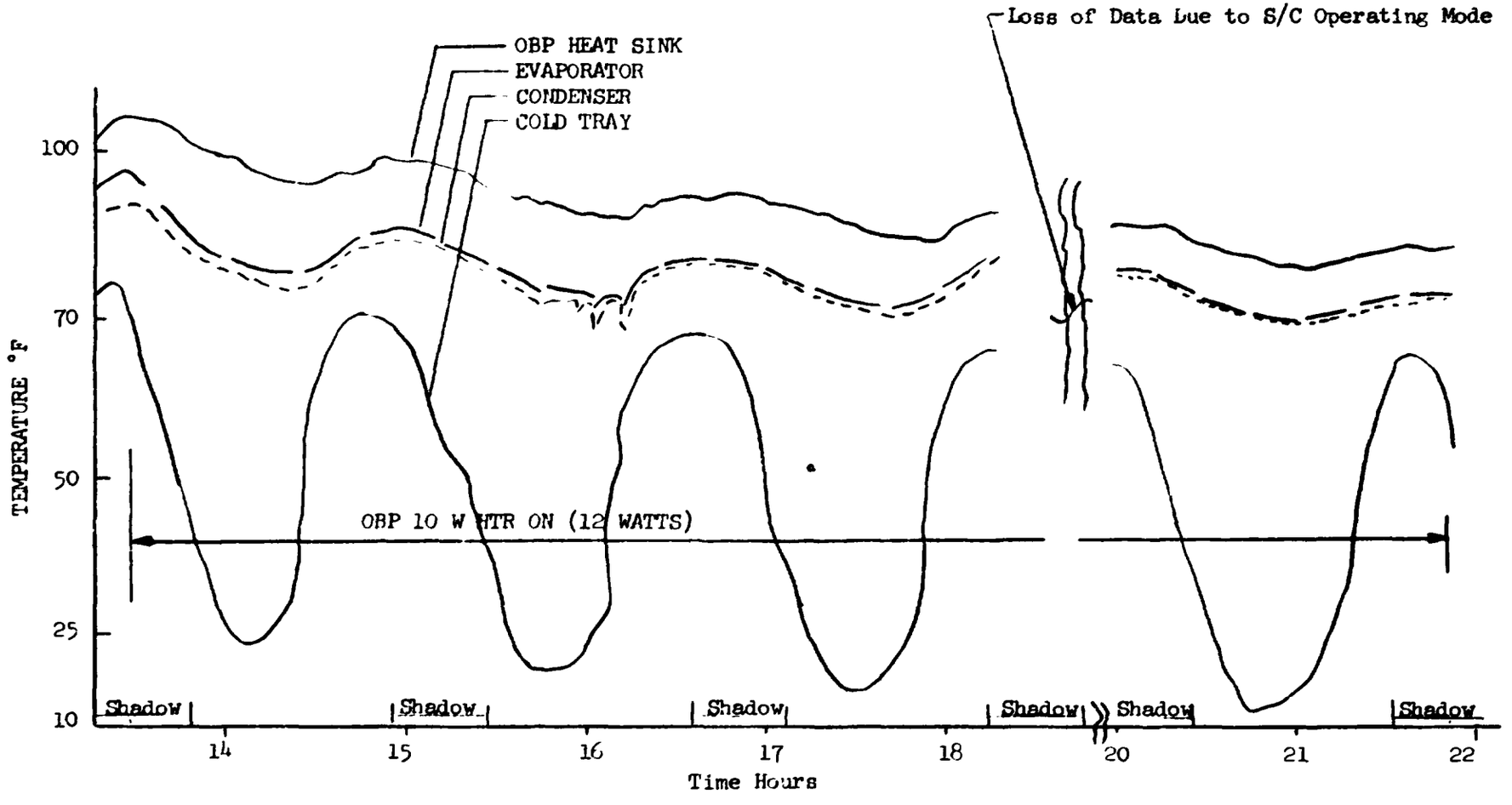

Figure 2-7c. OBP VCHP Temperature History - Mode 2.

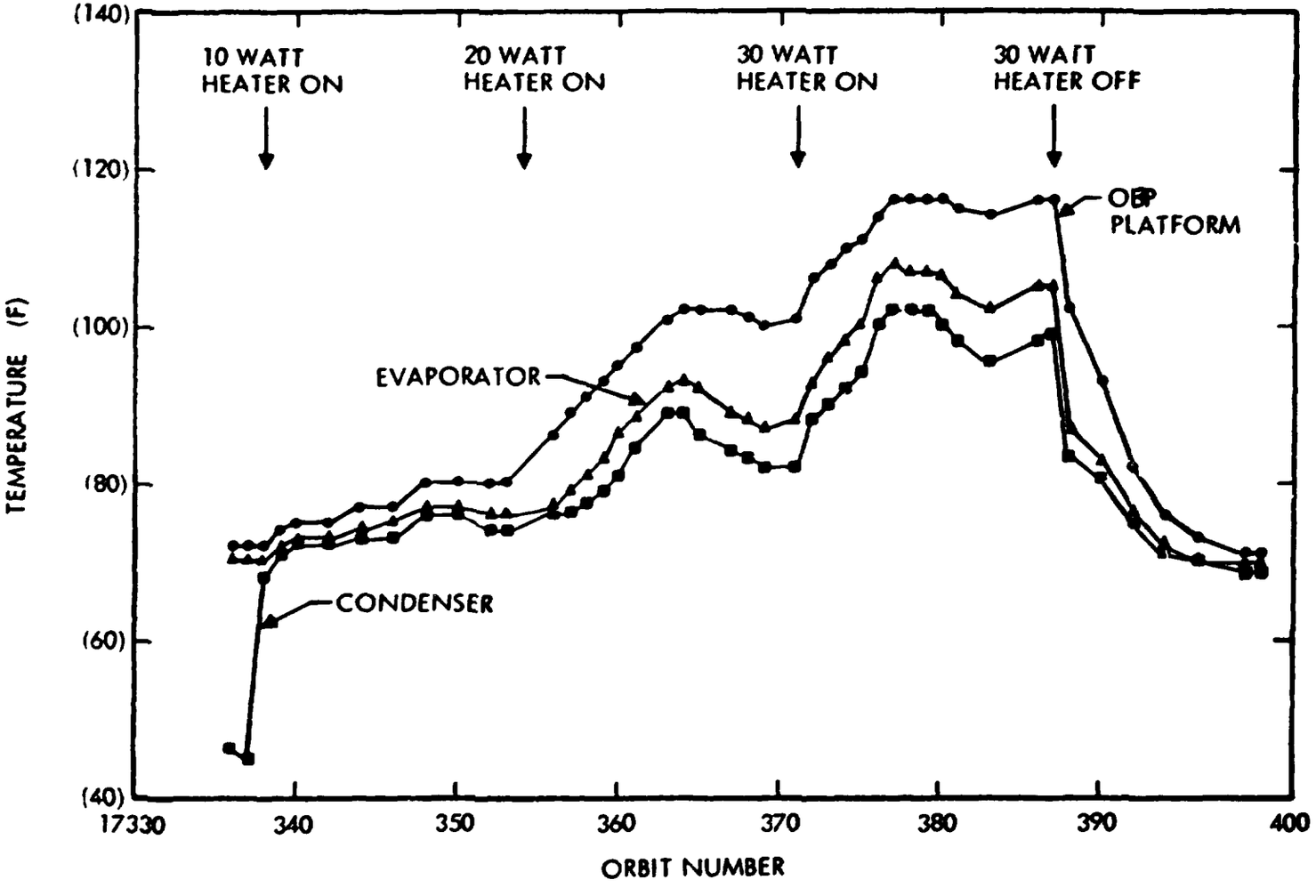

Figure 2-8. OBP VCHP Performance (From Ref. 6).

shows that none of the pipes have degraded in performance since launch. In particular:

a. All four heat pipes have performed their spacecraft housekeeping functions without any detectable change in performance.
b. The OBP VCHP continues to show an offset in control range of 4°F. This is most probably due to heat leak from the equipment heat sink to the cold trap. There is no detectable change in performance over the 8 1/2 years.
c. Flight data in the heat pipe test mode for all four pipes after 8 1/2 years in orbit are in excellent agreement with equivalent early flight data and pre-flight data.
d. No indication of dryout was detected in any of the pipes in the high power heat pipe test mode.

All four heat pipes performed demonstrating that capillary forces in zero gravity will hold liquid in the capillaries and pump along the capillaries. In addition, heat fluxes as high as 8W/square in. (12W/in.) were handled without any indication of nucleate boiling. No non-condensible gases were detected in the FCHP demonstrating the compatibility of the aluminum/ammonia systems. No additional noncondensible gas was detected in the VCHP demonstrating the compatibility of the stainless steel/methanol system. No fluid was lost from any of the pipes demonstrating the adequacy of the manufacturing processes used by the three heat pipe manufacturers.

REFERENCES

1. Fine, H., Quadrini, J. and Ollendorf, S., "An Insight into the Features of the OAO-C Thermal Design", ASME Paper Number 73-ENAs-4.

2. Harwell, W., Edelstein, F., McIntosh, R., and Ollendorf, S., "Orbiting Astronomical Observatory Heat Pipe Flight Performance Data", AIAA Paper Number 73-758.

3. Wanous, D.J., Marcus, B.D., and Kirkpatrick, J.P., "A Variable Conductance Heat Pipe Flight Experiment: Performance in Space", AIAA Paper Number 75-725.

4. Bienert, W., Kroliczek, E., "Experimental High Performance Heat Pipes for the OAO-C S/C", ASME Paper Number 71-AV-26.

5. Caruso, C., et al, "The Orbiting Astronomical Observatory Thermal Test Program", AIAA Paper Number 69-995.

6. Eninger, J.E., Leudke, E.E., and Wanous, D.J., "Research Report No. 1, Flight Data Analysis and Further Development of VCHP's", CR-137782, Feb. 1976.

OAO-C End of Mission Tests
Thermal Control Coatings

by
W. Harwell
Grumman Aerospace Corporation
Bethpage, New York 11714

February 9, 1981

TABLE OF CONTENTS

SECTION 3
THERMAL CONTROL COATINGS

3.1 SUMMARY

The rate of degradation of the A-1 alzak and A-5 silver teflon skins has been determined over the 8 1/2 years of the OAO-C mission. The A-1 skin which was fabricated from an alzak panel known to be prone to severe UV degradation reached a limiting solar absorptance of 0.38. This should not be considered typical of flight quality alzak. The A-5 skin which is a composite of silver backed teflon and flight quality alzak reached a solar absorptance of 0.2. This equates to a value of 0.18 to 0.19 for the silver teflon alone.

3.2 INTRODUCTION

Two side skins of the OAO-C were instrumented to allow estimation of the rate of degradation of their external thermal control coatings. The coatings were alzak and silver backed teflon. The side skins chosen were on the A side of the vehicle, the side receiving the maximum cumulative solar insolation.

To ensure maximum accuracy of the data, the A-1 skin which is insulated on the inside was chosen for the alzak skin. A flight thermistor was bonded to the inside surface at the center of the skin. Late in the program during routine UV screening of test coupons taken from the individual skins, it was discovered that the A-1 alzak panel was of poor quality and would degrade quickly in space. As it was insulated from the internal spacecraft equipment (UCL or University College of London Experiment) it was allowed to fly as a guide to the worst case degradation. The UV tests showed that the A-1 skin was the only panel of the OAO-C which was prone to severe degradation. It is recommended, therefore, that the quantitative flight data for this skin be de-emphasized and the data only be viewed as indicative of qualitative degradation of alzak surfaces.

The silver backed teflon coating was flown on the A-5 (tape recorder) bay. The A-5 skin was in fact a composite skin consisting of silver backed teflon laid down on an alzak skin with double backed kapton tape. The silver teflon

covered 82% of the 16" x 28" skin, the remaining 18% being a picture frame of alzak around the silver teflon. The flight thermistor was bonded to the inside surface at the center of the skin.

3.3 OBJECTIVE OF TEST

The objective of the test is to evaluate the rate of degradation of the alzak and silver teflon thermal control coatings on the OAO-C spacecraft over the 8 1/2 years of flight.

3.4 METHODOLOGY

The A-1 (alzak) and A-5 (silver teflon) skins are each instrumented with a thermistor to monitor their orbital variations in temperature. Temperature data taken during the first 30 days of flight from these two sensors plus associated equipment were used to verify thermal math models of each of these skins (Ref. 1). The thermal models are shown schematically in Figure 3-1 and correlations of an analytical model with typical flight data on Figure 3-2. Assuming the emittance of the coatings have remained constant since launch, then degradation of the coatings can be determined simply by systematically varying the solar absorptance until the computed orbital temperature profile matches the measured profile.

Data availability over the 8 1/2 years of flight consisted of:

a. Tape recorder dumps during the first 2 years of flight. This gives continuous orbital data.

b. Contact data through the 8 1/2 years of flight. By selecting contacts, it is possible to piece together large sections of orbits. This restricts analysis to periods when the vehicle was in a stable beta angle orientation for a number o orbits or when several contacts were established in one orbit.

c. PPDS data - During the EOM tests, thermal parameters were stored in the PPDS during the orbit and dumped during the next contact. PPDS memory utilization was minimized by storing data at approximately 2 minute intervals.

All three types of data have been collected for the A-1 and A-5 skins and the degradation of the skins estimated as a function of time since launch.

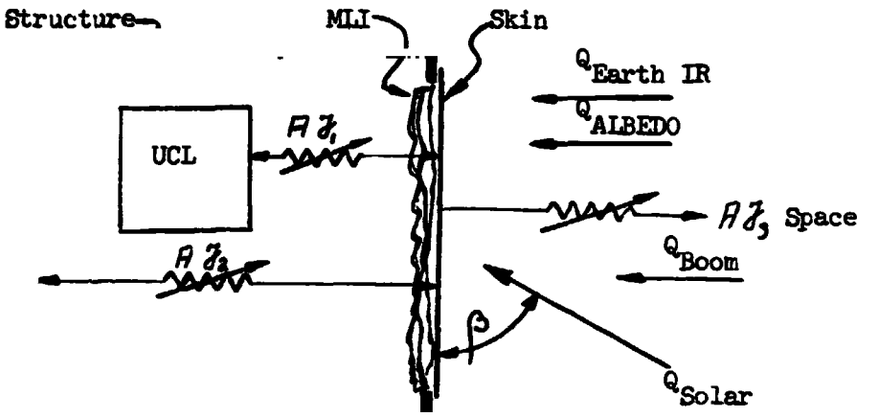

A-1 Skin (ALZAK) Thermal Model

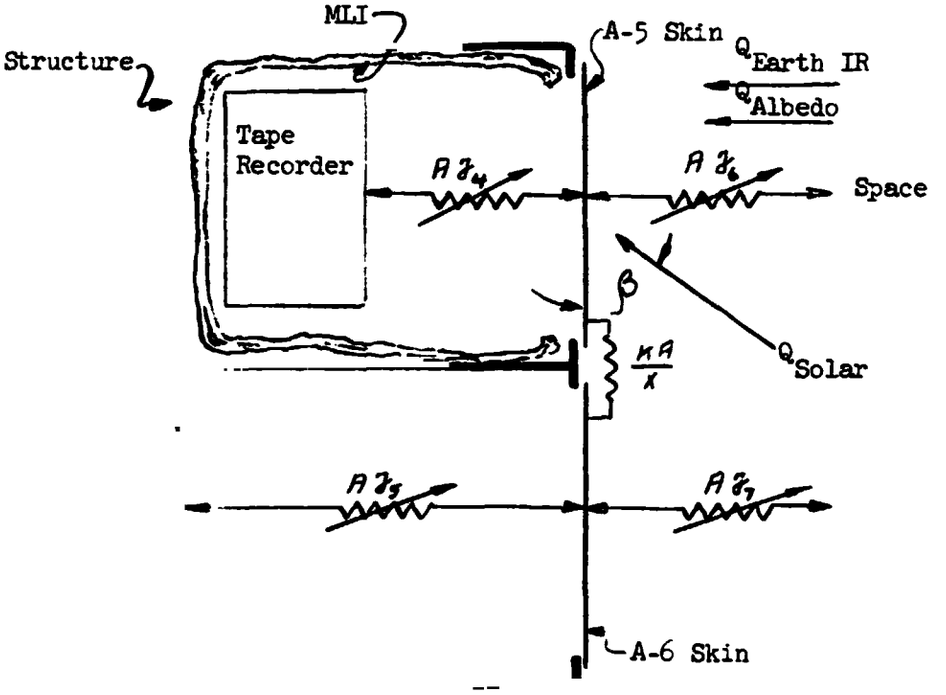

A-5 Skin (Silver Teflon) Thermal Model

Figure 3-1. Simple Thermal Models of Skins

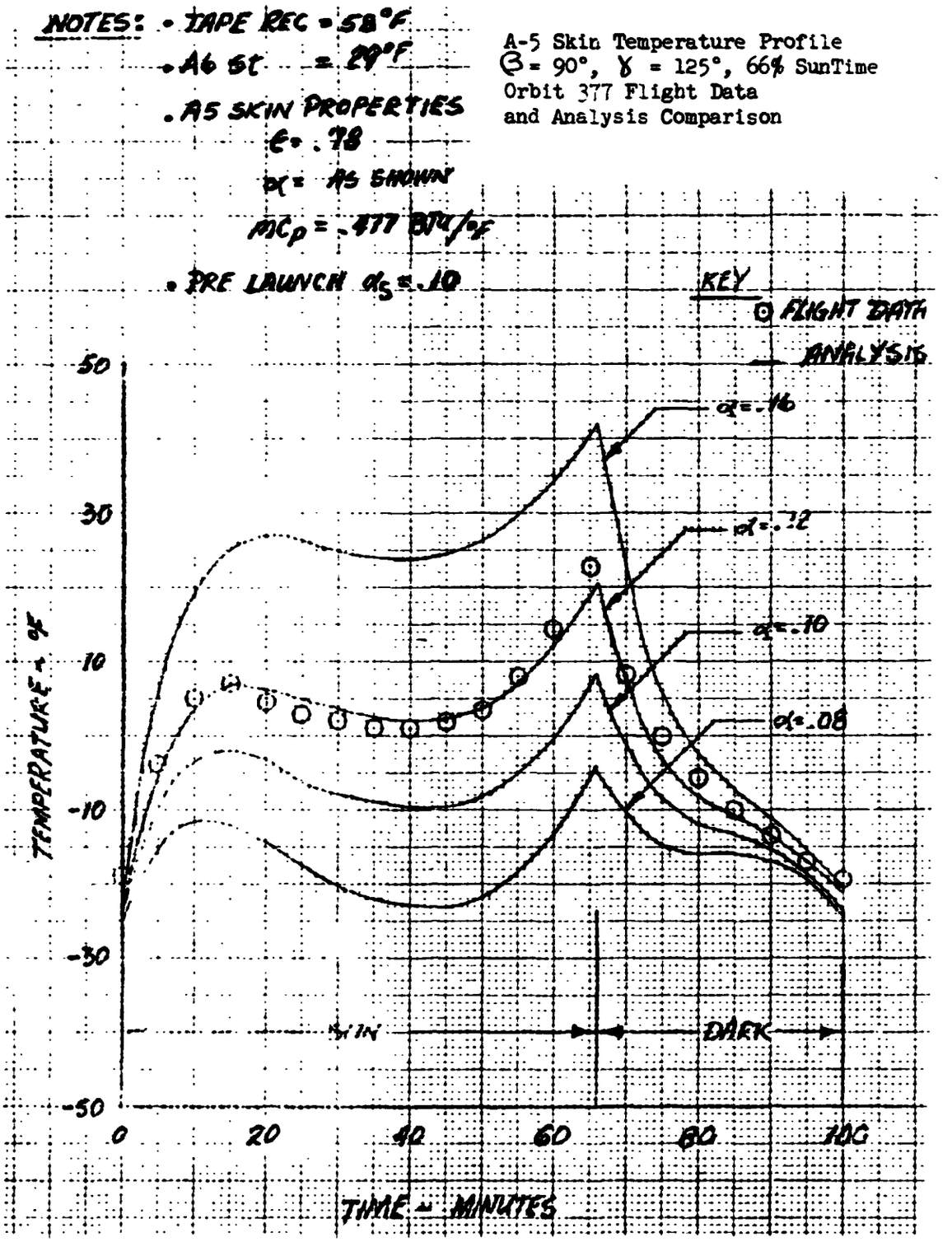

Figure 3-2. Correlation of Analytical Model and Flight Data.

The equivalent sun hours (ESH) of exposure of the A side skins were also computed as a function of time since launch. The ESH per orbit is simply

$$ESH = \frac{T.P. \sin \beta}{100}$$

where T is the orbit period (hours), P the percent suntime and β the angle between the earth/sun line and the vehicle optical axis. By definition, beta is also the angle between the plane of the A skins and the earth sun line. The cumulative equivalent sun hours of exposure (CESH) is simply the summation of each orbit ESH since launch. The beta angle, suntime data for the computation were taken from the OAO-C annual reports (Ref. 2). The variation of CESH with mission time is given in Figure 3-3.

3.5 DISCUSSION OF RESULTS

3.5.1 A-1 SKIN

Figures 3-4, 3-5, and 3-6 show typical orbit transient temperature data for the A-1 skin. Figure 3-4 data is a composite of four different contacts, each contact lasting 10 to 15 minutes. Figure 3-5 and 3-6 are data recorded by the PPDS then dumped during the next contact. Note that Figures 3-5 and 3-6 each show data for two consecutive orbits. The data within each set is very consistent. The estimated variation of solar absorptance with exposure time is shown on Figure 3-7. For simplicity, the data analysis has been restricted to nominal beta angles of 55 and 90°. Figure 3-7 shows the solar absorptance of the alzak skin to increase very rapidly over the first few thousand hours of exposure with data for both beta angles of 55 and 90 falling in line. The data for orbit 41926 at a beta angle of 55° equates to an absorptance of 0.36 then orbit 43846 (beta 90°) shows a drop to 0.27 followed by an increase to 0.38 at orbit 44136 (beta 53°). A repeat beta 90 test was run and again the absorptance came out low (0.28 at orbit 44576). The flight data was reviewed, but no problems were detected either with data transmittal or data reduction.

A beta angle of 90° is equal to the solar rays normal to the A-1 skin. With an insulated skin, one would expect normal incidence to equate to maximum skin temperature. Examination of Figures 3-5 and 3-6, however, show the beta 90 condition to be approximately 40°F colder than the beta 53° condition. Earlier flight data did not show this lower temperature effect. The data for orbit 43646

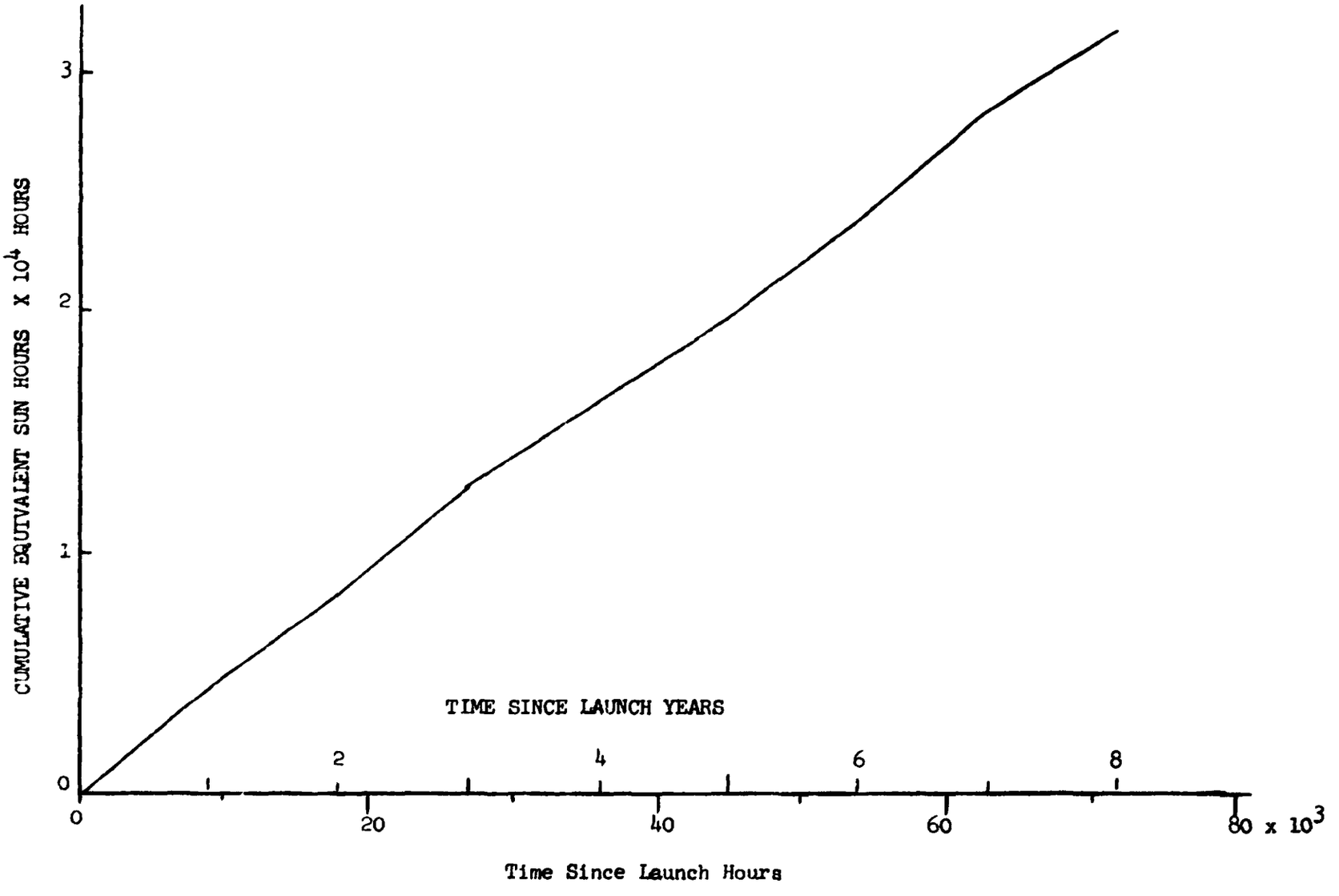

Figure 3-3. Cumulative Equivalent Sun Hours.

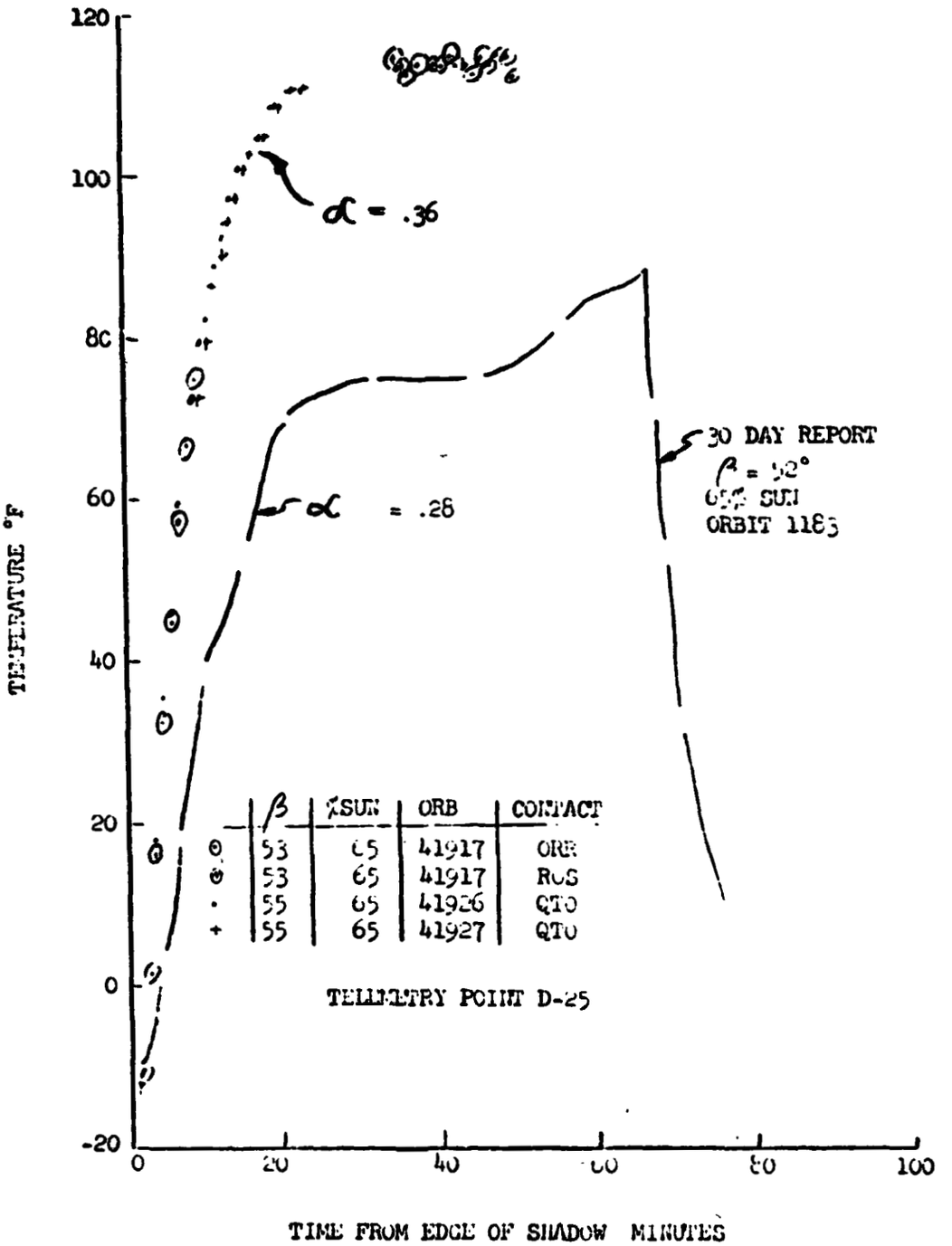

Figure 3-4. Temperature History A-1 Skin.

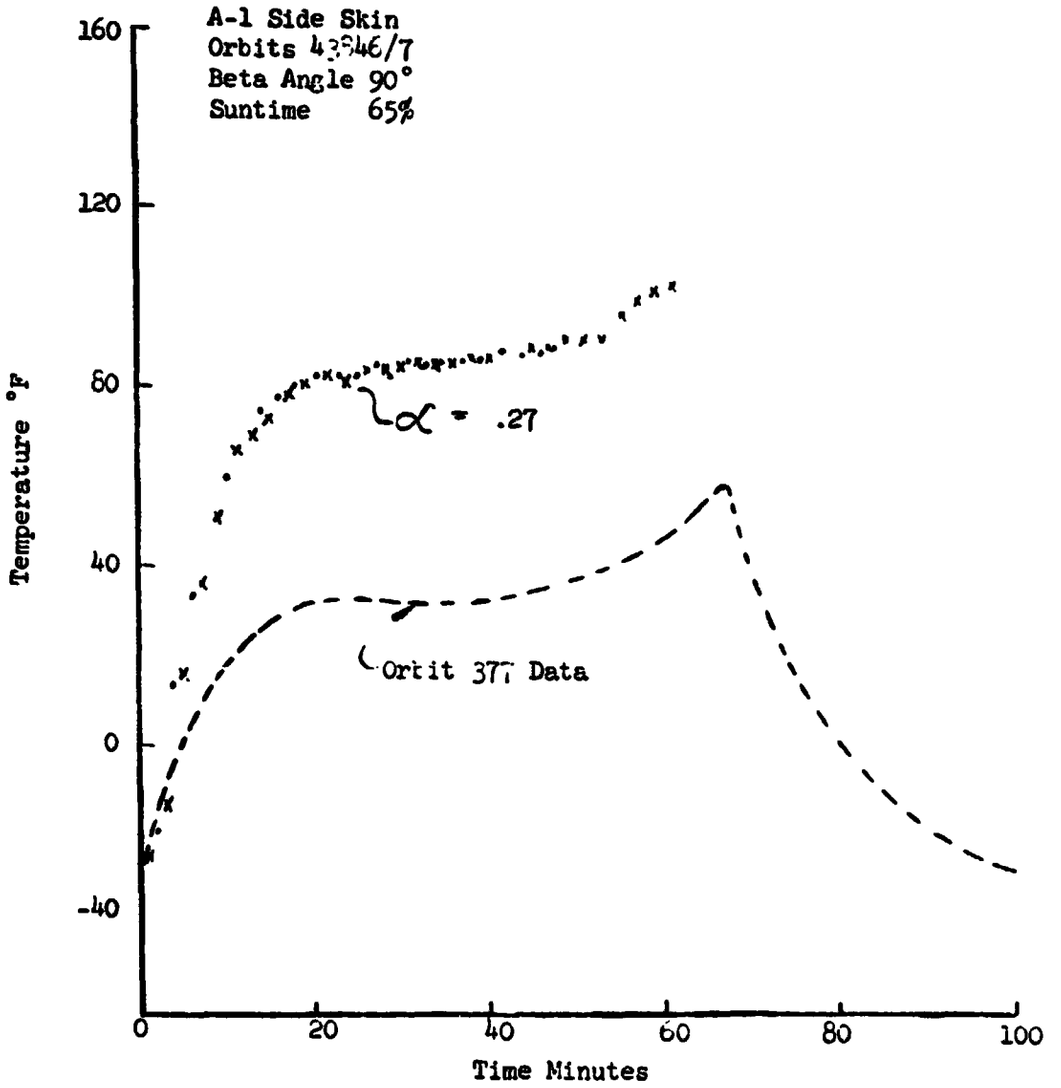

Figure 3-5. A-1 Skin Temperature History.

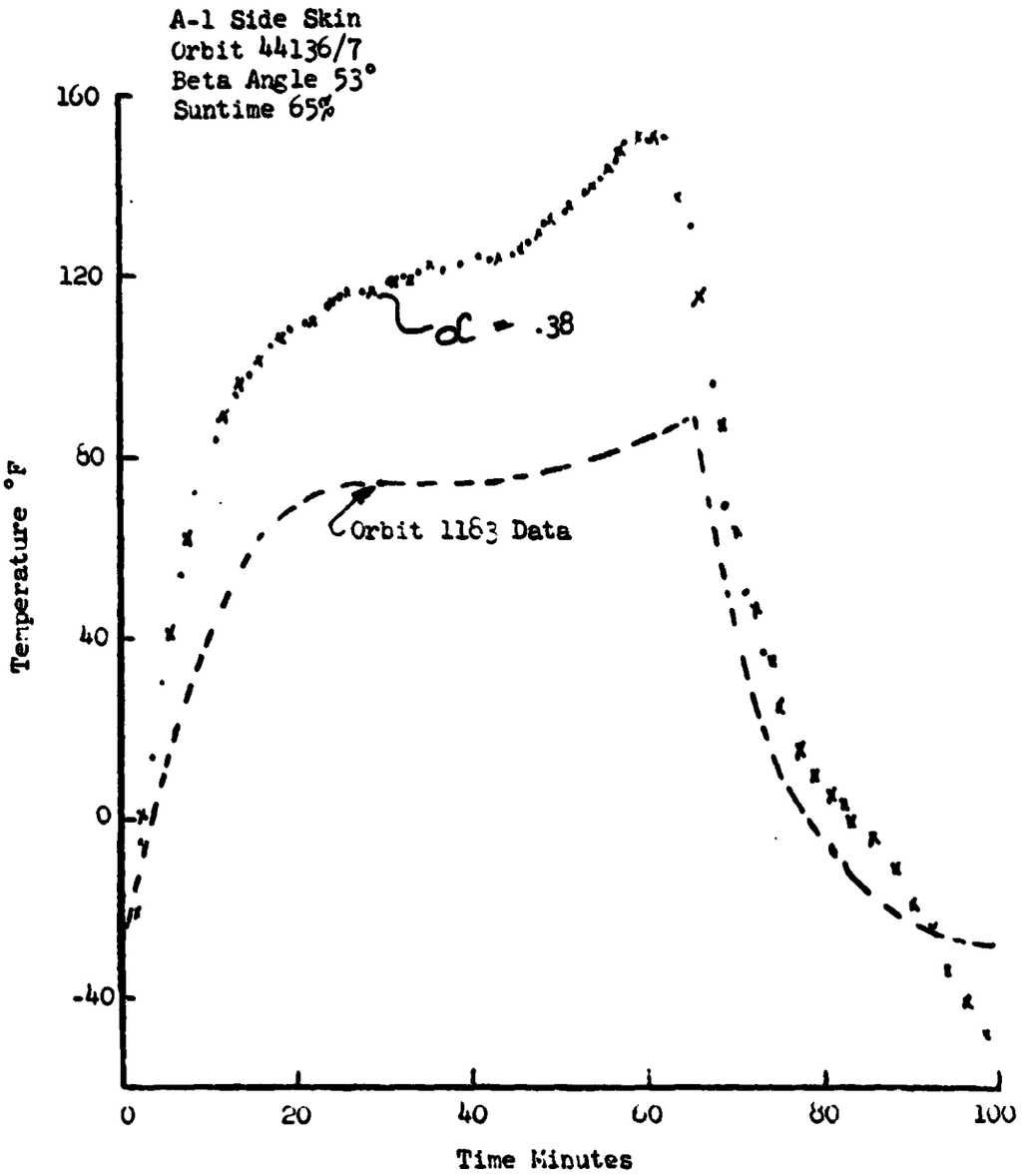

Figure 3-6. A-1 Skin Temperature History.

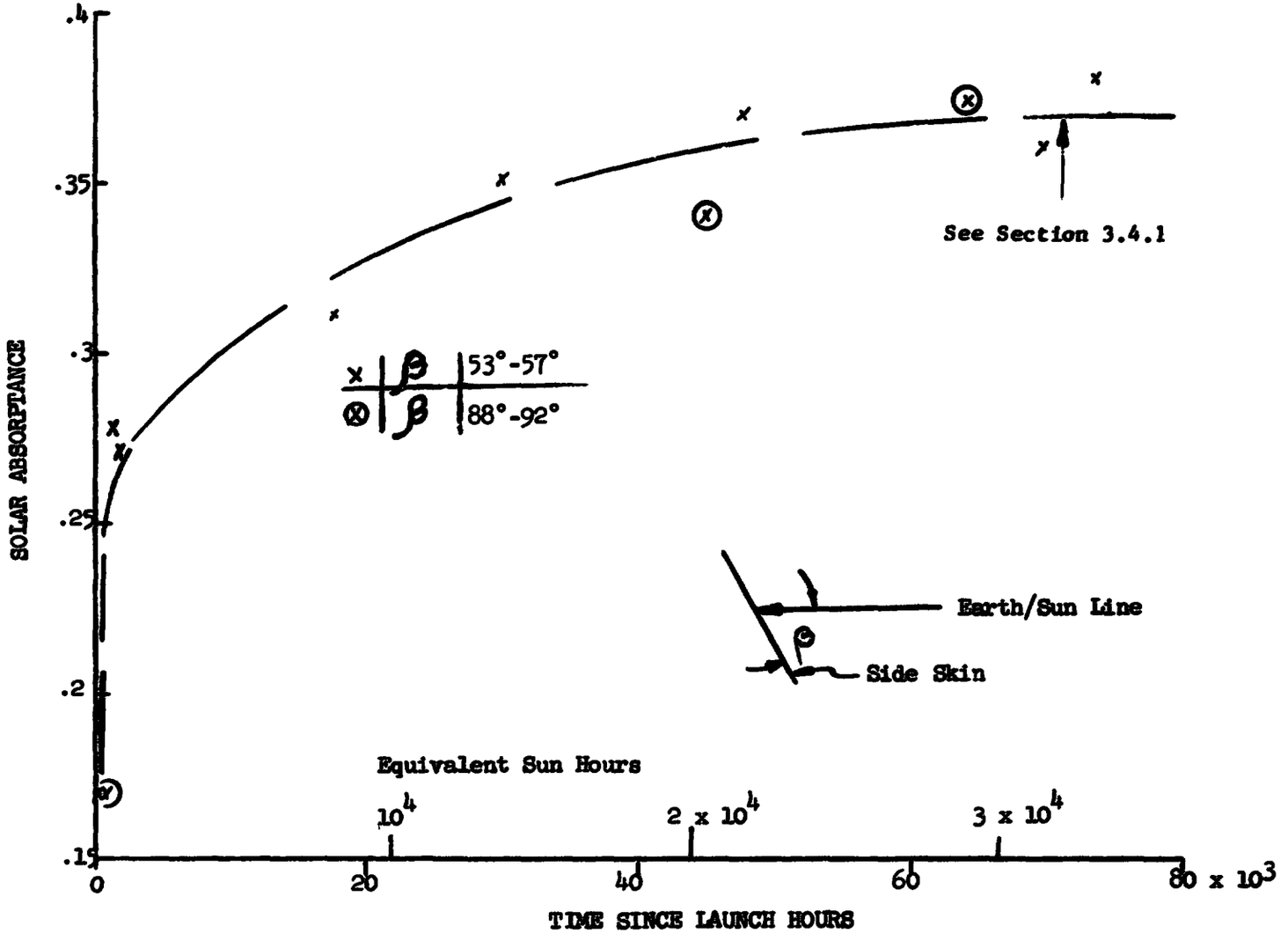

Figure 3-7. A-1 Skin (Alzak) Solar Absorptance.

beta 90 condition were reviewed to determine if any other anomalous conditions could be established. The results of this review were:

1. No anomaly was detected with the A-5 skin.
2. No anomalies were detected with either the lower left outboard or lower left inboard solar array temperatures.
3. The temperature of the upper right inboard array increased rapidly during the first 37 minutes of sunlight. The current drawn from the array at this time in orbit decreased rapidly indicating a switch to a new battery charging condition. Simultaneously with this decrease in power drawn from the array, the array temperature unexpectedly decreased. One would anticipate that as less energy is drawn from the array, then more of the insolent solar energy would be available in the form of thermal energy and the array temperature should increase. This must, therefore, be considered a second anomalous condition for this beta angle. Data are not available for orbit 44576 to determine whether or not a similar condition occurred during the most recent beta 90 orientation.
4. No other inexplicable data were found.

Possible reasons for the low temperature were reviewed and rejected as follows:

a. Loose thermistor - A loose thermistor would of course indicate an erroneous temperature which would lag the skin temperature. To postulate that, the thermistor could loosen, reheal itself and then loosen again in phase with the available data is unacceptable to the writer.

b. MLI - The temperature of the skin is highly dependent upon the inner MLI blanket. To postulate that, the blanked would fall off the skin, reposition itself and then fall off again is not believable.

c. Equipment temperature - The skin is very poorly coupled to the UCL and structure. Major temporary changes in couplings would be required to explain the data.

d. Spacecraft roll angle - The relatively small changes in absorbed earth infrared emissions due to changes in roll angle cannot explain the data.

e. Blocking of Solar Rays - Major blockage of the sun would be required to explain the 50 to 60°F reduction in temperature. In addition, there is nothing in the neighborhood which could block the sun.

In conclusion, the two beta 90 data points must be considered as anomalies and no solid reasons can be offered.

As stated in the introduction, this alzak panel cannot be considered typical of the other skins on the vehicle. This data should only be considered as indicating trends and possible worst case degradation of alzak.

3.5.2. A-5 SKIN

Temperature profiles for the A-5 skin are shown on Figures 3-8, 3-9, and 3-10. On Figure 3-8, the data were obtained for four contacts while Figure 3-9 and 3-10 are PPDS data with two orbits of data being shown on each figure. The data are very consistent within each data set. The estimated solar absorptance for the composite skin is shown on Figure 3-11 as a function of time since launch. Figure 3-11 shows the absorptance rapidly increased after launch and then stabilized at a value of about 0.2. The absorptance of the silver back teflon itself was estimated from

$$\alpha_{Composite} = 0.82\,\alpha_{ST} + 0.18\,\alpha_{ALZAK}$$

For this equation it was assumed that the absorptance of alzak started (at launch) at 0.14 and then degraded quickly to a constant value of 0.30 after 10^4 hours of equivalent sun time. This data is shown on Figure 3-12. For comparison, the effect of assumed alzak absorptance on the computed value for silver teflon is also shown on Figure 3-12. The effect is small and for most purposes can probably be neglected.

3.6 CONCLUSION

The rate of degradation of alzak and silver teflon has been estimated from data accumulated over the 8 1/2 years of the OAO-C mission. The following conclusions can be drawn:

1. The solar absorptance of the A-1 alzak skin reached a value of 0.38. The A-1 skin is not considered typical of flight quality alzak and the 0.38 value should only be considered as worst case for those alzak skins which are known to be prone to severe UV damage.
2. The solar absorptance of the A-5 silver teflon skin reached a value of 0.2 for the composite skin. This equates to 0.19 for the silver teflon alone assuming the alzak degraded to 0.24. More severe degradation of the alzak to an absorptance of 0.3 would result in a decrease in absorptance of the silver teflon to 0.18.

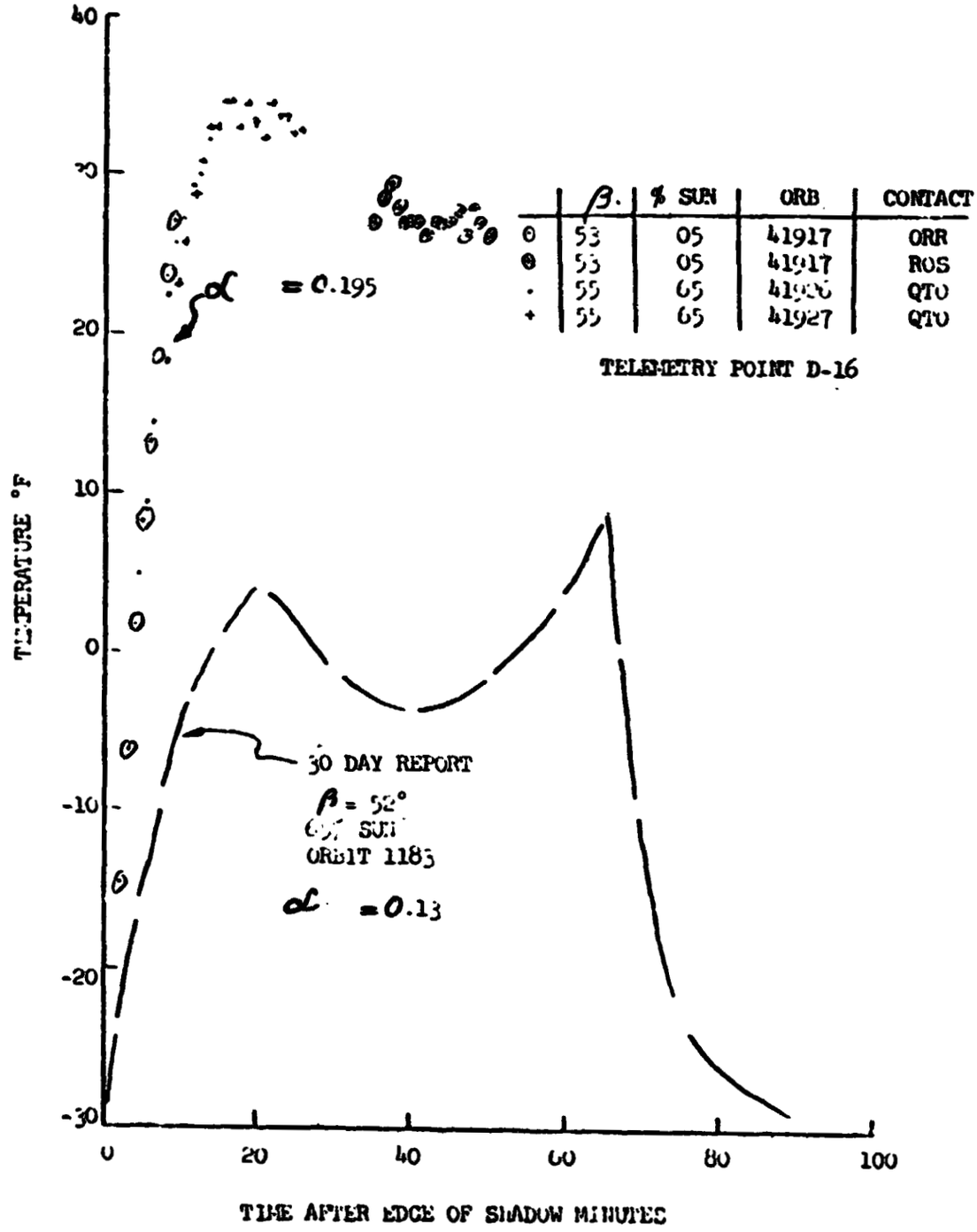

Figure 3-8. Temperature History A-5 Skin.

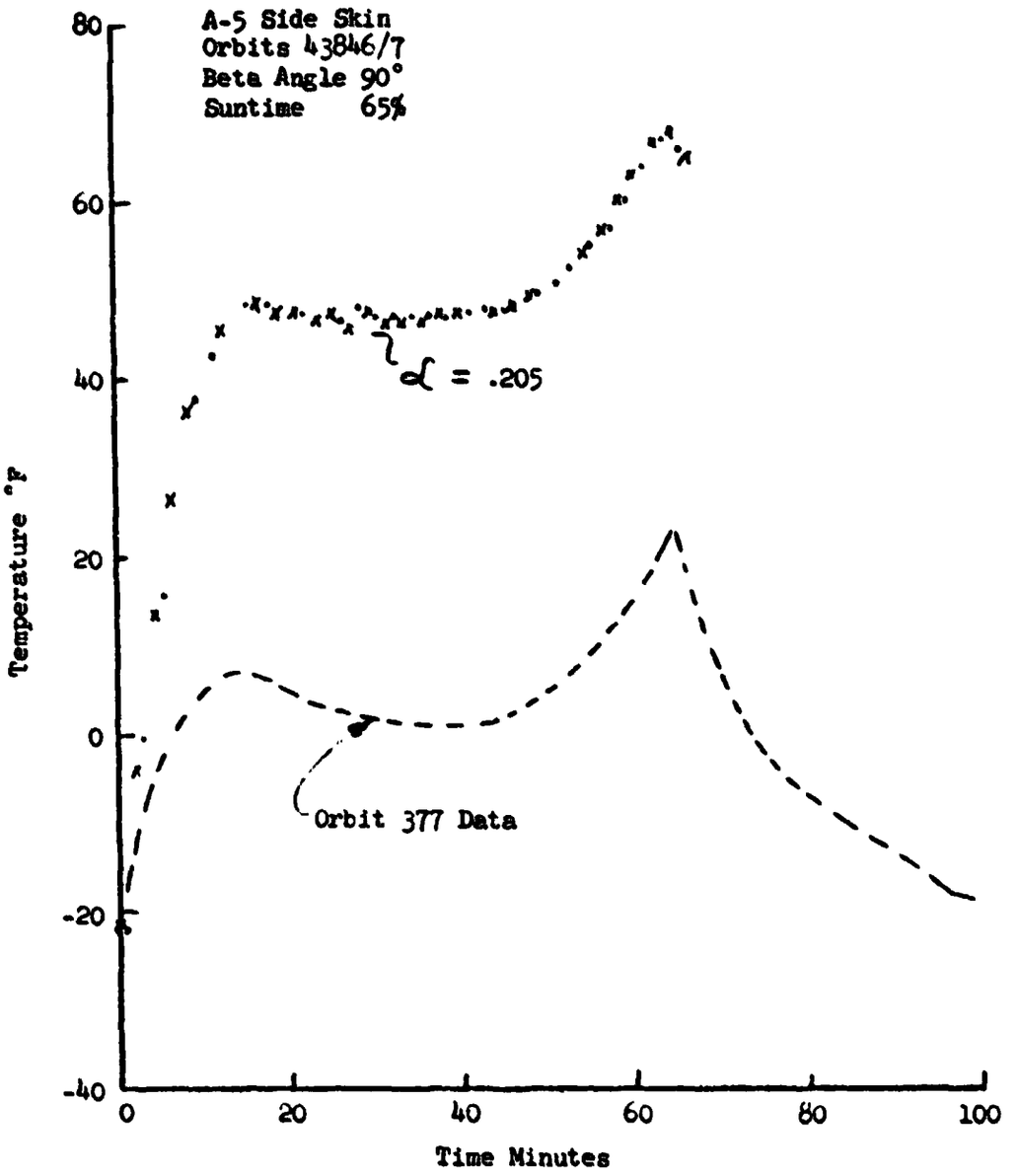

Figure 3-9. A-5 Skin Temperature History.

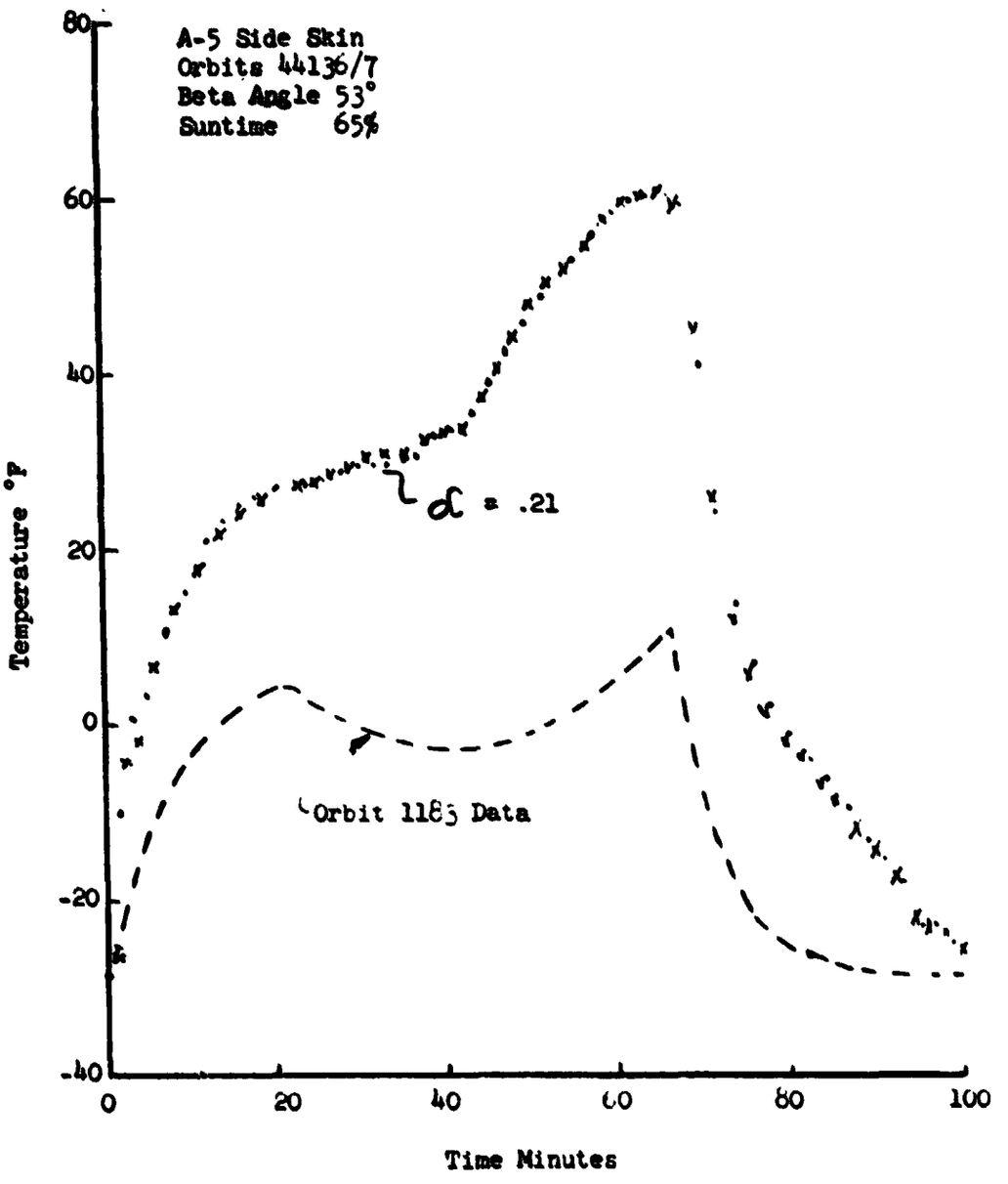

Figure 3-10. A-5 Skin Temperature History.

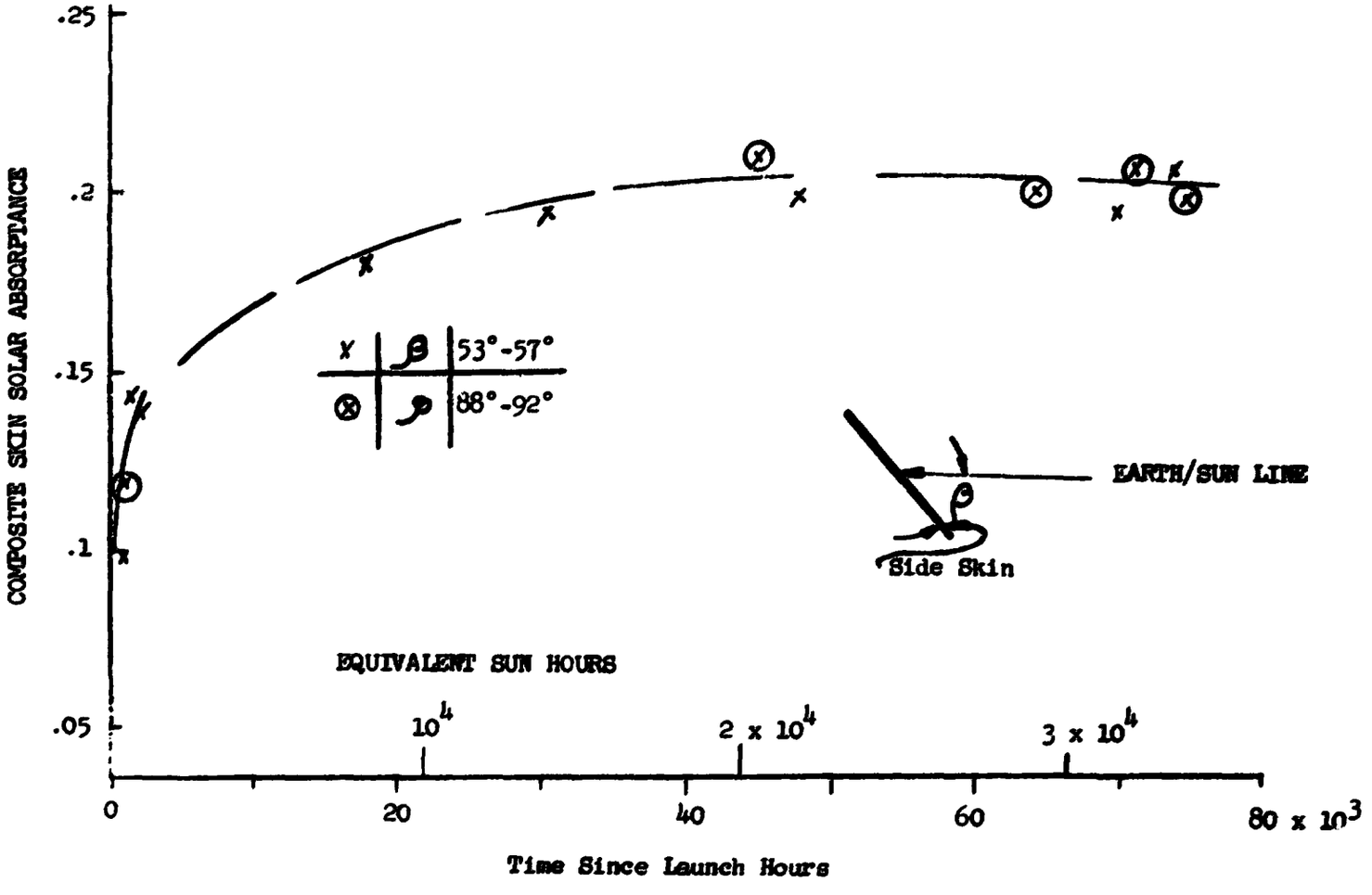

Figure 3-11. A-5 Skin (Silver Teflon) Solar Absorptance.

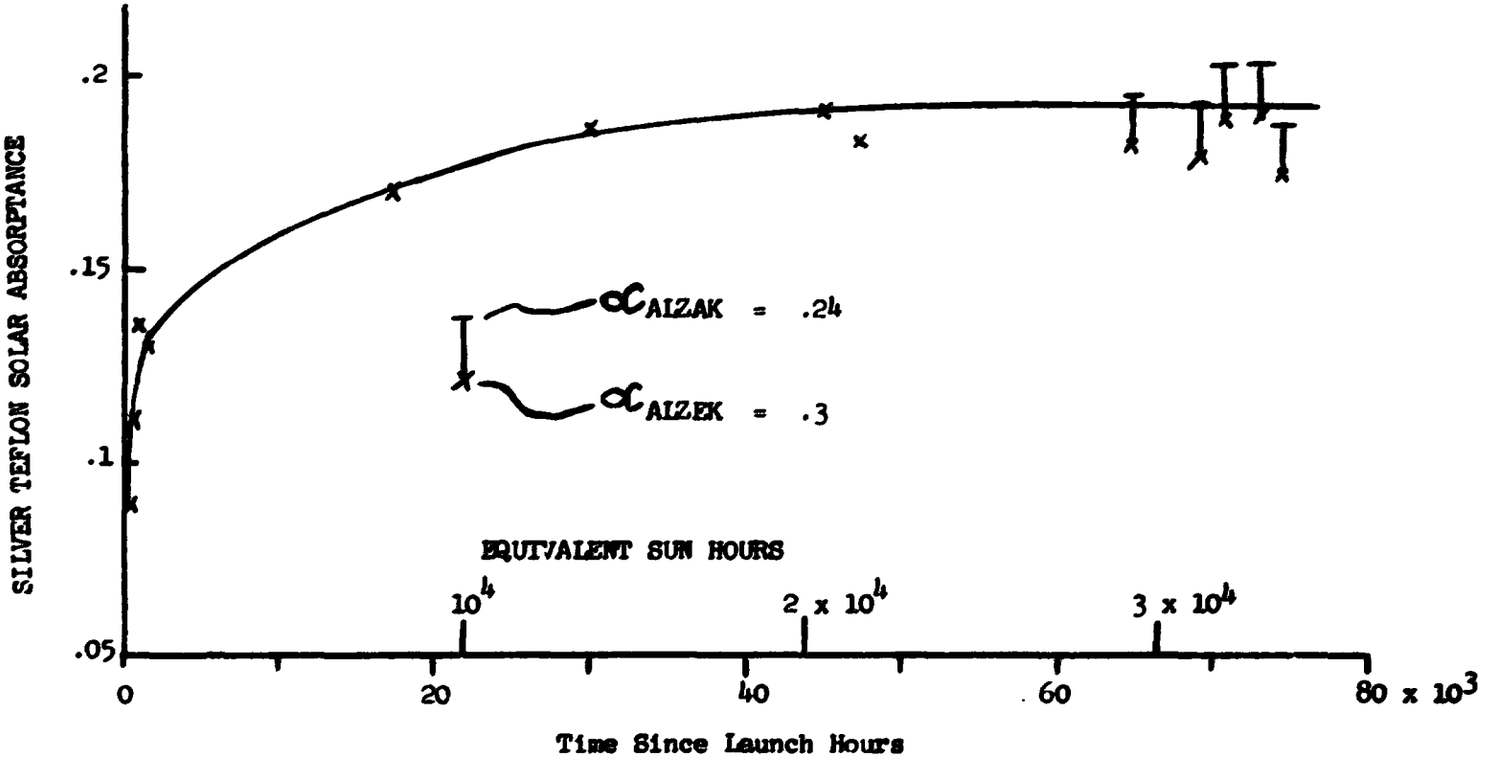

Figure 3-12. Solar Absorptance of Silver Teflon.

REFERENCES

1. Fine, H., Quadrini, J. & Ollendorf, S., "An Insight into the Features of the OAO-C Thermal Design", ASME Paper 73-ENAs-4.

2. OAO-C Copernicus Flight Evaluation Reports by Grumman Aerospace Corporation, NAS 5-20670.

OAO-C End of Mission Power Subsystem Evaluation

by
C. Michael Tasevoli
NASA/Goddard Space Flight Center
Space Power Applications Branch
Space Technology Division

May 1, 1981

TABLE OF CONTENTS

SECTION 4
POWER SUBSYSTEM EVALUATION

4.1 SUMMARY

End of mission tests were performed on the OAO-3 power subsystem in three component areas: Solar array, nickel-cadmium batteries and the On-Board Processor (OBP) power boost operation. Solar array evaluation consisted of analyzing array performance characteristics and comparing them to earlier flight data. Measured solar array degradation of 12 to 14.5% after 8 1/3 years is in good agreement with theoretical losses due to radiation damage. Battery discharge characteristics were compared to results of laboratory life cycle test performed on similar cells. Comparison of cell voltage profiles reveals close correlation and confirms the validity of real time life cycle simulation. The successful operation of the system in the OBP/power boost regulation mode demonstrates the excellent life, reliability and greater system utilization of power subsystems using maximum power trackers

4.2 INTRODUCTION

The Orbiting Astronomical Observatory (OAO) missions, starting in the late 1960's and spanning more than a decade of operation, were highly successful. The power subsystems for both OAO-2 and OAO-3 (Ref. 1) were similar and both performed successful until deactivated after more than 5 and 8 years of operation, respectively. Prior to the deactivation of the OAO-3 spacecraft, a variety of end of mission tests and evaluations were performed. This report presents the results of the end of mission tests and evaluations for the power subsystem.

The simplified block diagram of the OAO-3 Power Subsystem is shown in Figure 4-1. The subsystem consisted of a main solar array which recharges the batteries and provides additional power to the unregulated bus during the sunlight portion of the orbit, an auxiliary array to provide bus power to spacecraft loads, three nickel-cadmium batteries operated in parallel to power the bus during eclipse, and power regulation and control units for battery charging (Ref. 2).

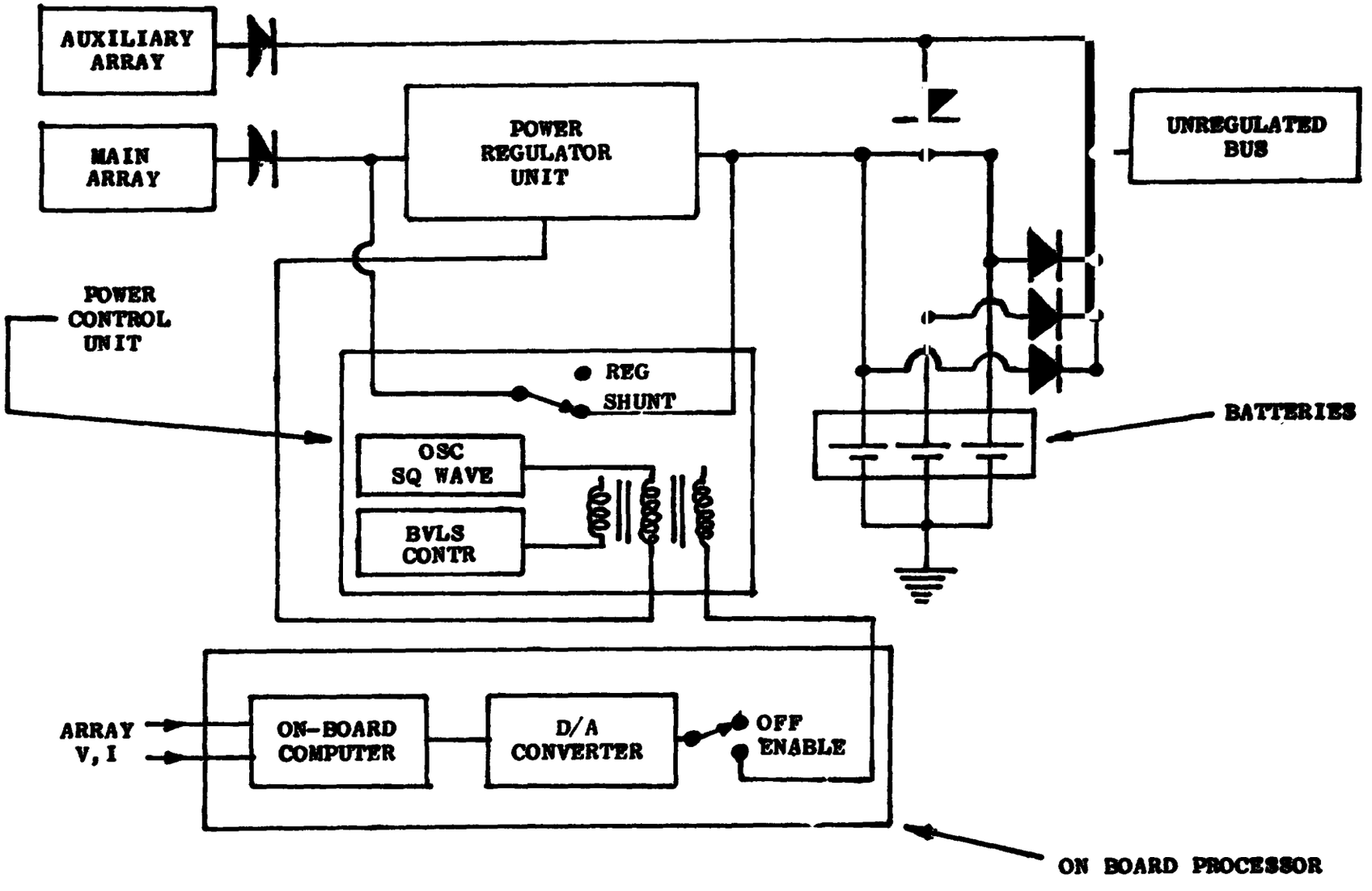

Figure 4-1. Block Diagram of OAO-3 Power Subsystem.

The solar array consisted of eight co-planar solar panels as shown in Figure 4-2. Of these, the lower left outboard (LLO) and lower right outboard (LRO) panel formed the auxiliary array and the remaining six panels comprise the main array. In addition to the power generating circuits of the solar array, two radiation detector (RD) solar cell circuits were installed on the array as shown in the figure. These detectors were each connected to a 68.1 ohm load and their output voltage measured as a telemetry point. All the cells were 1 x 2 centimeters, 12 mils thick, N/P silicon solar cells with a nominal base resistivity of 2 ohm-centimeters, manufactured by Heliotek, Inc.. The series-parallel configuration of the cells for the various paddles is noted in Figure 4-2. Each cell was individually protected by a 6 mil thick, fused silica coverglass with a MgF anti-reflective coating and a multi-layer ultraviolet reflective filter manufactured by Optical Coating Laboratory, Inc.. Dow Corning P.63-489 adhesive was used to bond the glasses to the cells. Beginning of life current/voltage (I-V) curves are shown in Figure 4-3.

Each of the three batteries consisted of 22 series-connected, 20 ampere-hours nickel-cadmium cells, manufactured by Gulton, Inc.. The three batteries were packaged into two mechanical assemblies. Each assembly contained 11 cells of each battery with two battery assemblies isolated on separate thermal baseplates. The batteries had a design life of 1 year in low earth orbit with a 15 to 20% depth-of-discharge (DOD). The temperature design range was 5 to 20°C and a 35°C over-temperature thermostat protected the batteries from high temperature conditions. The batteries were charged and discharged in parallel. A more detailed description of the OAO-3 battery performance appears in Ref. b. Battery cell design details are provided in Table 4-1. Throughout the 8 1/3 year mission, the nickel-cadmium batteries provided trouble-free performance. Battery depth-of-discharge has been approximately 15% and battery temperatures have remained between 5 and 10°C. During the entire mission battery voltage and current divergence have been within telemetry resolution.

The three batteries were charged in parallel from the Power Regulator Unit (PRU) using eight commandable, temperature compensated, battery voltage levels (see Figure 4-4). The PRU consisted of a series of power switching transistors which are turned off and on at a fixed repetition rate. The regulator's output voltage is adjusted by varying the ratio of "on" time to the repetition rate. This duty cycle is controlled by the current through the magnetic amplifier control winding in the Power Control Unit (PCU). The control

MAIN	AUXILIARY	RADIATION DETECTORS
46,080 cells 480 strings 96 cells in series	9464 cells 104 strings 91 cells in series	40 cells 2 strings 20 cells in series

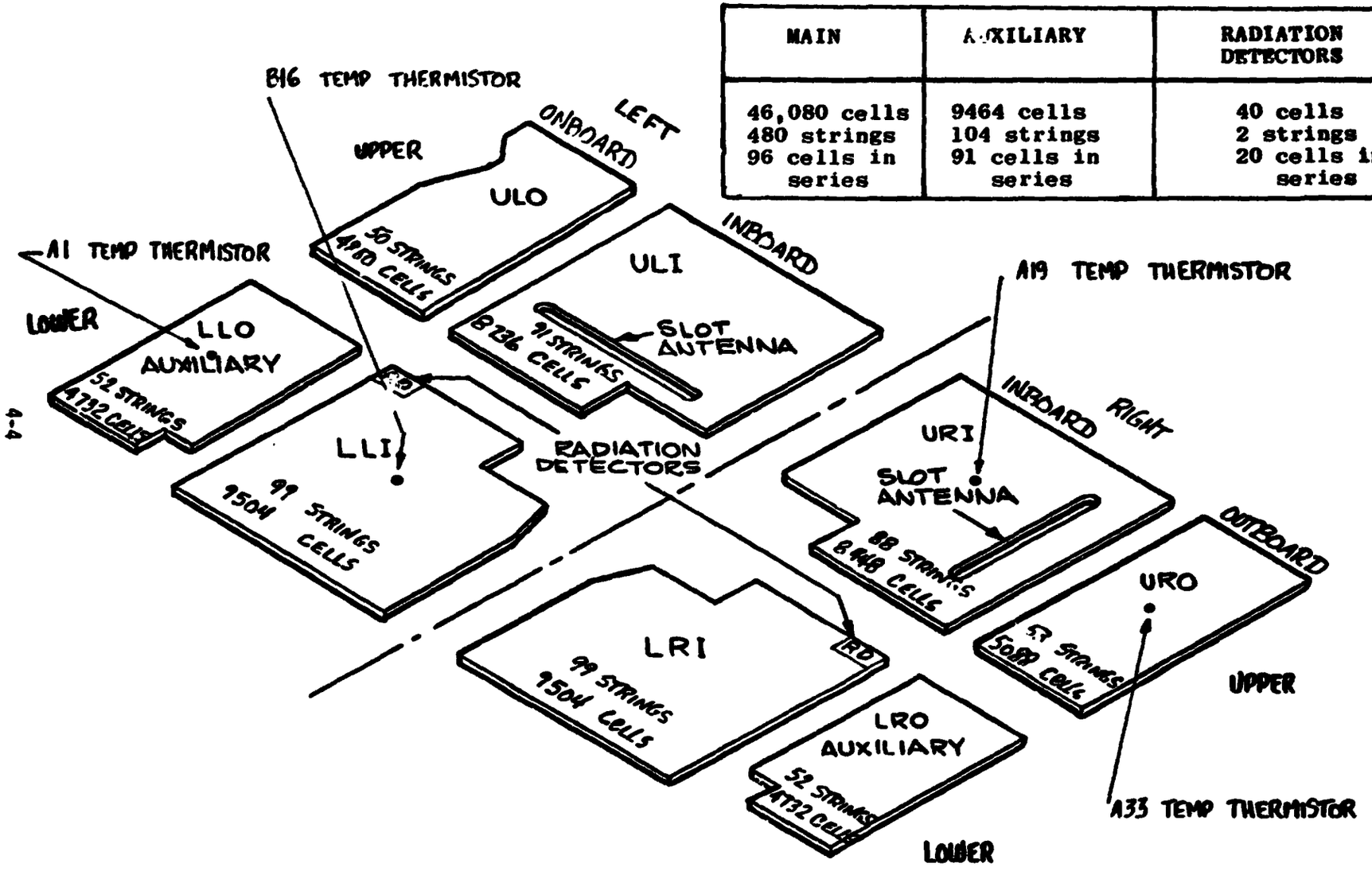

Figure 4-2. OAU-3 Solar Array Paddle Arrangement.

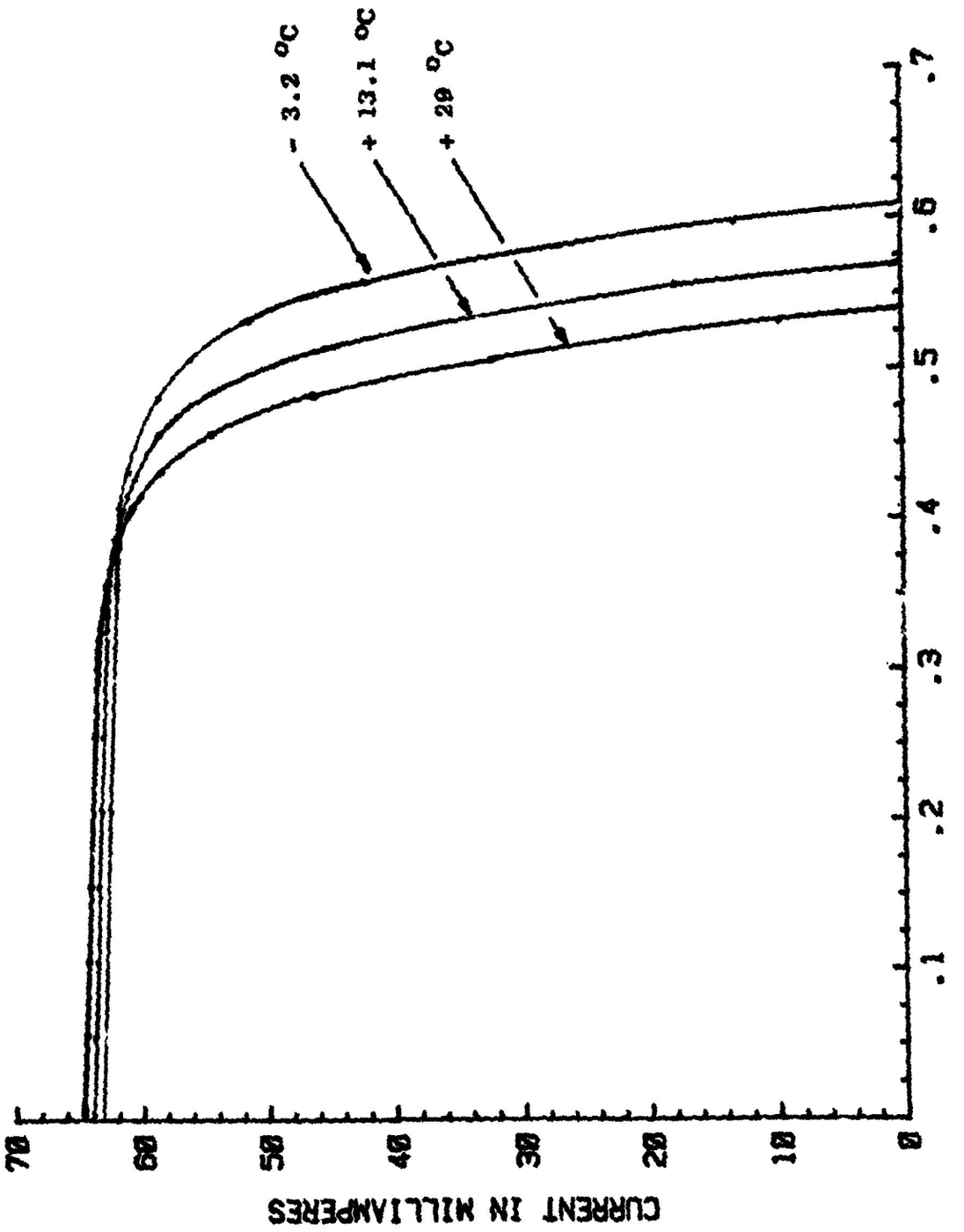

Figure 4-3. DAU-3 Solar Cell Characteristics (BOL).

TABLE 4-1

OAO-C NICKEL-CADMIUM CELL DESIGN FEATURES

CELL MANUFACTURER:	GULTON
CELL CAPACITY:	20AHR NOMINAL
SEPARATOR:	PELLON 2505
ELECTROLYTE:	34% KOH 66 cc

	POSITIVE PLATE	NEGATIVE PLATE
NUMBER	9.0	10.0
AREA	0.91 dm^2	0.91 dm^2
THICKNESS	0.0345 in.	0.0309 in.
POROSITY	46.7%	66.5%
PLATE LOADING	16.1 gr/dm^2	16.95 gr/dm^2
CAPACITY/AREA	4.12 AH/dm^2	4.20 AH/dm^2
FLOODED CAPACITY	27.7 AH	39.8 AH*

*CAPACITY MEASURED TO -1.0V

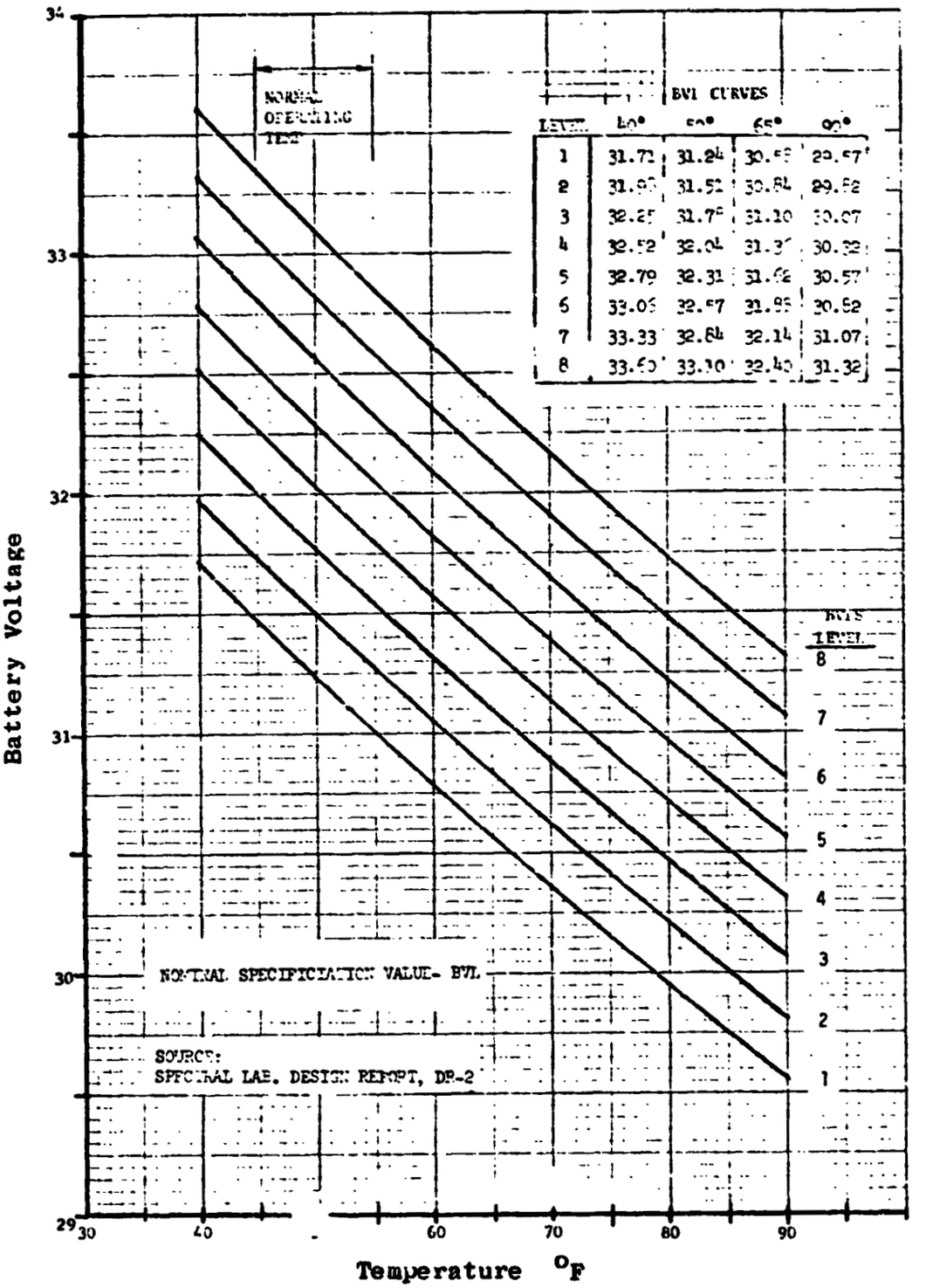

Figure 4-4. Battery Voltage Levels.

current is generated either by the battery voltage limit (BVL) controller to maintain a fixed battery voltage limit, or by the On-Board Processor (OBP) to maximize array power. As the spacecraft enters sunlight, battery charging commences either in the shunt mode where the solar array connects directly to the batteries or in the power boost mode where the PRU is under direct control of the OBP. When the charge bus reaches the voltage limit established by the BVL controller, the charge mode is changed from the shunt or the power boost mode to the regulated mode. The PRU then maintains the bus at the voltage limit. The battery charge current tapers for the remainder of the sunlight period. In the power boost mode, the power boost routine within the OBP allows the solar array to operate at higher power level than is available when the array is clamped to the battery voltage during the initial sunlight period. This increased power level results in higher initial battery charge current and higher charge-to-discharge ampere-hour ratio. Under the direction of this subroutine, the OBP monitors array voltage and current and updates array power every 6 seconds. Based on the power calculation, the OBP through the D/A converter provides a control current to the auxiliary winding of the magnetic amplifier in the PCU. This control current varies in discrete steps to either maintain the array power at 1,000 watts or track the maximum array power if it drops below 1,000 watts. This operation continues until the battery voltage reaches the charger voltage limit. At this point, the OBP releases control to the BVL controller which provides an output signal to the magnetic amplifier to maintain the output of the PRU at the voltage limit for the remainder of the sunlight period (Ref. 3).

Because of the successful performance, extensive life and excellent reliability of the OAO power subsystem, the concept was selected for the Modular Power Subsystem (MPS) for the Multimission Modular Spacecraft (MMS) (Ref. 4). In particular, the OBP power tracking mode was a forerunner to the MPS/MMS Standard Power Regulator Unit (SPRU). However, because of a chip failure in the OBP early in the misison, the power boost worker was removed and the power boost mode had never been energized during the mission. The end of mission power subsystem tests and evaluations provided a unique opportunity to obtain an increased understanding of the operation of maximum power tracking systems in degraded power subsystems. It was anticipated that, because of the commonalities of the OAO power systems, this understanding would be especially useful. In addition, performance analysis and determination of real time degradation of the solar array and batteries were expected to provide useful information relative to existing degradation models and, perhaps lead to improved models.

4.3 OBJECTIVES

The objectives of the end of mission power subsystem tests were:

a. To aquire and analyze engineering data on total real time solar array and battery degradation after more than 8 years in low earth orbit.
b. To use this analysis in determining the validity of empirical models used for predicting array and battery lifetime and,
c. To acquire and analyze the performance data for power subsystem operation in the power boost regulation mode.

4.4 METHODOLOGY

The test procedures used to acquire the necessary engineering data for the solar array, OBP/Power Boost and battery discharge analyses were as follows.

4.4.1 SOLAR ARRAY

Solar array data including temperatures, voltages and currents were collected at 1 or 2 minute intervals for a 10 minute period starting 1 minute after entry into sunlight. For these measurements, the array orientation was normal to the sun line* and the battery voltage level was set for Level 1. This data was analyzed and compared to the earliest available data, collected on the third day of flight during orbit 46.

4.4.2 OBP/POWER BOOST REGULATION MODE

In order to evaluate the Power Boost Regulation Mode, the software subroutine was reloaded into the OBP. The program remained unchanged except that the array power limit was changed from 1,000 watts to 900 or 1,300 watts to accommodate each test phase. The initial check out phase required a spacecraft orientation of Beta 78°, BLV-1, 900 watt power limit and power system data transmitted in real time for the first 12 minutes of sunlight. Since the peak array power was determined to be greater than 900 watts at this Beta angle, the PRU under the direction of the OBP limited it to the software limit of 900 watts.

*The spacecraft Beta angle is the angle between the spacecraft optical axis and the earth-sun line. The solar array paddle angle, the angle between the spacecraft optical axis and the plane of the solar array, is 33.75°. Therefore, the solar array plane is normal to the sun line at approximately Beta 57°.

The final was performed initially with the power subsystem in the shunt mode (without the power boost enabled) at a Beta 90° and BVL-2. Power system data was collected every 2 minutes for one complete orbit. This data established the baseline operating condition with which the power boost operation was compared. Finally, without altering any spacecraft loads or orbit parameters, the power boost routine was enabled and data collected real time. Because real time contacts were limited to approximately 10 minutes each, a number of passes over various ground stations were necessary in order to obtain data for a complete orbit.

4.4.3 BATTERY DISCHARGE CHARACTERISTICS

In order to analyze end of mission battery voltage characteristics, the three 20AH nickel-cadmium batteries were discharged in parallel over two orbits to the lowest allowable bus voltage. This was accomplished by disabling the undervoltage trip and orienting the spacecraft with the array at a high Beta angle to the sun causing the bateries to discharge even during the sunlight period.

Initially, the batteries were fully charged at BVL-2 with a spacecraft orientation of Beta 90°. As the spacecraft entered a designated eclipse period, BVL-4 was commanded while data was collected and stored for later transmission to a ground station. During the following sunlight period, the spacecraft was slewed to Beta 122°. Real time data, which is available when the spacecraft is in contact with ground stations, was used to determine when to terminate the test. After the discharge, the spacecraft was commanded back to Beta 90° and BLV-2. Following a period of 24 hours which was sufficient to fully recharge the batteries, the same procedure was repeated. For this test, Beta angle was 124° and additional loads were added.

4.5 ANALYSIS AND RESULTS

4.5.1 SOLAR ARRAY

The output characteristics of the radiation detector, the auxiliary array and the main array were each analyzed separately to determine solar array degradation. Solar array data collected during orbits 46 (August 24, 1972; third day in orbit 44,058 (December 20, 1980; 8 years and 118 days later) is shown in Tables 4-2 and 4-3.

TABLE 4-2

BEGINNING OF MISSION SOLAR ARRAY CHARACTERISTICS

Orbit 46 B = 58 = 0 BVL = 1 Day 237 T Bat = 50°F

TIME IN ORBIT	SET	UNREG. BUS CURR. (U-59)	CONV. INPUT CURR. (E-57)	TOTAL BUS CURR. (AMPS)	UNREG. BUS BOLT (U-29) (VOLTS)	UNREG. BUS LOAD (WATTS)	ARRAY LLA CURR. (U-05)	ARRAY LRA CURR. (U-18)	TOTAL AUX. ARRAY CURR. (AMPS)	RAD. DET. LRI (U-31)	RAD. DET. LLI (E-44)	AVG. RAD. DET. VOLT
L+0 min.	6137											
L+1 min.	6134	8.22	8.98	17.2	28.18	484.7	3.30	3.31	6.61	4.27	4.19	4.2
L+2 min.	6147	8.14	8.82	17.0	28.58	485.9	3.32	3.33	6.65	4.27	4.19	4.2
L+3 min.	6153	8.06	8.82	16.9	29.04	490.8	3.34	3.35	6.69	4.27	4.31	4.2
L+4 min.	6157	8.06	8.82	16.9	28.97	489.6	3.40	3.39	6.79	4.31	4.25	4.2
L+5 min.	6163	8.13	8.74	17.1	29.11	497.8	3.42	3.41	6.83	4.33	4.29	4.3
L+6 min.	6167	7.98	8.74	16.7	29.50	492.7	3.44	3.45	6.89	4.37	4.31	4.3
L+7 min.	6173	8.14	8.66	16.8	29.17	490.1	3.46	3.46	6.92	4.37	4.33	4.3
L+8 min.	6177	7.98	8.66	16.8	29.50	489.7	3.48	3.49	6.97	4.39	4.35	4.3
L+9 min.	6203	8.31	8.58	16.9	29.90	505.3	3.47	3.47	6.93	4.39	4.35	4.3
L+10 min.	6207	7.90	8.58	16.5	29.90	493.4	3.46	3.46	6.92	4.37	4.35	4.3
AVG OF 10					29.16	492.0	3.41	3.41	6.82	4.33	4.28	4.3

TABLE 4-2

BEGINNING OF MISSION SOLAR ARRAY CHARACTERISTICS (Continued)

Orbit 46 B = 58 ? = 0 BVL = 1 Day 237 T Bat = 50°F

TIME IN ORBIT	SET	VOLTS (D-30)	ARRAY UL CURR. (E-13)	ARRAY UR CURR. (E-39)	ARRAY LLI CURR. (E-26)	ARRAY LRI CURR. (E-52)	TOTAL MAIN CURR. (AMPS)	ARRAY TEMPERATURES (°F) LLI (B-16)	URI (A-19)	LLO (A-1)	URO (A-33)	AVG. ARRAY TEMP. (°F)
L+0 min.	6137											
L+1 min.	6143	29.37	9.26	9.19	6.26	6.27	30.98	-40.4	-26.7	-42.8	-30.2	-35.0
L+2 min.	6147	30.10	9.44	9.25	6.30	6.31	31.30	-28.4	- 6.8	-20.6	- 6.8	-15.7
L+3 min.	6153	30.10	9.57	9.31	6.38	6.35	31.61	-20.6	).3	- 5.9	10.9	- 1.6
L+4 min.	6157	30.10	9.57	9.43	6.42	6.43	31.85	- 8.8	23.2	6.9	27.8	12.3
L+5 min.	6163	30.58	9.69	9.49	6.50	6.47	32.15	0.4	37.3	20.9	44.9	25.9
L+6 min.	6167	30.58	9.81	9.61	6.54	6.55	32.51	7.7	48.2	33.0	58.3	36.8
L+7 min.	6173	30.58	9.87	9.67	6.54	6.55	32.63	16.3	58.3	44.2	69.2	47.0
L+8 min.	6177	31.05	9.81	9.67	6.58	6.59	32.65	26.3	66.6	54.6	79.8	56.8
L+9 min.	6203	31.06	9.87	9.67	6.62	6.59	32.75	34.4	74.7	62.8	88.5	65.1
L+10 min.	6207	31.30	9.81	9.61	6.58	6.55	32.55	42.2	80.6	68.6	95.4	71.7
AVG OF 10		30.48	9.67	9.49	6.47	6.47	32.10					26.3

TABLE 4-3

END OF MISSION SOLAR ARRAY CHARACTERISTICS

Orbit 44058 B = 57° = 0 BVL = 1 %Sun = 65% Day 355 T Bat = 49°F

TIME IN ORBIT	SET	UNREG. BUS CURR. (0-59)	CONV. INPUT CURR. (E-57)	TOTAL BUS CURR. (AMPS)	UNREG. BUS VOLT (D-29)	UNREG. BUS LOAD (WATTS)	ARRAY LLA CURR. (0-05)	ARRAY LRA CURR. (0-18)	TOTAL AUX. ARRAY CURR. (AMPS)	RAD. DET. LRI (0-31)	RAD. DET. LLI (E-44)	AVG. RAD. DET. VOLTS
L+1 min.	2454	7.74	8.90	16.64	28.38	472.2	3.13	2.64	5.77	4.01	3.81	3.91
L+3 min.	2464	7.66	8.82	16.48	28.51	469.8	3.19	2.66	5.85	4.09	3.89	3.99
L+5 min.	2474	7.66	8.74	16.40	28.64	469.7	3.28	2.70	5.98	4.17	3.97	4.07
L+7 min.	2504	7.58	9.06	16.64	29.24	486.5	3.30	2.72	6.02	4.23	4.05	4.14
L+9 min.	2514	6.14	8.98	15.12	29.30	443.0	3.32	2.70	6.02	4.23	4.07	4.15
AVG OF 5					28.81	468.2	3.24	2.68	5.92	4.142	3.95	4.05

TIME IN ORBIT	SET	VOLTS (D-30)	ARRAY UL CURR. (E-13)	ARRAY UR CURR. (E-39)	ARRAY LLI CURR. (E-26)	ARRAY LRI CURR. (E-52)	TOTAL MAIN CURR. (AMPS)	ARRAY TEMPERATURES (°F) LLI (B-16)	URI (A-19)	LLO (A-1)	URO (A-33)	AVG. ARRAY TEMP. (°F)
L+1 min.	2454	29.37	7.93	8.34	5.45	5.58	27.30	-12.0	34.4	-12.0	-----	3.5
L+3 min.	2464	29.37	7.99	8.31	5.33	5.54	27.20	13.2	70.6	20.9	-----	34.9
L+5 min.	2474	30.10	7.99	8.40	5.45	5.54	27.38	38.0	96.3	48.8	-----	61.0
L+7 min.	2504	30.34	7.99	8.52	5.37	5.58	27.46	58.3	115.8	70.6	-----	81.6
L+9 min.	2514	30.34	7.99	8.46	5.29	5.54	27.28	75.4	128.5	87.7	-----	97.2
AVG OF 5		29.90	7.98	8.41	5.38	5.55	27.32					55.6

4.5.1.1 Radiation Detector Degradation

For orbit 44,058, the degradated detectors generated an average of 4.05 volts at an average temperature of 13.1°C. This corresponds to an individual cell current of 59.47ma for the 68.1 ohm load. Applying the solar intensity correction factor of 0.967 for the date of the test, results in a corrected cell current of 57.50ma. For orbit 46, the average detector voltage was 4.31 volts at an average temperature of -3.2°C. The individual cell current in this case was 63.29ma. In order to make comparison of the data on a common basis, this current was adjusted for temperature using a coefficient of 0.050ma/°C. For the temperature difference of 16.3°C, the adjustment is 0.81ma, resulting in a current of 64.1ma. Correction for intensity using a factor of 1.02 for the date of measurement yields a current of 64.38ma. The comparison of corrected data shows a degradation or 7.88ma or 12%.

4.5.1.2 Main Array Degradation

Because the average spacecraft load was 492 watts for orbit 46 and 460 watts for orbit 44,058, an analysis was made to determine if the change in the array operating point was significant enough to require any additional correction. The operating point for the cells of the main array during orbit 46 is the array voltage of 30.48 volts plus a diode drop of 0.8 volts or 31.28 volts. Therefore, the individual cell voltage was 0.326 volts. For orbit 44,058, the main array voltage was 29.90 volts, and including the same diode voltage drop, the individual cell voltage was 0.320 volts. Since the change in the operating voltage of the cells in the main array was only 6mv, any correction would be insignificant in view of the neglibible slope on the short circuit current side of tne I-V curve and the resolution of the telemetry.

For orbit 46, the average main array voltage was 30.48. Including a 0.8 volt diode drop, the individual cell voltage was 0.326 volts. This voltage corresponds to a cell current of 62.33ma. Including the increase of 0.81ma for the temperature increase of 16.3°C, the adjusted current is 63.14ma. Assuming equal contribution from each of the 480 cell strings and applying the solar correction factor of 1.02, the adjusted and corrected main array current for orbit 46 is 30.91 amperes. For orbit 44,058, the degraded array delivered 26.41 amperes. After correction for solar intensity using the factor of 0.967, the current loss is determined to be 4.50 amperes or 14.5%.

4.5.1.3 Auxiliary Array Degradation

The auxiliary array voltage was not measured directly, but was calculated from the unregulated bus voltage and by assuming a diode drop and line losses caused by an estimated 20 milliohm line resistance from the array terminals to the unregulated bus.

Using the above method, the cell voltage was found to be 0.330 volts for orbit 46 and 0.326 volts for orbit 44,058. The operating points are again slightly different, but require no further correction.

For orbit 46, the auxiliary array voltage was 30.09 volts. The individual cell voltage was 0.330 volts with a corresponding cell current of 62.30ma. The cell current adjusted by 0.81ma for the temperature increase is 63.11ma. Assuming equal contribution from each of the 104 cell strings and using the solar intensity correction factor of 1.02, results in an adjusted array current for orbit 46 of 6.69 amperes. For orbit 44,058, the degradated auxiliary array delivered 5.72 amperes, corrected for solar intensity. Therefore, the loss equals 0.97 amperes or 14.5%.

One highlight of the auxiliary array data is the current imbalance of approximately 0.5 amperes between the two auxiliary paddles. This discrepancy was observed and reported during the mission. This imbalance is probably caused by the loss of one cell string on the right auxiliary paddle.

These calculated current losses may now be compared to the theoretical short circuit current losses due to 1MeV electron fluence. Based on the OAO-3 circular orbit of 740km and inclination of 35°, the annual equivalent fluence of 3.55×10^{13} 1-MeV electrons per cm^2 was calculated using reference e. The calculations assumed infinite backshielding and no losses due to coverglass darkening. Figure 4-5 illustrates the normalized short circuit current loss vs. electron fluence for a conventional silicon cell similar to the OAO cell design. The theoretical loss is 14.0% for a total, 8.3 year fluence of 2.95×10^{14} 1-MeV electrons per cm^2. Losses calculated from flight data vary from 12 to 14.5% and are considered in good agreement with the theoretical value. This agreement indicates that almost all of the degradation observed was due to radiation damage.

4.5.2 ON-BOARD PROCESSOR/POWEER BOOST REGULATION

4.5.2.1 Initial Trial

During the first trial of the power boost mode, the power boost routine was energized for only the first 12 minutes of sunlight to verify the operation

ORIGINAL PAGE IS
OF POOR QUALITY

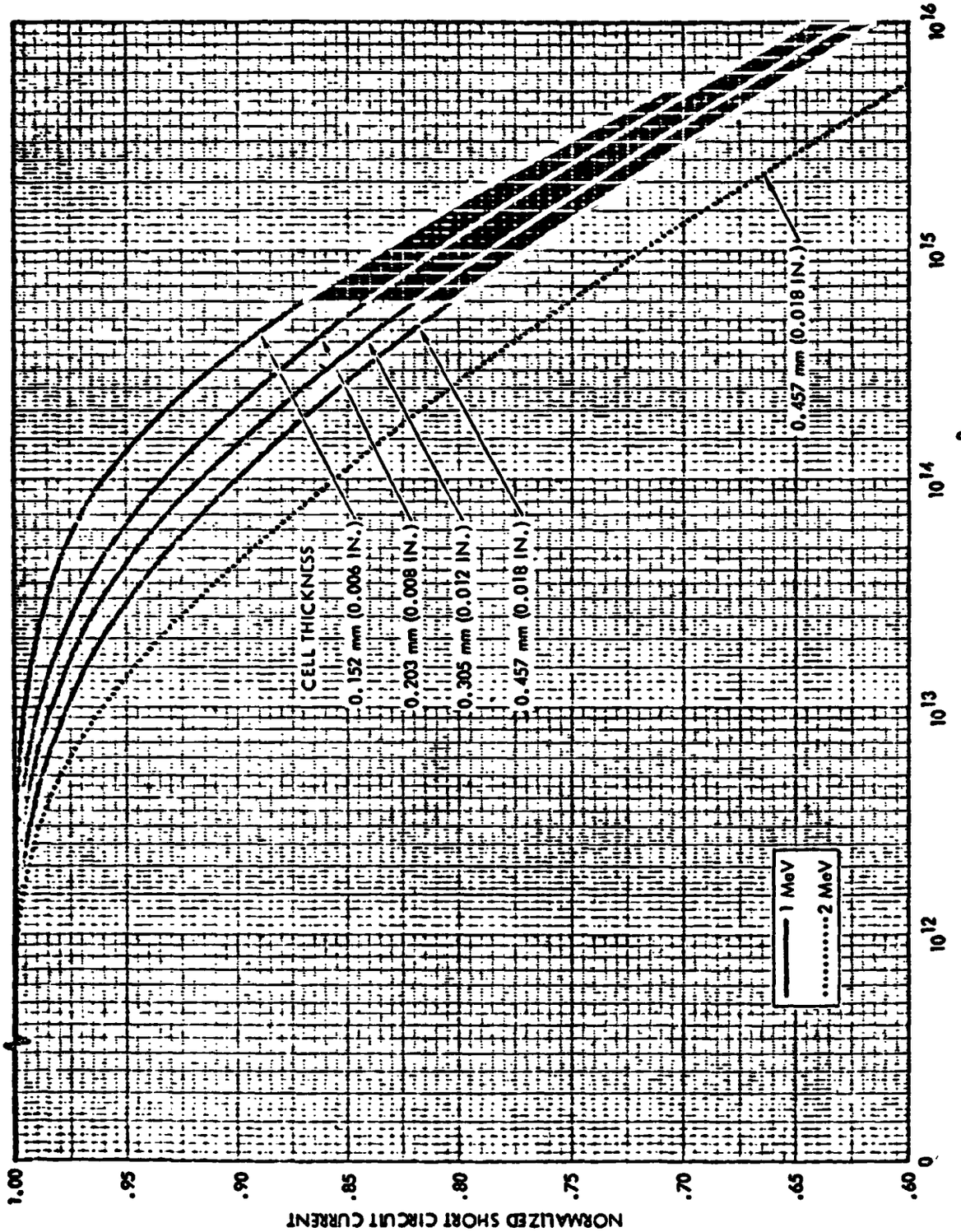

Figure 4-5. Normalized Short Circuit Current vs. 1 MeV Electron Fluence for 2 Ohm-cm n/p Conventional Silicon Cells. (At 135.3 mW/cm^2 AMO Illumination, 30°C)

of the worker and power subsystem components. Figure 4-6 illustrates the array power which the OBP calculates every 6 seconds prior to shifting the duty cycle of the PRU to maintain array power at 900 watts. Figure 4-7 shows the measured array voltage during the same period.

For the first 3 minutes, the array operating point varies as much as 250 watts above and below the software limit and gradually drops off due to the loss of array power with increasing temperature. The slope of array power vs. time is an indication of the rate at which the array power curve shifts due to array heating. Three minutes into sunlight, the calculated array power falls below 900 watts causing the OBP to alter the array operating point above 900 watts. This condition occurs again after 6 minutes into sunrise. OBP control is terminated after 9 minutes when the battery voltage reaches the battery voltage limit.

4.5.2.2 Final Evaluation

The final test required collecting power system data for one complete orbit prior to and after enabling the power boost worker. Figures 4-8 through 4-11 represent array and battery data during one complete orbit starting with the eclipse period for both the baseline condition (Figures 4-8 and 4-9) with the power system in the shunt mode (PRU by-pass relay closed) and in the power boost mode (Figures 4-10 and 4-11) with the OBP in control of the PRU (by-pass relay open). The orbit period is approximately 98 minutes long with 35 minutes eclipse and 63 minutes sunlight. In the shunt mode, array power is limited because the array voltage is clamped to the battery voltage. Individual battery currents remain withon 0.1 amperes of each other throughout the orbit. During the initial sunlight period, battery charge currents are limited to approximately 4 amperes. After 34 minutes in sunlight, the battery voltage reaches the voltage limit and triggers the BLV controller to adjust the PRU to maintain the battery voltage level. The average end of light (EOL) battery current is approximately 0.83 amperes. The battery charge-to-discharge ampere hour ratio (C/D) is 1.02. The end of light battery temperature is approximately 7.9°C.

With the power boost enabled and the OBP array limit set to 1,300 watts, the OBP will automatically attempt to adjust the PRU to track the maximum array power. The initial battery charge currents are approximately 6 amperes. After 21 minutes of sunlight, the OBP releases control to the BLV controller as the battery charge currents taper to an average of 0.7 amperes. The battery recharge ratio (C/d) is approximately 1.05 and the end of light battery temperature is 8.7°C.

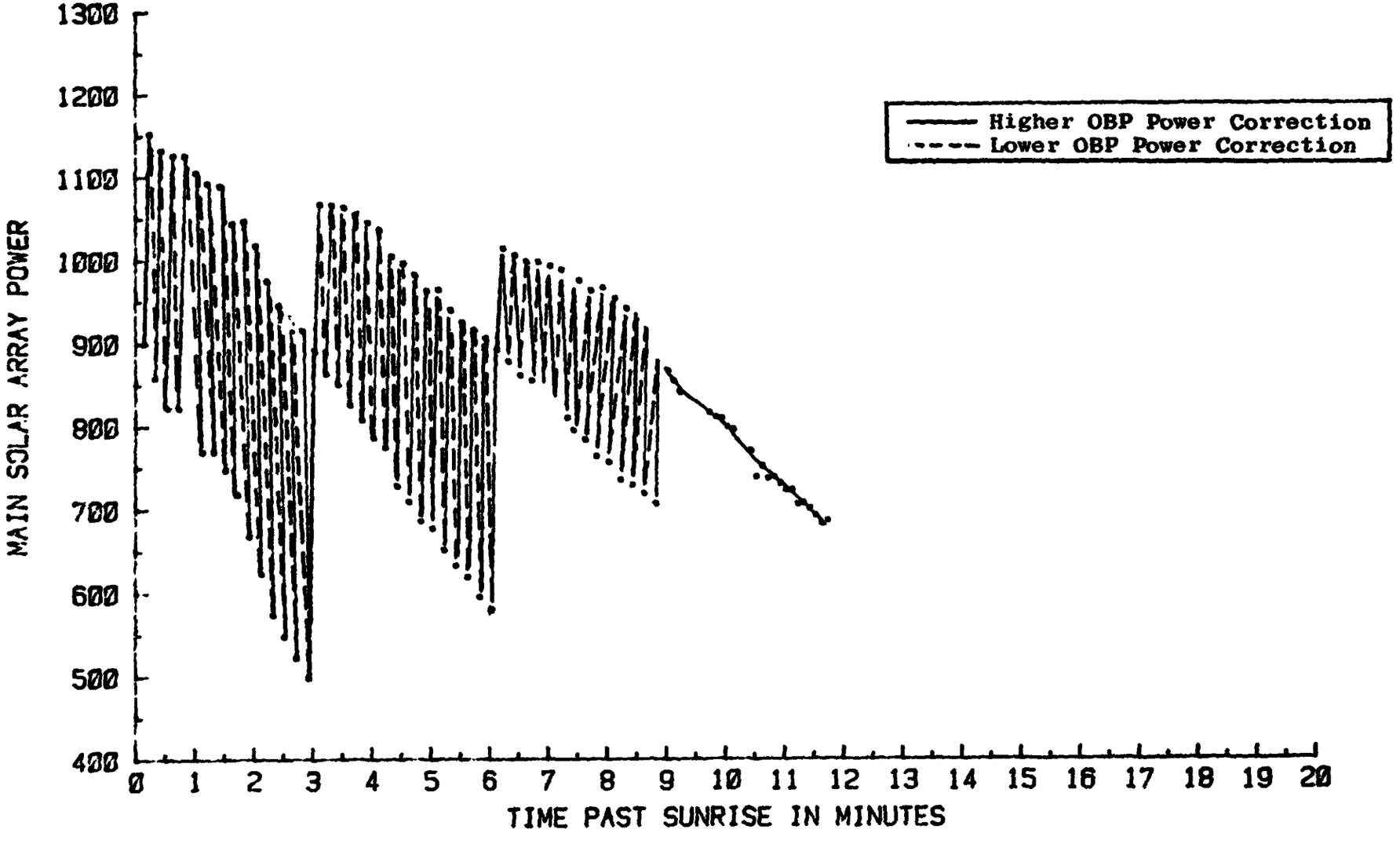

Figure 4-6. OBP Power Boost Evaluation 900 Watt Power Limit Beta 78.

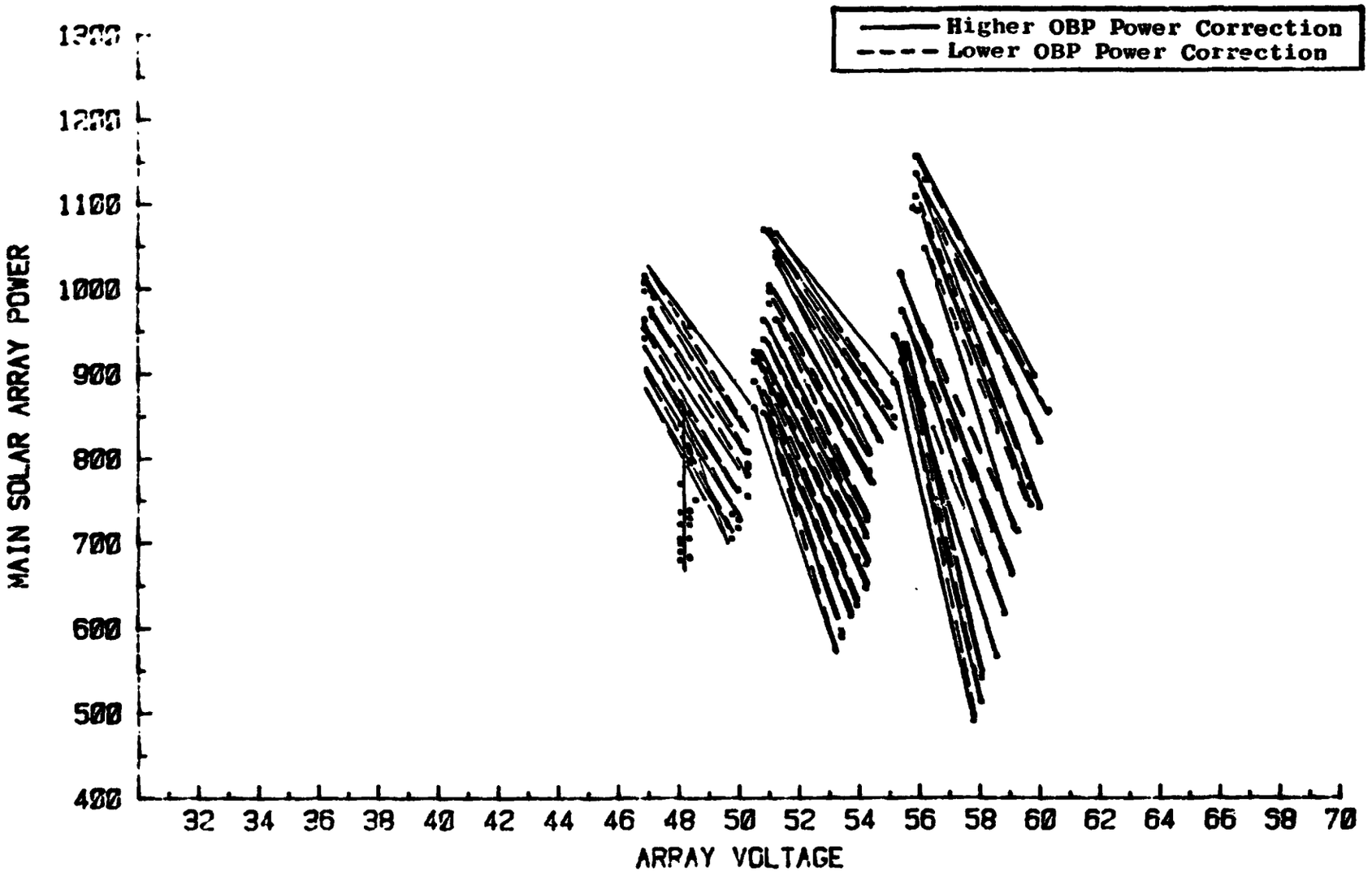

Figure 4-7. OBP Power Boost Evaluation 900 Watts Power Limit Beta 78.

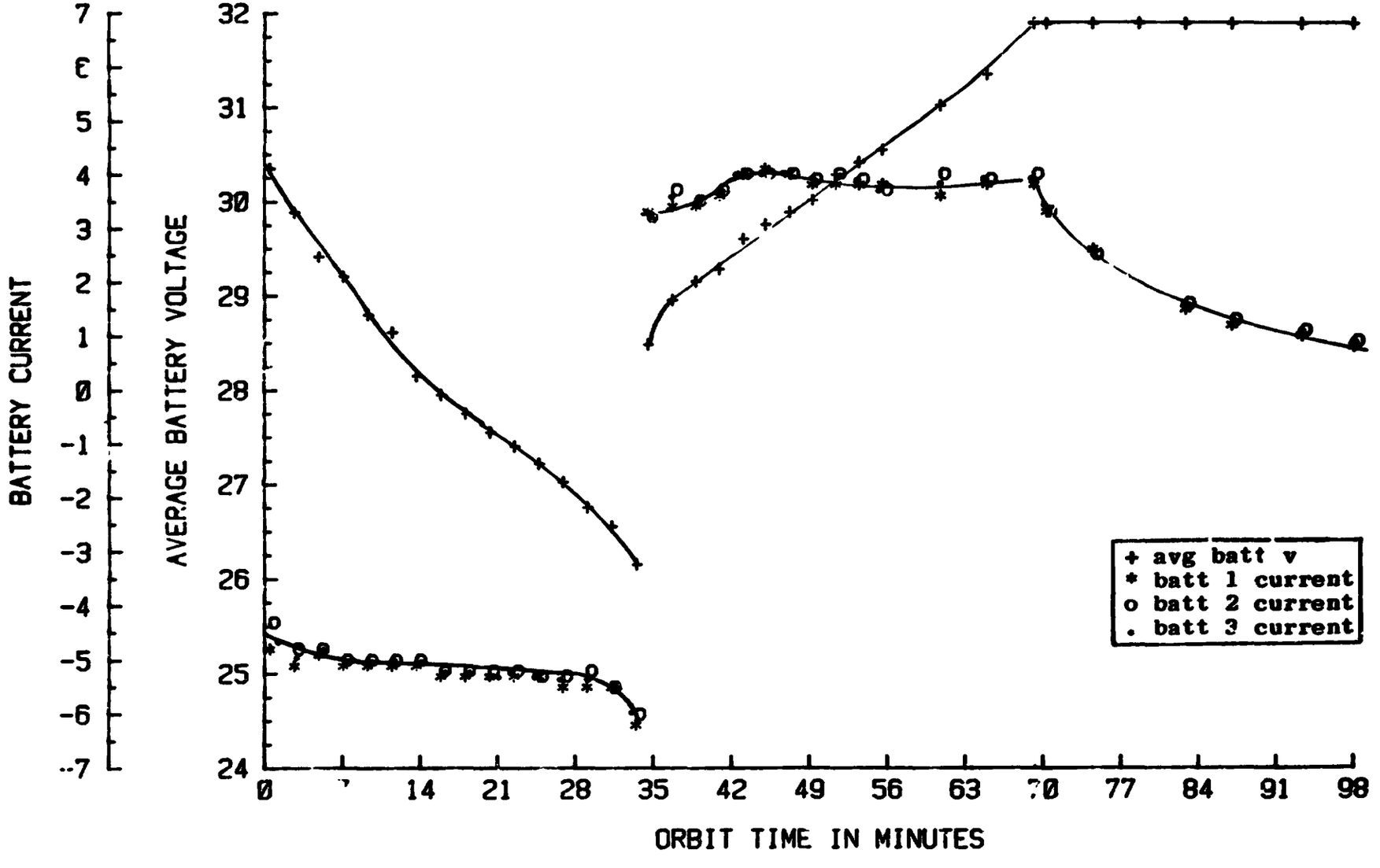

Figure 4-8. OBP Power Boost Evaluation Shunt Regulation Mode Beta 90.

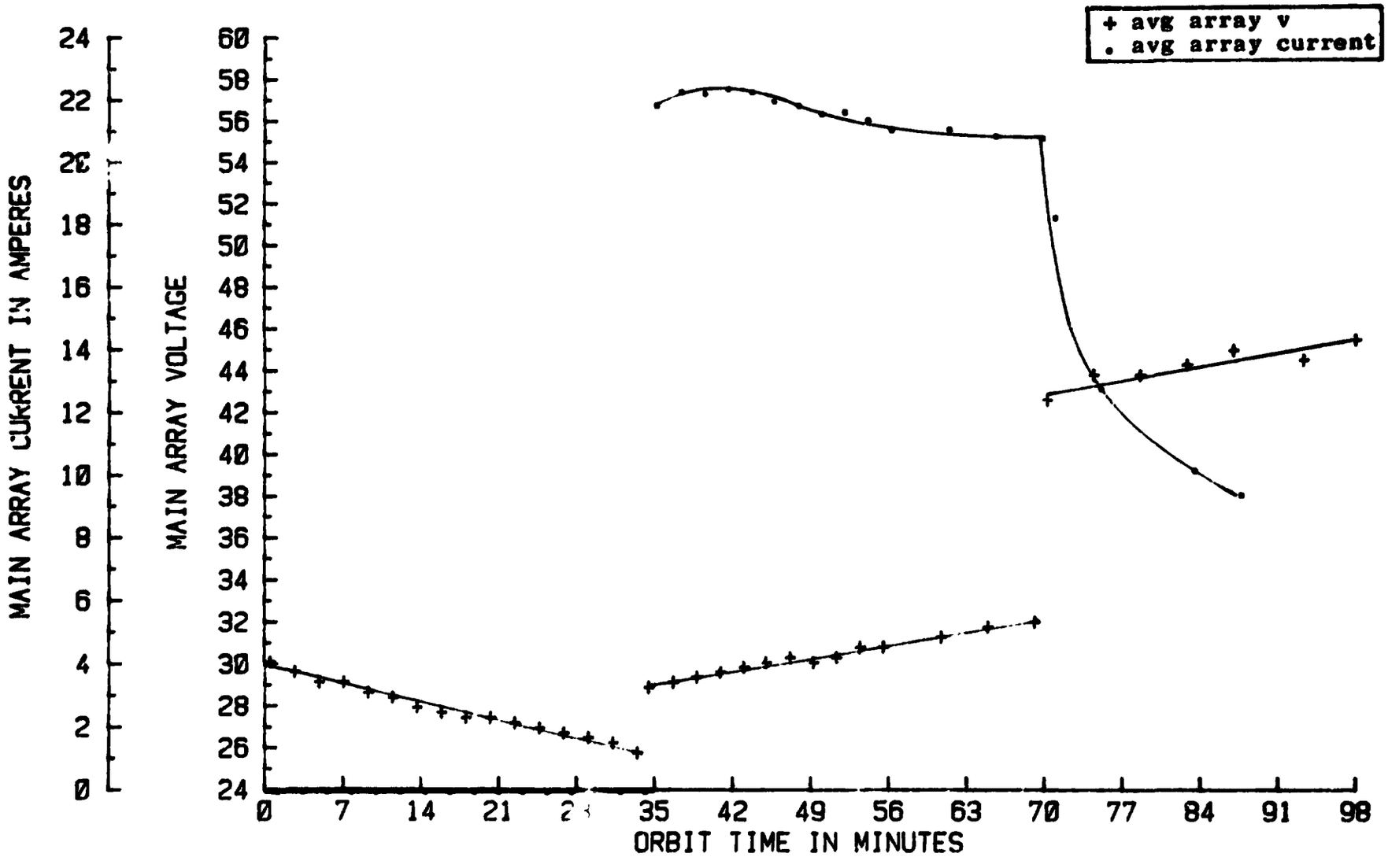

Figure 4-9. OBP Power Boost Evaluation Shunt Regulation Mode Beta 90.

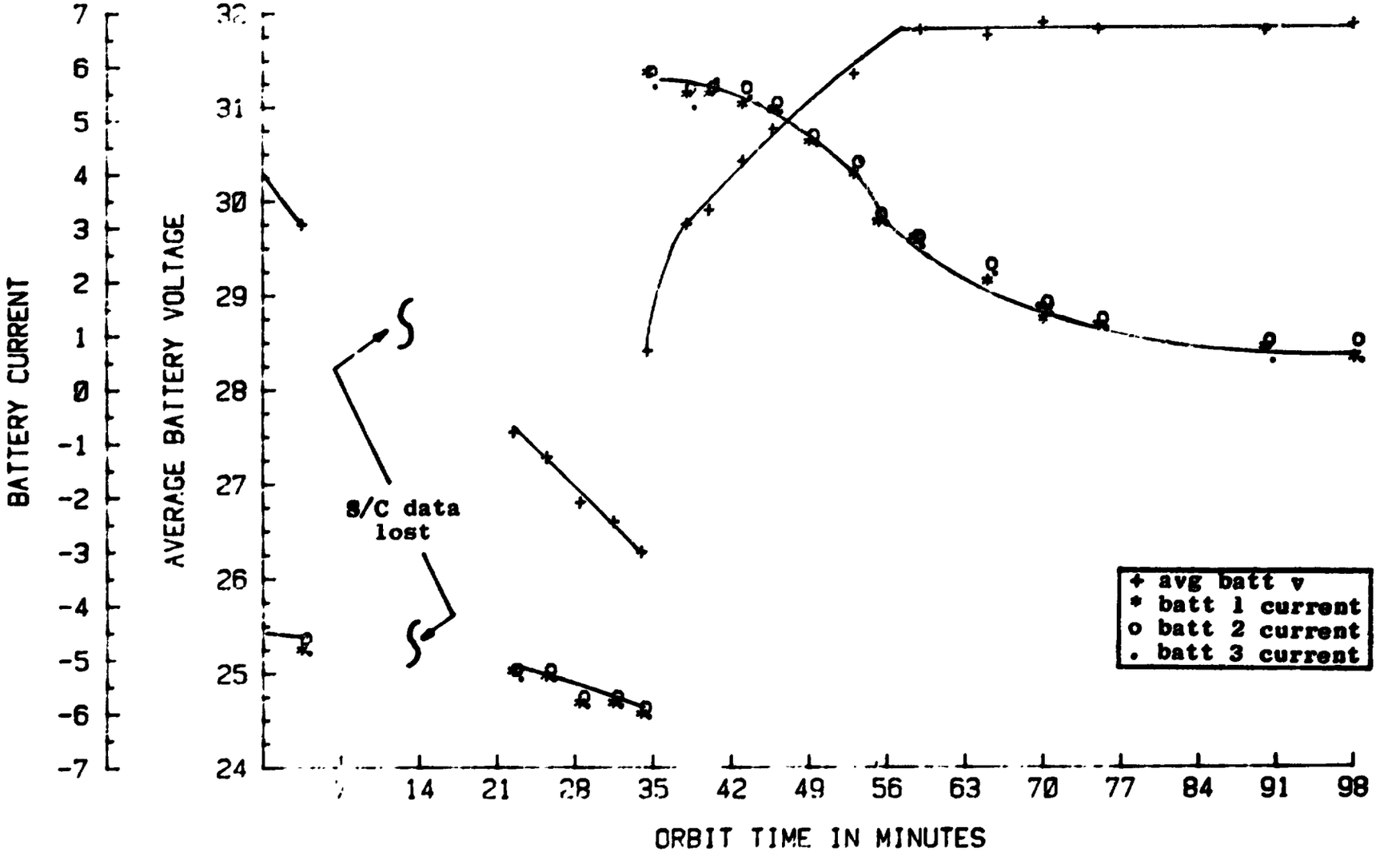

Figure 4-10. OBP Power Boost Evaluation Maximum Power Tracker Beta 90.

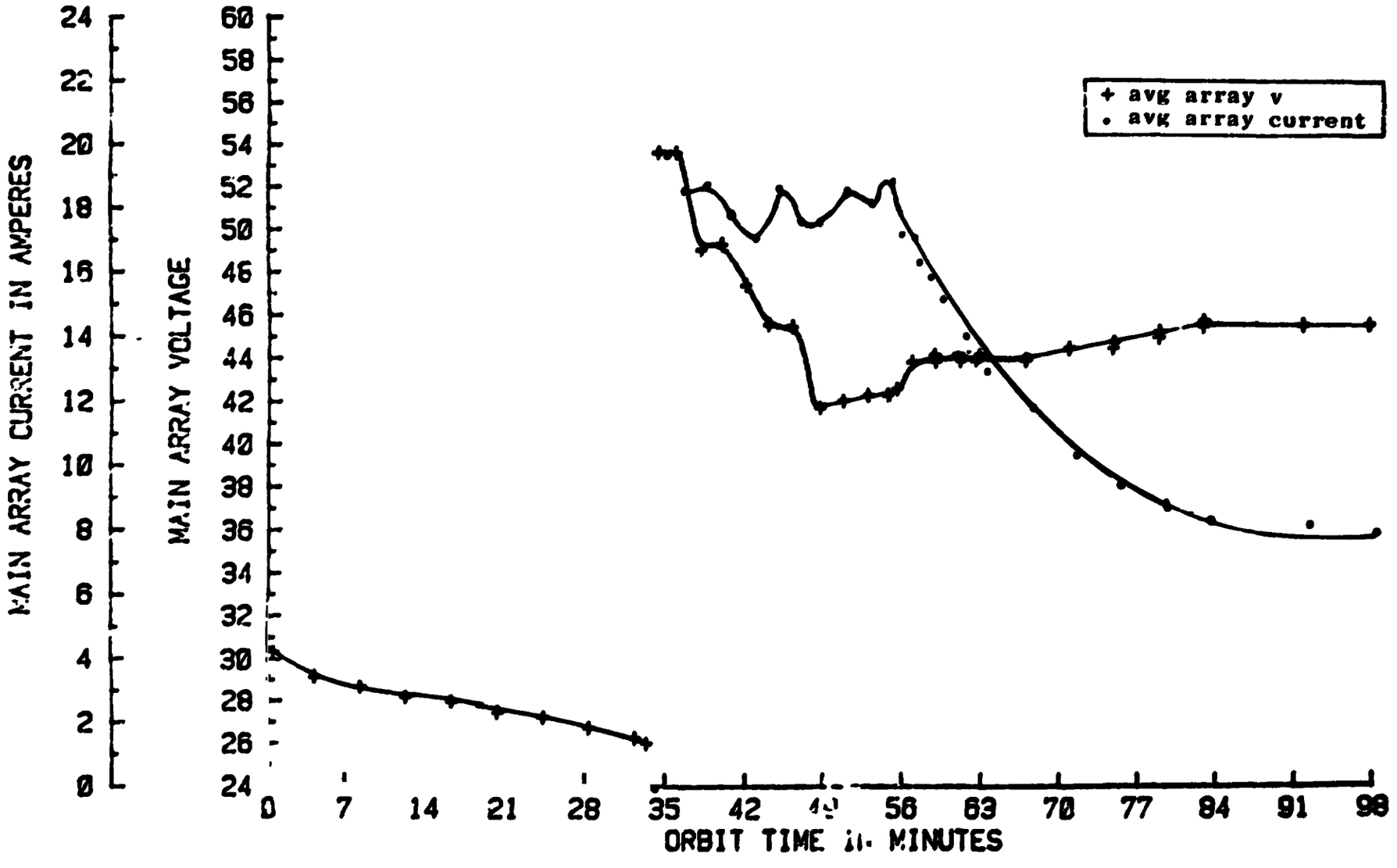

Figure 4-11. OBP Power Boost Evaluation Maximum Power Tracker Beta 90.

There are significant differences in the operation of the power subsystem between the shunt mode and the OBP array power tracking mode. Because the PRU regulates to the maximum array power point when power boost is enabled, more array power is available to recharge the battery resulting in higher initial battery charge current. With this, the battery voltage reaches the BVL in less time than in the shunt mode, resulting in higher percent recharge and temperature. Figure 4-12 shows array power vs. time since sunrise for both the shunt mode and the power boost mode. The array power shown for the power boost trial represents maximum and minimum excursions around the peak power point to which the OBP has adjusted the PRU. The additional array power available in the power tracking mode is the difference between the array power in the shunt mode and the power boost mode.

Table 4-4 summarizes the final OBP power boost evaluation compared to the pre-flight performance determined during acceptance thermal vacuum testing (ATV). While a direct comparison between pre-flight and end of mission performance is difficult, the higher initial and average battery charge current and greater percent recharge using the power boost mode indicates succesful array power tracking by the OBP/PRU.

4.5.3 BATTERY DISCHARGE CHARACTERISTICS

Prior to conducting the end of mission battery discharge tests, Princeton scientists requested a spacecraft orientation which oriented the main telescope toward the sun for the purpose of evaporating surface contaminates. During this manuever, the batteries continuously discharged from one eclipse period through the following sunlight period and again through another eclipse prior to regaining a more favorable attitude. It was determined that battery capacity was approximately 9 ampere hours down to the bus voltage between 21 and 22 volts prior to terminating the test. Following this discharge, the batteries were allowed to recharge for several days prior to performing the end of mission battery discharge tests.

The battery discharge tests were performed as described earlier. Data was collected continuously and are shown in Figure 4-13 for the first test and in Figure 4-14 for the second test.

The individual battery voltages were within less than 5mv of each other while battery currents varied only 0.2 amperes between batteries during the entire discharge test. The results of both tests suggest a voltage plateau at a battery voltage of 22.75 volts or approximately 1.034 volts per cell.

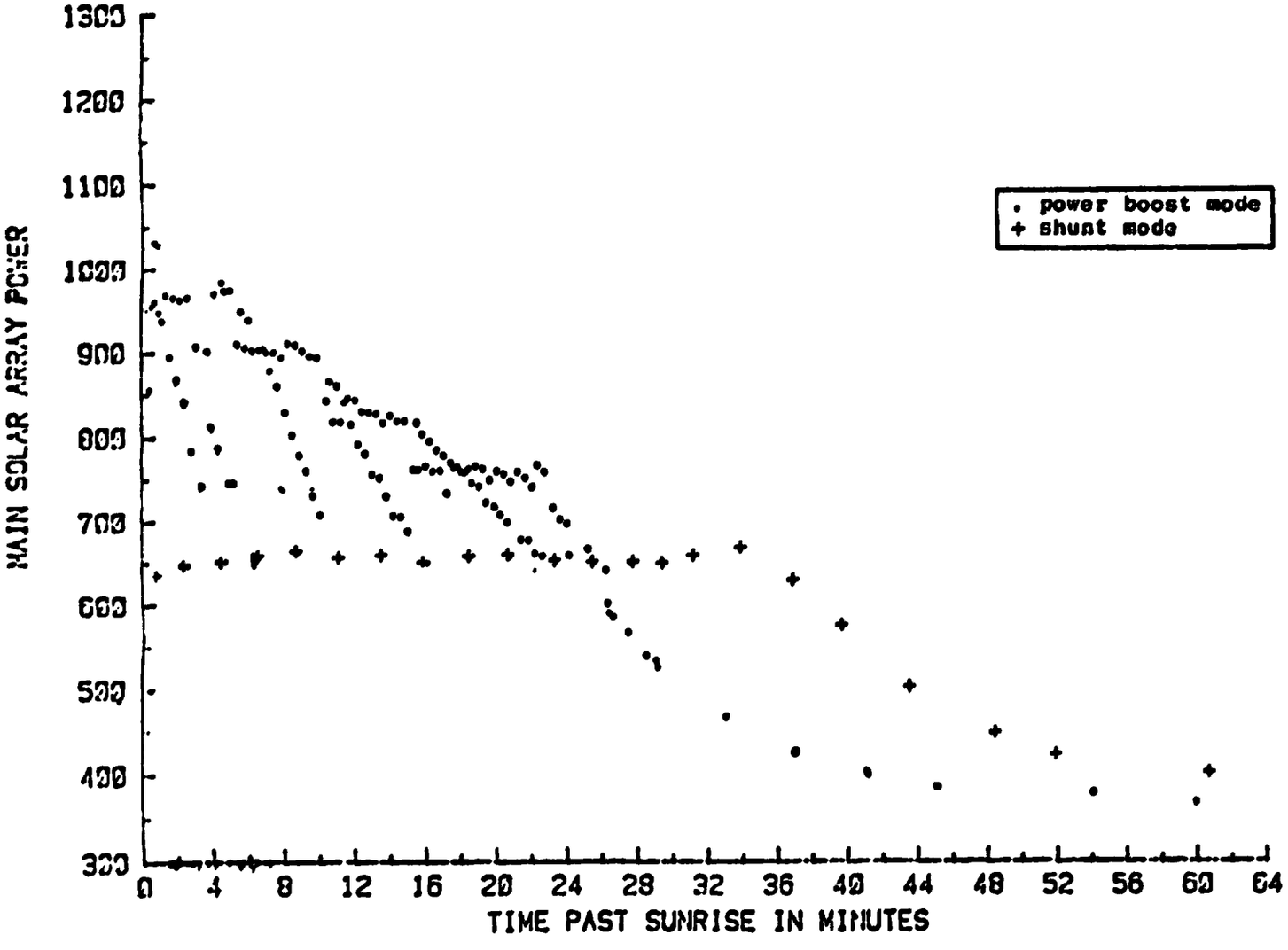

Figure 4-12. Shunt Regulation vs. Power Boost Mode Beta 90.

TABLE 4-4

OBP POWER BOOST EVALUATION SUMMARY

PARAMETER	PRE-FLIGHT MEASUREMENTS WITHOUT POWER BOOST	PRE-FLIGHT MEASUREMENTS WITH POWER BOOST	END OF MISSION TEST DATA WITHOUT POWER BOOST	END OF MISSION TEST DATA WITH POWER BOOST
ORBIT(S)	ATV	ATV	44,703	44,744 to 44,756
BETA	15	15	90	90
BLVS	4	4	2	2
DISCHARGE AH	3.85AH	3.85AH	3.3AH	3.3AH
BATTERY EOD* VOLTAGE	27.25V	27.35V	26.15V	26.28V
BATTERY EOL** CURRENT	2.0 AMP	0.9 AMP	0.83 AMP	0.66 AMP
BATTERY EOL TEMP.	9.2°C	10.2°C	7.9°C	8.7°C
PERCENT RECHARGE	103%	105%	102%	105%
BATTERY SOL*** CURRENT	4.3 AMP	6.2 AMP	3.2 AMP	6.0 AMP
BATTERY CURRENT PRIOR TO BVLS	4.0 AMP	4.5 AMP	3.9 AMP	4.2 AMP
AVERAGE BATTERY CURRENT FROM SOL TO BVLS	4.2 AMP	5.0 AMP	3.8 AMP	4.8 AMP

*END OF DISCHARGE
**END OF LIGHT
***START OF LIGHT

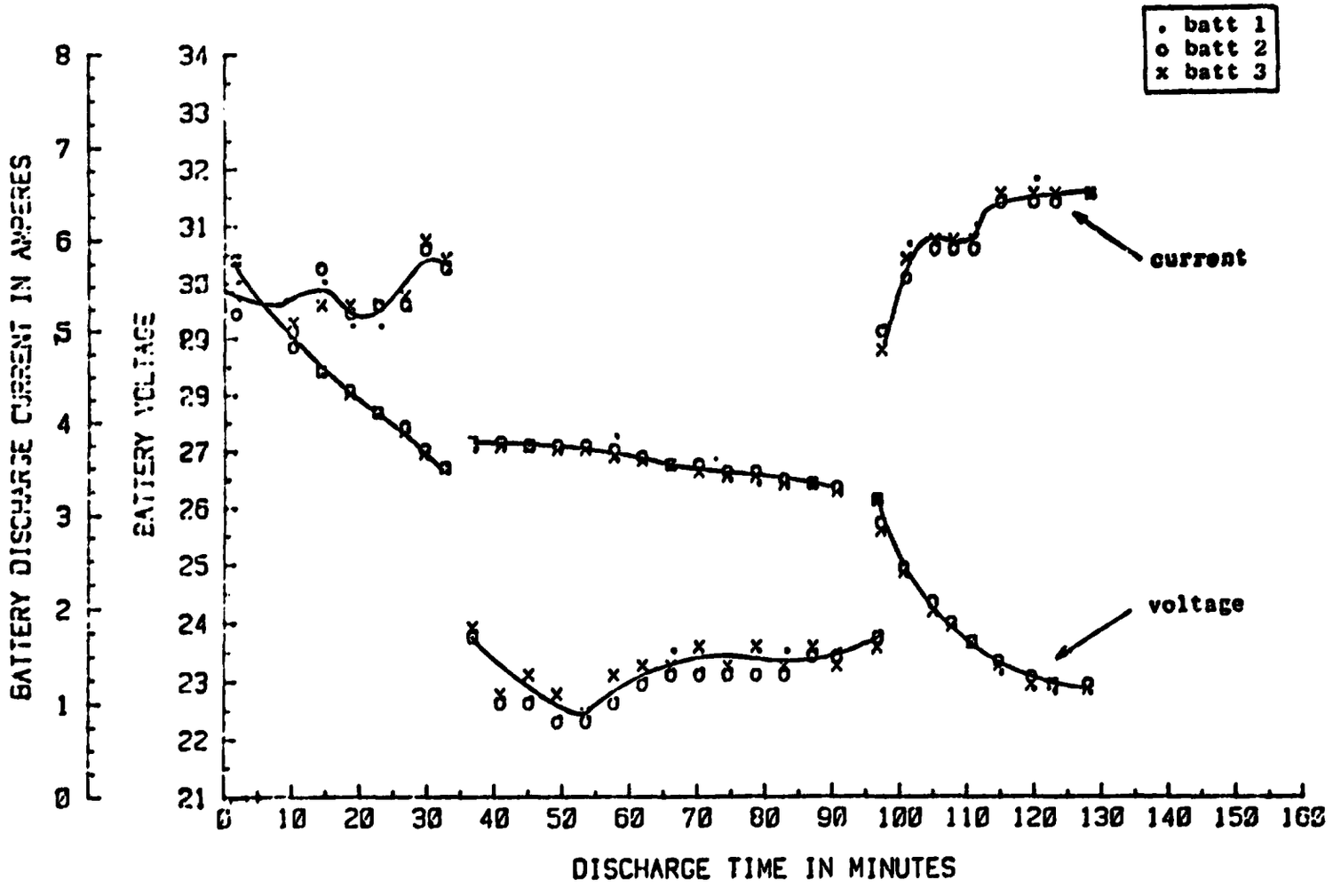

Figure 4-13. OAO-3 Battery Capacity Discharge Test 1.

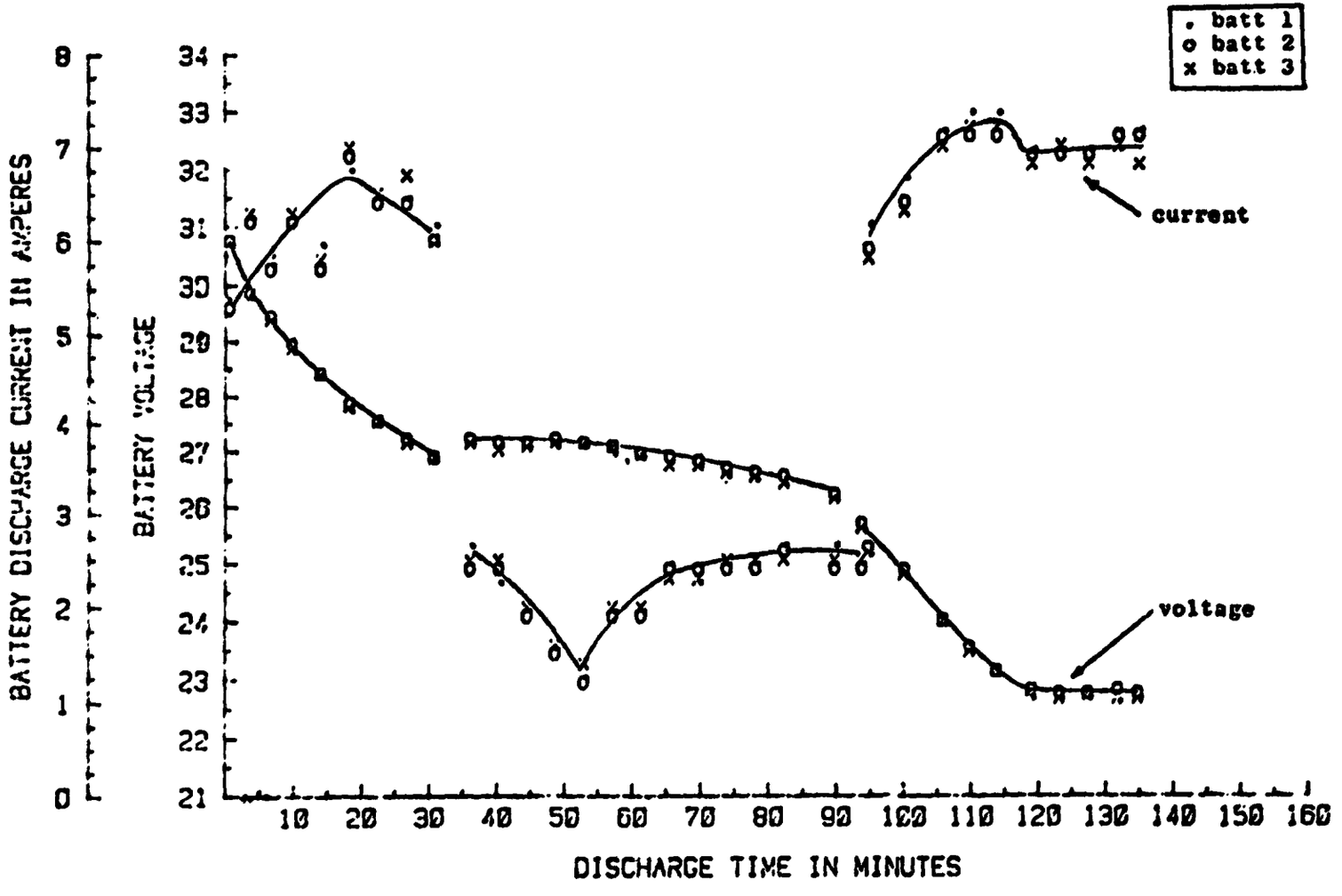

Figure 4-14. OAO-3 Battery Capacity Discharge Test 2.

Battery cells from the OAO-3 flight lot were evaluated and life cycled by the Quality Evaluation and Engineering Laboratory at Crane, Indiana. The results and analyses of the initial evaluation and life cycling testing appear reference f and g, respectively.

Figure 4-15 compares the two battery discharge tests with the life cycle data from the Crane. Pack 4C was cycled at 15% DOD and 10°C in a simulated low earth orbit regime and completed over 33,000 cycles without cell failure prior to discontinuing the test. The discharge capacity data is shown for cell S/N 559 at several times during the life cycle test. The pre-cycling capacity was approximately 27 ampere-hours to a cell voltage of 1.00 volts. As a result of cell aging, the discharge voltage characteristics change significantly as seen by later capacity discharges. Of major importance is the existence of the second voltage plateau apparent during the capacity measurement on cycle 33,298 which is similar to that observed during the OAO-3 discharge tests. The average battery capacity measured for the first test was 7.3 ampere-hours to 1.04 volts per cell and 10.0 ampere-hours to 1.03 volts per cell for the second discharge test.

4.6 CONCLUSIONS AND RECOMMENDATIONS

The end of mission power subsystem engineering analysis provided significant information degraded power subsystem components. Specific conclusions are listed below.

4.6.1 SOLAR ARRAY

a. Measured current degradation are as follows:
   (1) Radiation detector, 12%
   (2) Main array, 14.5%
   (3) Auxiliary array, 14.5%
b. Measured current degradations are in good agreement with theoretical losses.
c. Observed degradations are almost entirely due to radiation damage.

4.6.2 OBP/POWER BOOST REGULATION

a. Maximum array power trackers provide increased system utilization by providing:
   (1) Additional array power supplies more energy to recharge the battery or for increased load capability.
   (2) Increased flexibility in science data collection.

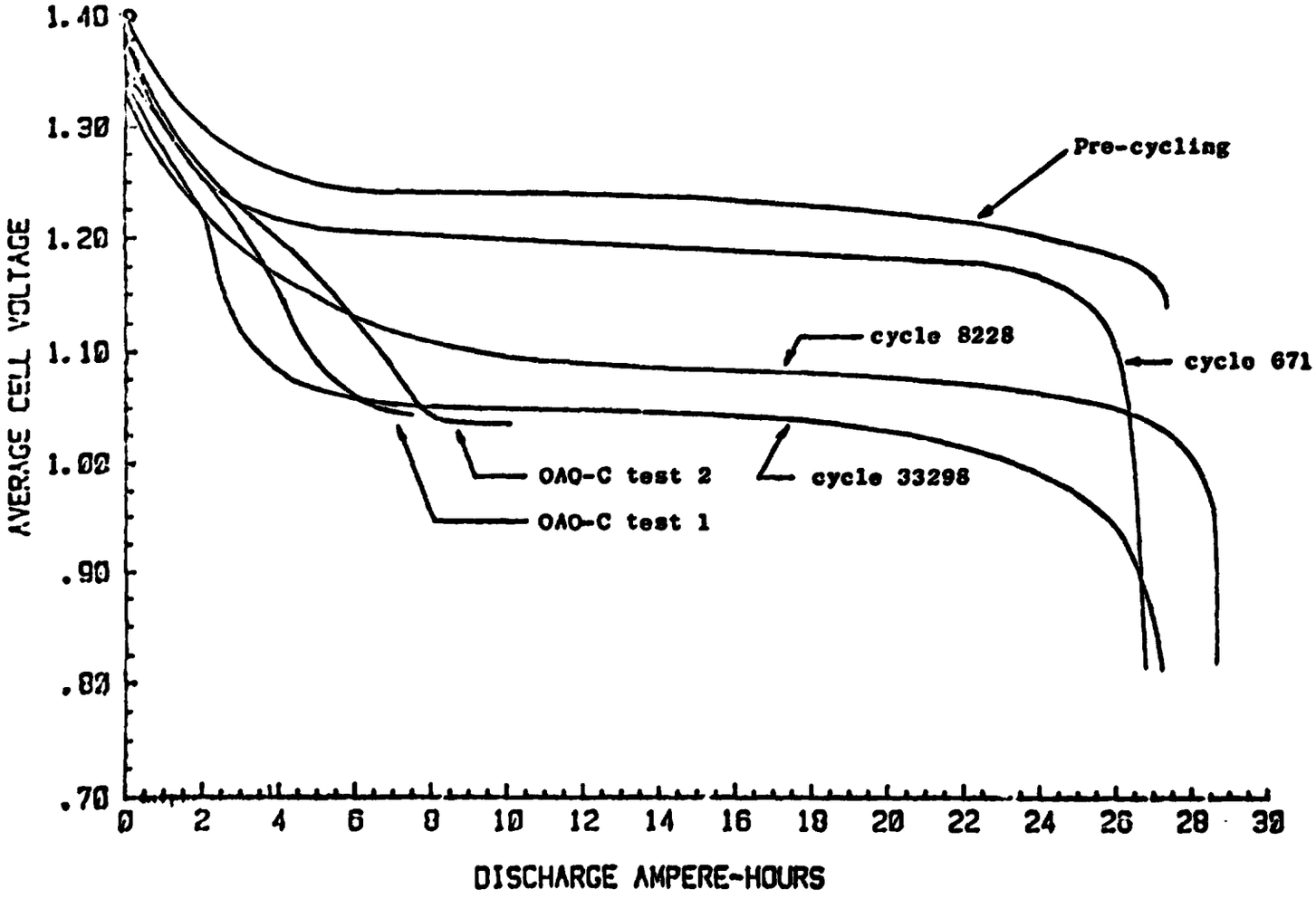

Figure 4-15. OAO-3 Battery and Crane Discharge Comparisons Pack 4c Cell S/N 559 15% DOD 10°C.

b. Operation of nickel-cadmium batteries in parallel through a single charger was demonstrated.

4.6.3 BATTERY DISCHARGE CHARACTERISTICS

a. Confirmed existence of second voltage plateau at approximately 1.03 volts per cell.

b. Degraded voltage characteristics are in close agreement with life cycle simulations.

c. Life cycle simulations form an accurate data base for mathematical modeling of cell lifetime.

d. Limited pre-flight testing of flight batteries during spacecraft integration contributed to trouble-free battery performance.

REFERENCES

1. "Characteristics and Limitations of MPS/MMS Battery Charging System," F. Ford, C. Palandati, J. Davis, C. M. Tasevoli, November 1980, TM 81983.

2. "OAO Functional Operations Manual, Power Subsystem," Document Number FO-G 0127-C, Vol. B, August 1972.

3. "OAO Functional Operations Manual, On-Board Processor (OBP), Document Number FO-G-0127-C, Vol. F, August 1972.

4. "Low Cost Modular Spacecraft," NASA/GSFC, X-700-75-140, May 1975.

5. "Solar Cell Radiation Handbook," H. Tada and J. Carter, TRW Systems Group, Rendondo Beach, California, November 1, 1977, NAS-7100.

6. "Initial Evaluation Tests, 20AH Nickel-Cadmium Spacecraft Cells," QEEL/C 73-459, December 3, 1973.

7. "Ninth through Fifteenth Annual Report of Life Cycle Test," 1973 through 1979, Quality Evaluation Laboratory, NAD Crane, Indiana.

ACKNOWLEDGEMENTS

The author acknowledges the contributions of Michael Malison, Harry Walsgras, and David Lozinsky of the Grumman Aerospace Corporation for their assistance during the end of mission power subsystem tests; Luther Slifer of the Goddard Space Flight Center for technical support in analyzing the data, and Terry Schmitt and William Anderson of the OAO Corporation for their help in repregramming the OBP.

OAO-3

COMMUNICATIONS AND DATA HANDLING SYSTEM END OF LIFE TESTS

DONALD L. MARGOLIES

TABLE OF CONTENTS

SECTION 5
COMMUNICATIONS AND DATA HANDLING
SYSTEM END OF LIFE TESTS

5.1 SUMMARY

The communication and Data Handling Subsystem (CDHS), with a few exceptions survived the flight of OAO-3 very well. The status of the CDHS was generally monitored throughout the life of the observatory as a normal extension of operations. The purpose of the CDHS tests performed prior to mission termination was to verify that functions which had not been tested previously were still functional.

The results of the testing indicated that:

1. Command Receiver Equipment is working properly.
2. Wideband Transmitter No. 1 is still outputting more than 10 wattsand yielding good quality data even though its center frequency has shifted down below specification limits.
3. Wideband Transmitter No. 2 is performing well, however, it has exhibited a shift of center frequency upward and slightly beyond specification limits.
4. Narrowband Transmitters 1 and 2 are operating very close to prelaunch values.
5. The Spacecraft and Experimenters' Data Handling Equipment were both operating properly with apparently no degradation noted.
6. The Spacecraft Systems Controller Unit exhibited some degradation.

5.2 INTRODUCTION

End of mission tests were performed on elements of the CDHS in order to determine if redundancy still existed and if generally unused operating modes were still functioning. References 1 through 5 define the tests originally proposed.

5.3 COMMAND RECEIVER EQUIPMENT (CRE)

The OAO-C CRE, SN6, was manufactured by AVCO, Inc.; Cincinnatti, Ohio early 1970. It was integrated into the observatory in September 1970 and with one brief period of exception has remained with the observatory ever since.

The tests performed consisted primarily of sending commands and monitoring AGC and combiner input voltages along with selected bilevel data. Interactions between receivers, due to AGC joining and output combining, were observed. The condition of the CRE, at this time, is consistent with that indicated on page 9-142 of the 30 day report prepared by the Grumman Aerospace Corporation (GAC) in February 1973. The report noted that when strong signal levels were present receiver 3 quieted receiver 1 by an unexpectedly large amount. GAC was correct in asserting that this would not have been the case had the zero tone been present between commands. During the extensive preflight calibrations of the CRE, measurements were made under two different sets of conditions.

In the first, a CW signal was impressed, with equal amplitude, on each of the antenna ports and curves of AGC volts vs input level were made. An example of such a curve is shown in Figure 5-1. In the second case, variable attenuators were added in series with each antenna port and a CW signal modulated by a zero tone was injected. By changing the attenuator values a simulation of varying observatory aspect with respect to the ground antenna was created.

AGC voltage vs input level curves were generated for 11 different conditions. A typical curve is shown in Figure 5-2. In the test at hand, an unmodualted CW signal was utilized by the ground station except when actually commanding. It is concluded that the excessive quieting of receiver 1 by receiver 3 under these curcumstances is normal since the receiver exhibits expected performance when properly commanded (Table 5-1). All bilevel telemetry indications were normal and all power sources to the receivers appeared to be working properly.

The GAC 30 day report also stated that "Detector #1 cannot be used as an accurate indication of RF input level if relatively high input levels are present at receiver #3 input." The data at hand suggests that under the circumstances none of the detectors provides an accurate indication except under conditions where the RF signal received at each antenna port was nearly equal. The correction factors provided in the 30 day report do not seem to be adequate. Observed data indicates that the RF level was as high as -50 Dbm or about 15-20 Db higher than the calibration curves suggested and 8-10 Db higher than the best case link analysis value. The reason for this, of course, is that the calibration curve used was taken under a fixed set of conditions and the observatory did not operate under those fixed conditions.

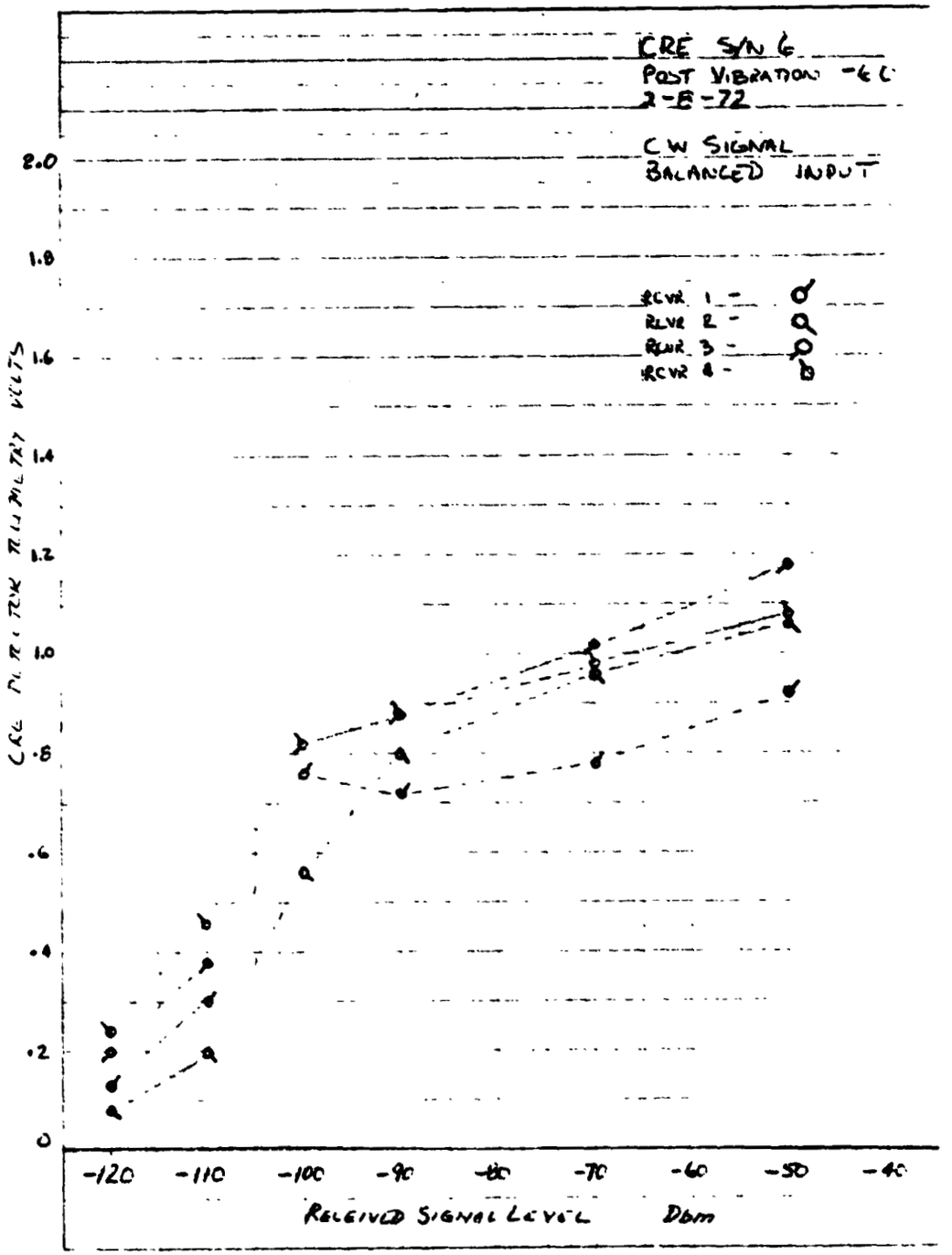

Figure 5.1. Receiver AGC Volts vs. CW Signal Level.

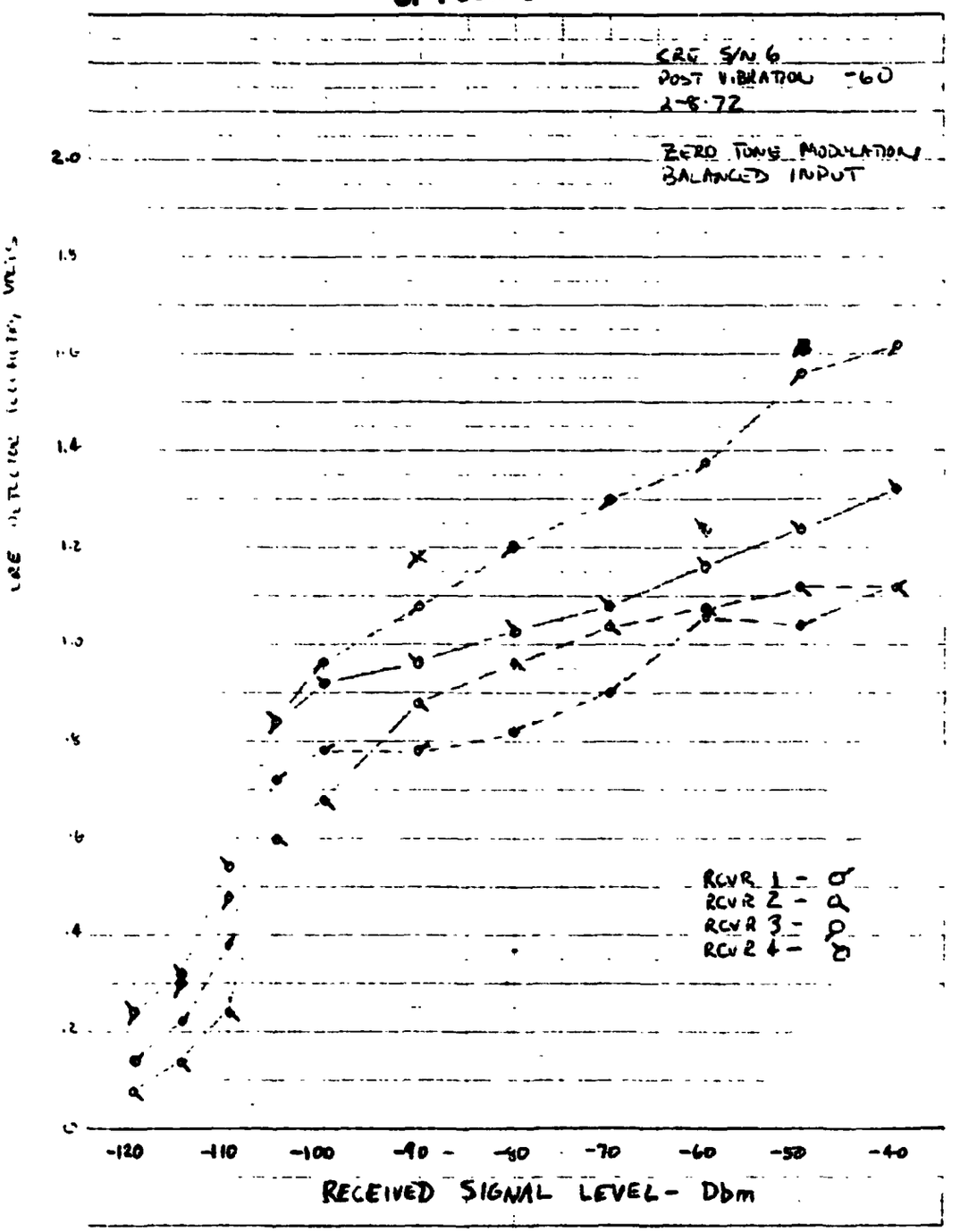

Figure 5.2. Receiver AGC Volts vs. Modulated Carrier Signal Level.

TABLE 5-1

RECEIVER AGC VOLTAGE - ORR44377

RCVR	1	2	3	4
Volts from				
Telemetry	1.10	1.16	1.44	1.14
B-3db Calibration Curve. - 55dbm	1.08	1.12	1.44	1.12
Telemetry	1.28	1.28	1.06	.82
B-20db Calibration Curve. - 66dbm (Approximately)	1.30	1.22	.94	.80
Telemetrys	1.12	1.18	1.26	.96
B-6db Calibration Curve. - 62dbm	1.12	1.12	1.24	1.04

5.4 WIDEBAND TRANSMITTERS (WBT)

5.4.1 WIDEBAND TRANSMITTER NO. 1

WBT No. 1 (SN4) was provided as GFE to the observatory. It was manufactured at the GSFC in 1971 and put in bonded storage. It underwent retest in mid 1972 and was subsequently installed in the observatory. WBT 1 has performed well throughout the life of OAO-C with one notable exception; that being a steady drift, downward, of the center RF frequency (which was easily accommodated by the STDN receivers). This was first observed approximately 2-3 years into the flight and degradation since then has been very slight. The specification for the WBT called for a center frequency of 400.550 MHZ$\pm$12KHZ. Data taken during 51 contracts between January 1980 and December 1980 indicate that the WBT center frequency is approximately 400.50 MHZ (ref. 6). The range of frequencies noted is from 400.591279 to 400.498580 MHZ, a differerce of 92.7 KHZ. This data was taken at different transmitter temperatures and at different times during the pass. In some cases data could have also been modulating the carrier. Any of these factors will affect the readings slightly. Preflight data shows that the transmitter frequency was typically 400.555 MHZ.

Other data taken during orbits 44835 through 44852 indicate transmitter RF power still exceeds 10.5 watts and is consistent with data taken during the first 30 days (Table 5-2).

5.4.2 WIDEBAND TRANSMITTER NO. 2

WBT No. 2 was manufactured by Hughes Aricraft, Culver City, California, and has not seen much service during the mission. A review of data indicates that it is still operating properly. Its' center frequency has drifted upward and is now slightly out of spec according to the data of Reference 6 (400.571 MHZ vs 400.550 MHZ). Prelaunch frequency was recorded as 400.558 to 400.564 MHZ. RF power output, as determined from the analog telemetry monitor varies from a high of 9.64 watts at 50.8°F to a low of 5.79 watts at 89.3°F (Table 5-3). The specifications called for a minimum of 7 watts except at 130° where it is allowed to drop to 5.5 watts. All data received at the ground, via WBT No. 2, was of satisfactory quality.

TABLE 5-2
WBT #1 POWER OUTPUT

STATION/ORBIT	INTERNAL TEMP °F	TLM VOLTS	Po (WATTS)
ORR 44833	56	3.62	10.5
ORR 44835	61.6	3.64	10.5
QTO 44838	52.9	3.64	10.5
QTO 44839	51.3	3.64	10.5
QTO 44852	60.4	3.64	10.5
First 30 days	---	3.64±.04	10.5

TABLE 5-3
WBT #2 POWER OUTPUT

STATION/ORBIT	INTERNAL TEMP °F	TLM VOLTS	Po (WATTS)
ORR 44760	67.2	1.12	7.00
ORR 44762	57.1	1.22	8.29
QTO 44767	50.8	1.32	9.64
ORR 44789	75.7	1.08	6.51
ORR 44792	79.5	1.06	6.27
SNT 44841	81.9	1.04	6.03
QTO 44845	89.3	1.02	5.79
Prelaunch	--	--	5.9W
Prelaunch-ETV	--	--	7.44W

5.5 NARROWBAND TRANSMITTERS (NBT)

NBT #1 was the primary source of housekeeping data throughout the mission. NBT #2 was turned on occasionally to verify operation. The data taken recently indicates that both transmitters are operating almost exactly as they did at the time of liftoff and during the first 30 days. RF power telemetry is within one telemetry count of beginning of life values, indicating that no degradation has taken place (either in the transmitters or antenna system (See Table 5-4). The total frequency drift over the mission life time has been less than 2 KHZ (reference 6).

5.6 SPACECRAFT DATA HANDLING EQUIPMENT (SDHE)

The SDHE, manufactured by Radiation, Inc., Melbourne, Florida, has been operating continuously since launch with no apparent malfunctions. The tests performed verified that those operational modes which could be verified, within operational constraints, were in fact operating properly. The modes run were:

- o cyclic data
- o four frames/minutes
- o four frames/two minutes

Data recovered from these modes was satisfactory.

5.7 EXPERIMENTERS' DATA HANDLING EQUIPMENT (EDHE)

Tests of the EDHE were not performed due to non-availability of time; the experimenters made continual use of it. No indication of degradation of the EDHE was noted during the mission.

5.8 SPACECRAFT SYSTEMS CONTROLLER UNIT (SSCU)

The SSCU, manufactured by the IBM Corporation, provided most of the relay switching capability in the observatory. Relays were arranged in simplex, duplex and triplex (voter) configurations for reliability purposes. The tests performed were intended to verify that "secondary" contacts were still functional and that logic still performed properly. The test sequence originally proposed is described in Reference 4 and then subsequently run in Reference 7. The relay tests were run, in part, and the results described in Reference 8. No anomalies were observed though a number of duplex relays were not cycled due to an error in setting up the command sequence.

TABLE 5-4
NBT POWER OUTPUT

NBT #1		NBT #2	
Representative Readings			
Temperature °F	Po (Watts)	Temperature °F	Po (Watts)
73.5	1.38	65.9	1.38
74.2	1.34	68.6	1.45
74.9	1.36	Prelaunch	1.27 - 1.75
Prelaunch	1.33 - 1.76		

During a subsequent test of RAPS operations and IRU gyro shutdown commands to activate RAPS AC power would not respond. Investigation showed that the zero decode latch in the T sector of the SSCU failed to become enabled and thus the commands sent to turn on RAPS were not executed. Subsequent testing showed that sector R and S zero decode latches were operative and thus redundant contacts were used to turn RAPS on. Reference 9 describes the problem in greater detail. No attempt was made to determine the probable cause of failure and no other failure modes were noted.

5.9 CONCLUSIONS

Based upon a review of data collected during the end of mission tests, along with other data taken during the lifetime OAO-3, it is concluded that the C&DH subsystems performed in an excellent manner. With the exception of the anomaly
noted in SSCU sector T, there is no reason to believe that these subsystems would not have provided satisfactory service for many more years to come.

REFERENCES

1. GAC Memo MOP-4-IMO-80-026; End of Mission Command RCVR Test

2. GAC Memo MOP-4-IMO-80-027; End of Mission Transmitter Test

3. GAC Memo MOP-4-IMO-80-028; End of Mission SDHE and EDHE Mode Test

4. GAC Memo MOP-4-IMO-80-029; End of Mission SSCU Relay Test

5. 710.2/Technical Management Office Memo; End of Mission Tests on OAO-C Spacecraft; August 25, 1980

6. GAC Memo MOP-4-IMO-81-020; End of Mission Transmitter Test

7. GAC Memo MOP-4-IMO-81-006; End of Mission SSCU Relay Test

8. GAC Memo MOP-4-IMO-81-019; End of Mission SSCU Relay Test-OAO-3

9. GAC Memo MOP-4-IMO-81-021; OAO-3 End of Mission Engineering Tests

ACKNOWLEDGEMENTS

The fact that the writer was able to review test data taken more than 8 years after the launch of OAO-C is a testimonial to the many people who made it happen. The Engineering, Integration and Test Team and field support groups of the Grumman Aerospace Corporation and the design, test and integration engineers at the Goddard Space Flight Center deserve special thatks. The tremendous support of the major subcontractors is appreciated. This group includes, but is not limited to:

1. IBM Corporation, FSD	-PPDS/PPSC and SSCU
2. Radiation, Inc.	-SDHE/EDHE
3. AVCO, Inc.	-CRE
4. Dorne & Margolin	-Diplexer
5. Hughes Aircraft Co.	-RTB, NBT, WBT #2
6. RCA Astro Electronics	-Tape Recorder
7. Goddard Space Flight Center	-GFEI, OBP, WBT #1

The writer also wishes to specifically thank the operations team who kept OAO-C alive and well during this time.

APPENDIX

A listing of the transmitter frequencies for both wideband (400 MHz) and narrowband (136 MHz) transmitters as they were reported by the various ground stations supporting OAO-3 are presented in Table 5-5.

The frequencies listed from January 1980 thru to February 1981 are for WBT No. 1 and NBT No. 1. In February 1981, starting with Quito 44790, widband frequencies listed are for WBT No. 2. NBT No. 2 frequencies are listed starting with Quito 44881.

TABLE 5.5
MEASURED TRANSMITTER FREQUENCIES - OAO-3

Month	Contact	WBT #1 Frequency (MHz)	NBT #1 Frequency (MHz)
January 1980	ORR 39042	400.501209	136.259674
	ORR 39065	400.501490	136.259680
	ORR 39128		136.259573
	SNT 39191		136.256650
	SNT 39192	403.503066	
	ORR 39325	400.500102	136.259508
	ORR 39353	400.304947	136.259930
February 1980	ORR 39438	400.501663	136.259615
	ORR 39466	400.500685	136.259960
	ORR 39495	400.502244	136.259993
	ORR 39580		136.259389
	ORR 39595	400.503935	
	ORR 39652	400.500600	136.259366
	ORR 39661	400.502573	136.259397
	ORR 39724	400.502707	136.259578
	ORR 39752	400.500488	136.259370
March 1980	ORR 39851	400.591279	136.259515
	ORR 39879	400.500915	136.259446
	SNT 39975	400.501049	
	SNT 40004	400.500992	

TABLE 5-5
MEASURED TRANSMITTER FREQUENCIES - OAO-3 (Continued)

Month	Contact	WBT #1 Frequency (MHz)	NBT #1 Frequency (MHz)
April 1980	ORR 40369	400.500917	
	ORR 40392	400.496493	
	ORR 40463		136.259990
	ROS 40479	400.501210	
	ORR 40506	400.501407	
	ORR 40534		136.259973
	ROS 40551	400.500422	
	QTO 40561		136.260180
	ORR 40563	400.500425	
	ROS 40651	400.500552	
May 1980	ORR 40677	400.[illegible]502	
	SNT 40713		136.258693
	ROS 40722	400.515130	
	SNT 40743		136.259983
	ROS 40750	400.500510	
	ROS 40779	400.500390	
	ORR 40819	400.501974	
	ORR 40846	400.502593	136.260251
	ORR 40874	400.500836	136.259520
	ORR 40903	400.501172	136.259683

TABLE 5-5

MEASURED TRANSMITTER FREQUENCIES - OAO-3 (Continued)

Month	Contact	WBT #1 Frequency (MHz)	NBT #1 Frequency (MHz)
July 1980	ORR 41559	400.500741	136.259732
	ORR 41588	400.510817	136.260415
	ORR 41616	400.519953	136.260221
	SNT 41666	400.498580	
	ROS 41718	400.500076	
	ORR 41758	400.519874	136.260171
	ORR 41815	400.521661	136.259830
August 1980	ORR 42257	400.510110	136.259473
	ORR 42287	400.500532	
	ORR 42354		136.259477
September 1980	ORR 42457	400.519633	136.26040-
	ORR 42541	400.501356	136.259774
	ORR 42570	400.501568	136.259763
	ORR 42626	400.401475	136.260085
	ORR 42668	400.501547	136.259997
	ORR 42689	400.501339	136.259886
	ORR 42727	400.519187	136.259408
November 1980	ORR 43680	400.500993	136.258932
	ORR 43708	400.520044	
	ORR 43737	400.539815	

TABLE 5-5

MEASURED TRANSMITTER FREQUENCIES - OAO-3 (Continued)

Month	Contact	WBT #1 Frequency (MHz)	NBT #1 Frequency (MHz)
December 1980	ORR 44020	400.500388	136.259023
	ORR 44605	400.557306	136.258974
January 1981	SNT 44787	400.497244	
	ORR 44788	400.562718	
	QTO 44788	400.587720	
	ORR 44789	400.569131	
February 1981	QTO 44790	400.588960	
	ORR 44790	400.561739	
	ORR 44791	400.567130	
	ORR 44792	400.556789	
	QTO 44795	400.560000	
	SNT 44796	400.571140	
	SNT RR797	400.499478	
	ORR 44806	400.567165	
	SNT 44812	400.567975	
	SNT 44828	400.567020	
	SNT 44841	400.568885	
	QTO 44847	400.569730	
	SNT 44858	400.669726	
	QTO 44859	400.575537	
	QTO 44860	400.571442	

TABLE 5-5

MEASURED TRANSMITTER FREQUENCIES - OAO-3 (Continued)

#1 Frequency Month	Contact	WBT #1 Frequency (MHz)	NBT #1 Frequency (MHz)
February 1981 (Continued)	QTO 44861	400.570517	
	SNT 44870	400.570189	
	SNT 44872	400.568141	
	QTO 44873	400.570700	
	QTO 44874	400.570670	
	QRR 44876	400.567104	
	QTO 44881	400.566120	136.262330
	QTO 44882	400.556421	136.261471
	QTO 44883	400.573613	136.260470
	SNT 44884	400.570479	136.258610
	SNT 44885	400.567820	136.257334
	SNT 44886	400.568509	136.258400
	QTO 44887	400.566950	136.259530

OAO-3 END OF MISSION STAR TRACKER

SENSITIVITY TEST

by

Jerry Kull - NASA/Goddard Space Flight Center
Dr. Ford Kalil - NASA/Goddard Space Flight Center
Jim Gemmel - NASA/Goddard Space Flight Center
H. Kochevar - Westinghouse Electric Corporation

TABLE OF CONTENTS

SECTION 6
STAR TRACKER SENSITIVITY TEST

6.1 SUMMARY

The end of mission tests for the star tracker sensitivity characteristics were performed on three out of four gimballed star trackers on the OAO-3 spacecraft. A failure occurred on the fourth star tracker soon after launch. A family of linear curves were established for each star tracker sensitivity, by using the telemetry signal voltage data versus time for a number of guide stars whose magnitudes approximately covered the dynamic sensitivity range of each sensor.

A family of straight line curves were determined by applying the method of least squares to the data points to obtain the best fit straight lines.

The results on the graph show that all the curves have a very small slope and were either positive or negative. Evaluation of these results did not provide any conclusive evidence that a change occurred in the sensitivity of the three star trackers.

6.2 INTRODUCTION

The gimballed star tracker, whose sensitivity stability with time was determined, is an electro-mechanical-optical sensor that was needed for detection, acquisition and tracking of stars in a three dimensional space for the purpose of providing discrete coordinate information along all three spacecraft axis. The three star trackers, whose sensitivity was measured, consisted of Nos. 3, 4 and 5. Each sensor was located on the outer surface of the spacecraft frame structure as shown in Figure 6-1. The subsystem of the star tracker consisted basically of the gimballed tesescope and the star tracker electronics.

Each star tracker was mounted in a dual gimbal which permitted the sensor to scan an angle of $\pm$ 43° along each axis and produced a square angular field as illustrated in Figure 6-2. The normal attitude control of the OAO-3 was under a three axis strapdown gyro system called the Inertial Reference Unit (IRU).

ORIGINAL PAGE IS
OF POOR QUALITY

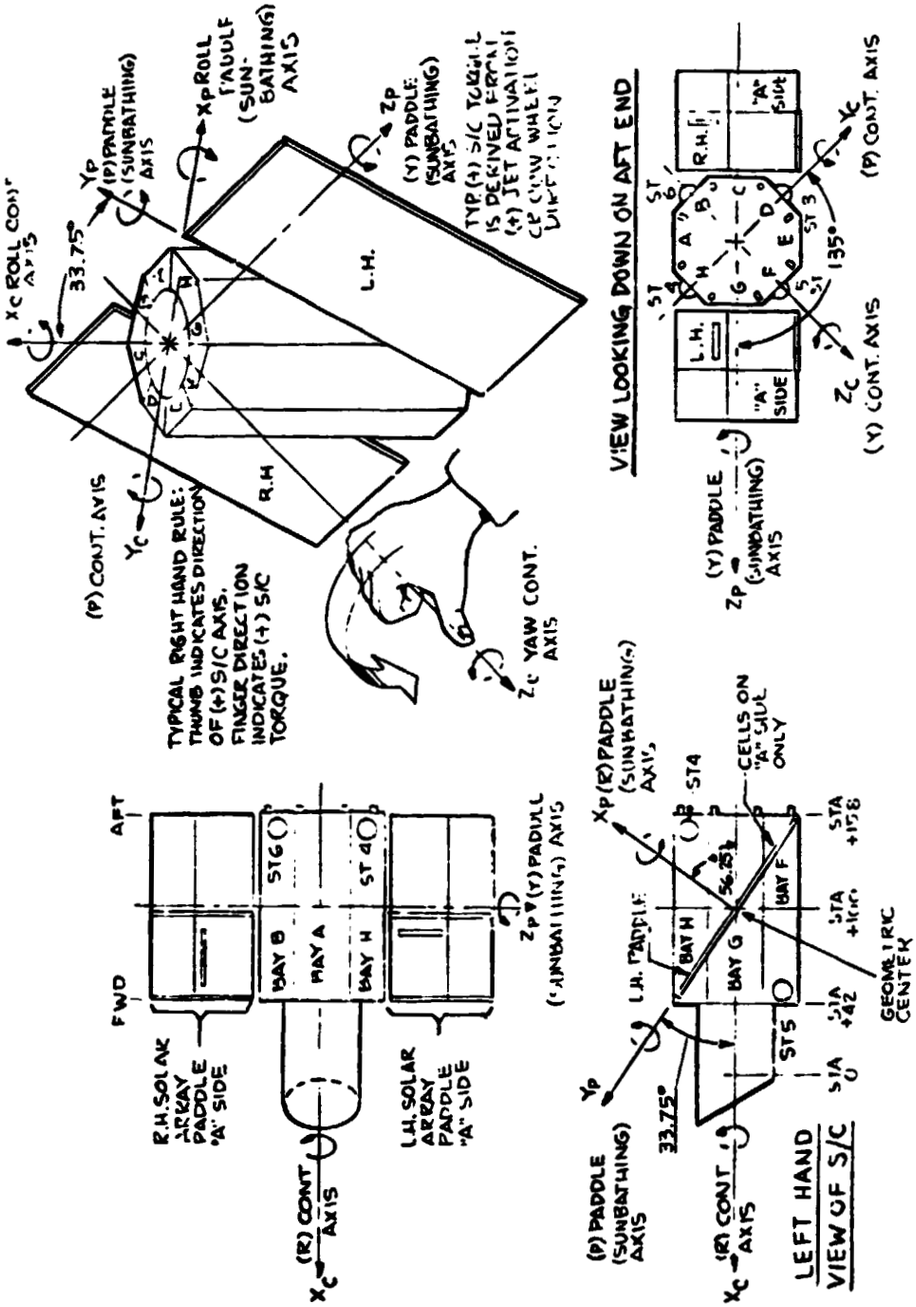

Figure 6-1. OAU-3 Spacecraft Coordinate Reference System.

ORIGINAL PAGE IS
OF POOR QUALITY

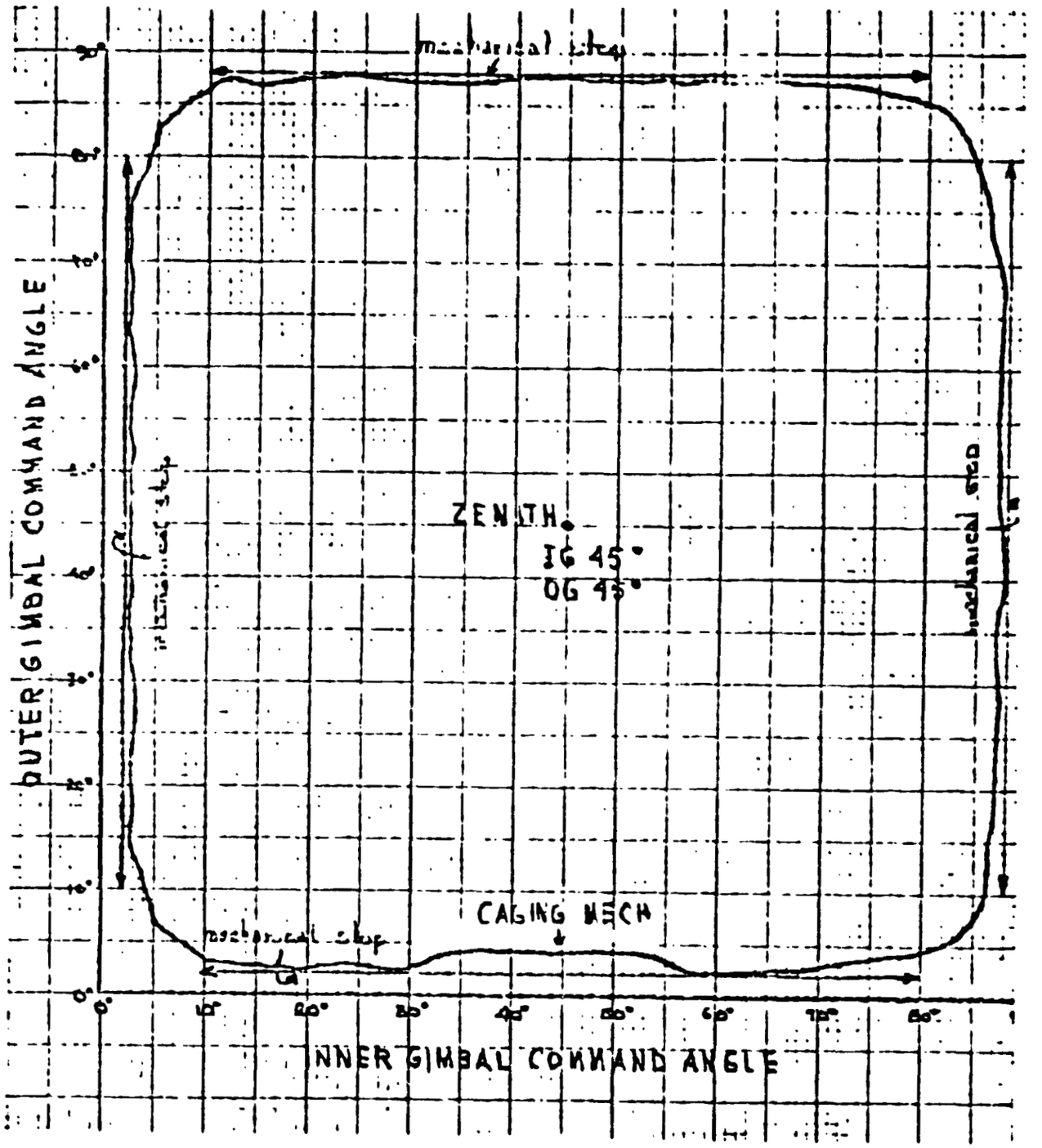

Figure 6-2. Typical Star Tracker Gimbal Travel with the Long Sun Shield.

The IRU's reference was periodically updated by commanding the spacecraft to Gimballed Star Tracker control and after allowing the spacecraft to settle, zeroing out the IRU errors, then switching back to IRU control.

Any time the attitude control was lost the spacecraft automatically went to sunbathing and switched to IRU control under reaction wheels and jets. To regain celestial reference, instead of going through the prelaunch designed procedure of L-Stab, Roll Search, Star Acquisition and Acquisition Complete, the following simplified procedure was devised:

When the spacecraft settled down at sunbathing an attitude determination was taken utilizing magnetometer and solar reference data which was accurate to within a couple of degrees. This information was provided to the Support Computer Processing System (SCPS) which then calculated sl[illegible]o return the spacecraft to its original position or to take it to the next s[illegible]ed pointing. Either one of these attitudes already had guide stars available [illegible]he correct gimbal angles already calculated for their Gimballed Star Tracker complement. At the conclusion of these slews a star search was initiated where the ground computer would command the star trackers to move in an ever increasing spiral until they acquired their specified star. They were then halted and the errors between the GST's and the IRU were read and the spacecraft was manually slewed to the correct pointing to reduce these errors to zero. The spacecraft control was then switched to GST control and after settling out the IRU was reset to the newly reacquired celestial reference.

6.3 OBJECTIVE

The purpose of the end of mission test on the gimballed star trackers was to determine what effects from space environment radiation and aging may have on the sensitivity of the sensors in the star trackers over a period of approximately eight years.

6.4 DESCRIPTION OF GIMBALLED TRACKER

6.4.1 OPTICAL SYSTEM

The star tracker, shown in Figure 6-3, employed a Cassegrainian reflector type telescope having a primary mirror of 3.5 inch (8.9 cm) diameter and 5.0 inch (12.7 cm) focal length of which only half was used. Individual beams of light reflected from a primary surface were passed back up the telescope barrel

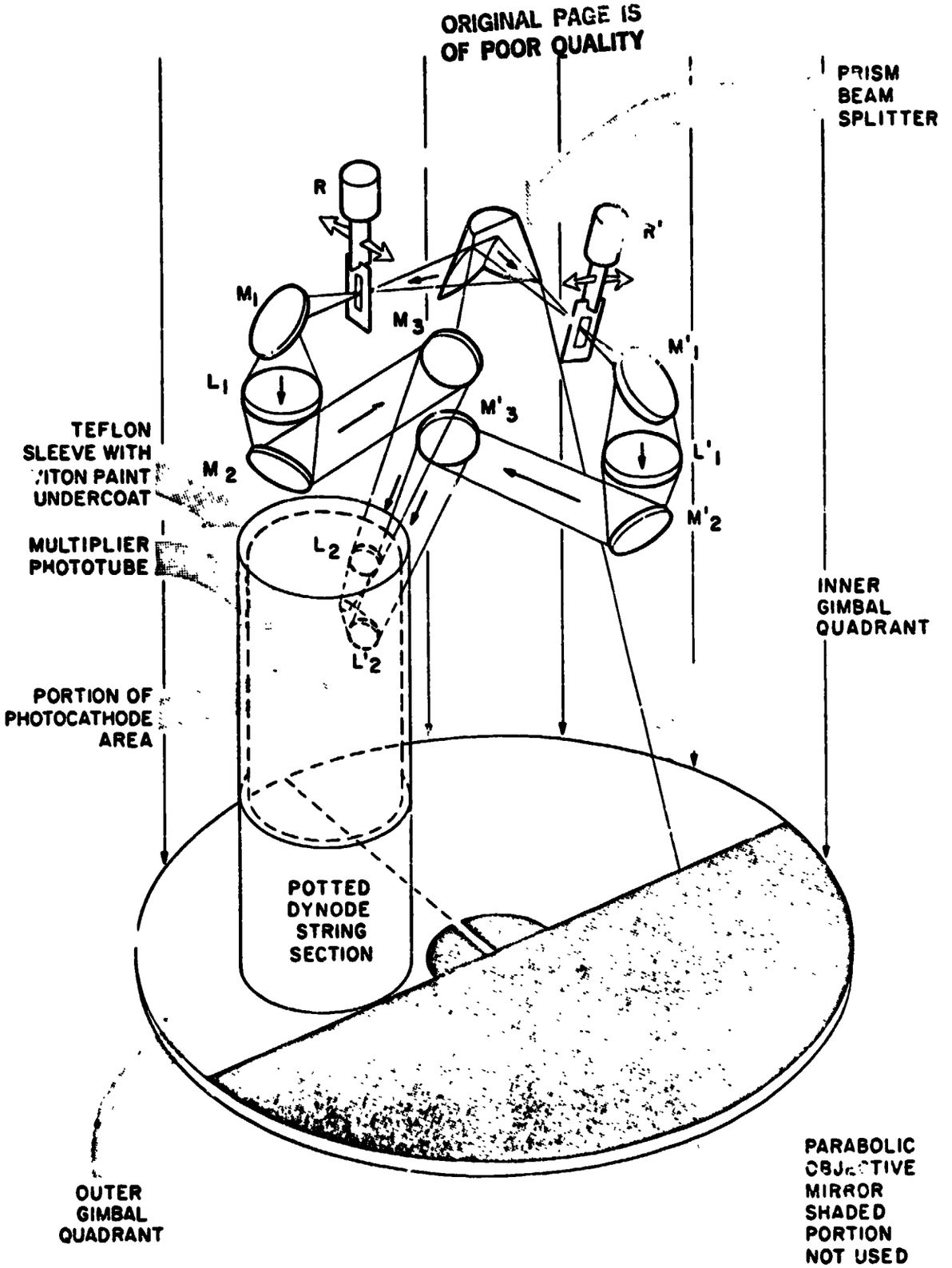

Figure 6-3. Schematic-Optical System Star Tracker.

where they were again reflected from two plane mirrors at an angle of 90° to each other and each making a 45° angle with the plane of the parabolic orbit mirror. The impinging beam was thereby split into two components at 90° to each other. Each beam was related to one of the gimbal axes. The beams passed back down the telescope barrel and then through the square window of a vibrating reed. One reed vibrated at 350 Hz and provided error information of the inner gimbal of the star tracker, while the other reed vibrated at 450 Hz and provided error information for the outer gimbal. The reeds were tuned to their natural frequencies of vibration at either one of the above frequencies to minimize reed drive power. The system could bring a star at infinity into focus in the plane of the reed windows. After passing through the reed, each beam was converged with refractive and reflective optical surfaces and was made to fall on the cathode surface of a nine stage photomultiplier tube. In the light path, just before the beam splitter mirror, was a solar operated shutter device. Whenever the sun was within 30° of the telescope line of sight, the shutter closed and blocked off all light falling on the photo-cathode to prevent permanent damage to the cathode surface. Another more sensitive earth sensor would trigger the shutter when the earth was within 8° $\pm$ 4° of the star line.

6.4.2 IMAGING AND ERROR GENERATION

With no light falling on the photo-cathode of the multiplier tube, the voltage on each dynode was 900 volts across the tube. When light impinged on the cathode surface, electrons were emitted. These were attracted to the first dynode where their impingement caused a greater number of lower energy electrons to be emitted (secondary emission). These in turn were accelerated towards the next dynode and liberated an even greater number of electrons. The current collected from the photo-tube was not steady, but was modulated by the vibrating reeds. The frequency of modulation was a function of reed frequency and the phase of modulation was a function of star image position. When the star was off to one side of the optical field of view, the window in the reed uncovered the image beam only once per oscillation. The output current of the phototube contained a large component at the frequency of the reed(s). The phase of this current depended on whether the star image was left or right, or up or down with respect to the center of the optical field. The output was amplified and then passed through 40 Hz bandpass filters tuned to 350 and 450 Hz. The filtered outputs were synchronously demodulated to yield a DC voltage whose polarity was a function of phase and whose

amplitude was a function of displacement magnitude. Two DC voltages were used as error signals for the two gimbal servo systems. When the star was centered in the field of view, the image was chopped twice by the reed for each oscillation. The modulated current from the phototube contained a large second harmonic signal at the reed frequency(s) while the fundamental component was at a null, and error drive signals to the servos indicated a null. A second pair of narrow band filters tuned to 700 and 900 Hz wre used to recover star brightness information when the star image was centered. The outputs of these filters were combined with the outputs of the 350 and 450 Hz filters to develop an AGC proportional to star brightness. This AGC voltage acted upon the photo-tube dynode voltage supply and caused it to drop from 900 volts with a ±2 magnitude star image to 600 volts with a -1 magnitude star image. This effect kept the output of the phototube constand for stars of different magnitudes, and maintained the error slope and servo loop gain constant.

6.4.3 TRACKER LOGIC

The star tracker produced several digital signals that affected the stabilization and control subsystem operation. A Star Presence signals was generated whenever a guide star having an S-4 magnitude of +2.5 or brighter appeared within the telescope field of view. The photo-tube had an S-4 spectral response curve peaking at 4000 Angstroms and since visual acuity peaks at 5500 Angstroms, it is obvious that S-4 and visual magnitudes can differ (Refer to Figure 6-4). The majority of stars are of type B-0, a bluer and hotter star then the sun which is a type G-0 with a peak black-body radiation output at 6000 Angstroms. A blue-white star of visual magnitude ±3.0 may appear as an S-4 star of +2.5, while a closer, reddish star may have a higher visual reading than S-4 magnitude. The tracker was calibrated to take into account the attenuation of light over the S-4 band so that a +2.5 magnitude star will be recognized in the vacuum of outer space. The threshold operated on the AGC voltage and was set at +2.5 magnitude so that a +2.0 magnitude star will always be recognized while a +3.0 magnitude star will never be recognized. This limited the guide stars to a maximum of 40 and actually only about 31 could be used. The others were too close to bright neighbors to permit accurate tracking. The star tracker tracked the center of light appearing in its field of view. If two stars, one of +2.0 magnitude and the other of +5.0 magnitude or more appeared together within the field of view, the star tracker would not point exactly at the +2.0 star, but would

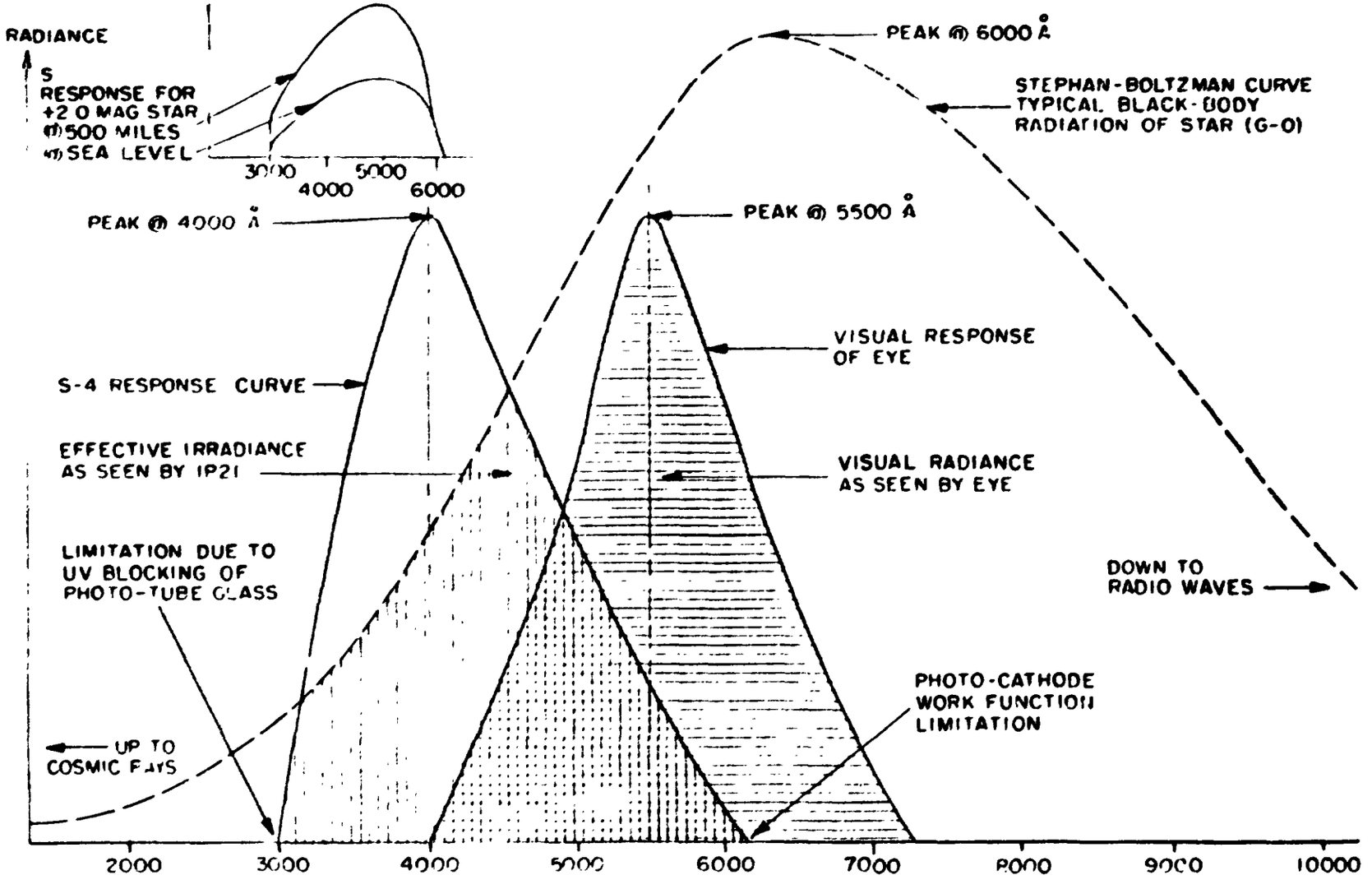

Figure 6-4. Angstroms (Wave Length).

point to some spont between the two stars. Thus, a tracking error occurred whose magnitude was a function of the difference in brightness and angular displacement between the two stars in the tracker's field of view

6.5 RESULTS AND ANALYSIS

There is a limitation to the accuracy that the star tracker sensitivity with time can be determined from the available data. The number of telemetry data measurements (signal voltage) of guide stars obtained by each star tracker varied considerably over a period of 2800 days (7-2/3 years). From the signal voltage data, the star's magnitude was determined by ground based computers. Stars with the greatest number of data measurements were, therefore, selected to provide the most accurate sensitivity characteristics of the sensor.

The approach taken to demonstrate the possibility of any aging effects that may have occurred on the sensitivity of the star trackers was to plot the signal voltage parameter versus the time in days for each star selected for the particular star tracker. The reason for selecting the signal voltage was that it contained less errors than the star magnitude parameter which is obtained via a calibration equation for converting the signal voltage to star magnitude (in some cases errors were made in the conversion). A comparison of the data in Table 6-1, between the measured magnitude and the corresponding signal voltage, shows a nonlinear correlation which indicates data reduction errors were occasionally involved in the computation process of the star's magnitude for star tracker No. 3.

The data points from all star trackers show a wide variation when plotted on a graph as linear curves and provided coarse average characteristics. These variations of data points are measurement errors resulting primarily from the coarse resolution and inherit noise in the telemetry system. One bit of telemetry data represents an increment of 0.02 signal voltage and a computed magnitude of 0.05.

TABLE 6-1
STAR TRACKER #3

Star	True Mag.	Meas. Mag.	Signal Volt.	Day
5	.35	.77	3.72	28
"	.35	.82	3.86	451
"	.35	.76	3.86	455
"	.35	.82	3.86	702
"	.35	.82	3.86	709
"	.35	.87	3.88	1159
"	.35	.92	3.90	1165
"	.35	.87	3.90	1167
"	.35	.87	3.88	1459
"	.35	.92	3.92	1509
"	.35	.87	3.90	2246
7	.20	.61	3.78	587
"	.20	.71	3.82	622
"	.20	.61	3.76	667
"	.20	.76	3.84	701
"	.20	.76	3.84	1655
"	.20	.82	3.86	1966
"	.20	.76	3.82	2478
22	1.75	2.41	4.48	462
"	1.75	2.31	4.44	463
"	1.75	2.41	4.46	464
"	1.75	2.31	4.44	514
"	1.75	2.31	4.42	536
"	1.75	2.31	4.42	592
"	1.75	2.36	4.42	638
"	1.75	2.41	4.48	1297

TABLE 6-1

STAR TRACKER #3 (Continued)

Star	True Mag.	Meas. Mag.	Signal Volt.	Day
32	1.20	1.90	4.32	453
"	1.20	1.95	4.26	665
"	1.20	1.90	4.28	677
"	1.20	1.95	4.30	686
"	1.20	1.95	4.30	709
"	1.20	2.05	4.34	1918
"	1.20	2.00	4.32	2244

To obtain the most meaningful results from the erratic data points, Xi, Yi where i = 1 --- n, the method of least squares was used to provide the best linear fit of a straight line. Calculations were performed by utilizing the linear regression line equation as follows (Ref. 1):

where, $y = a + bX$

a = y intercept of regression line

b = slope of regression line

The parameters a and b were determined from the following expressions:

$$a = \frac{\sum_{i=1}^{n} Y_i \sum_{i=1}^{n} X_i^2 - \sum_{i=1}^{n} X_i \sum_{i=1}^{n} X_i Y_i}{n\left(\sum_{i=1}^{n} X_i^2\right) - \left(\sum_{i=1}^{n} X_i\right)^2}$$

$$b = \frac{n\left(\sum_{i=1}^{n} X_i Y_i\right) - \sum_{i=1}^{n} X_i Y_i}{n\left(\sum_{i=1}^{n} X_i^2\right) - \left(\sum_{i=1}^{n} X_i\right)^2}$$

n = number of data points used

The sensitivity characteristics curves for star tracker No. 3, utilizing guide stars Nos. 5, 7, 22 and 32, were determined by using the above equations and are presented as linear lines in Figure 6-5. For each sensitivity curve the associated regression line equation containing its corresponding coefficients is shown on the graph. The parameter b in the equations for the linear lines in Figure 6-5 indicate that they all have a very small positive slope. Because of this factor there is no conclusive evidence that a change occurred in the No. 3 star tracker's sensitivity.

Similar graphs of sensitivity curves with their corresponding regression line equations were established for star tracker No. 4 from the data shown in Table 6-2, by utilizing guide stars No. 5 and 12, and are presented in Figure 6-6.

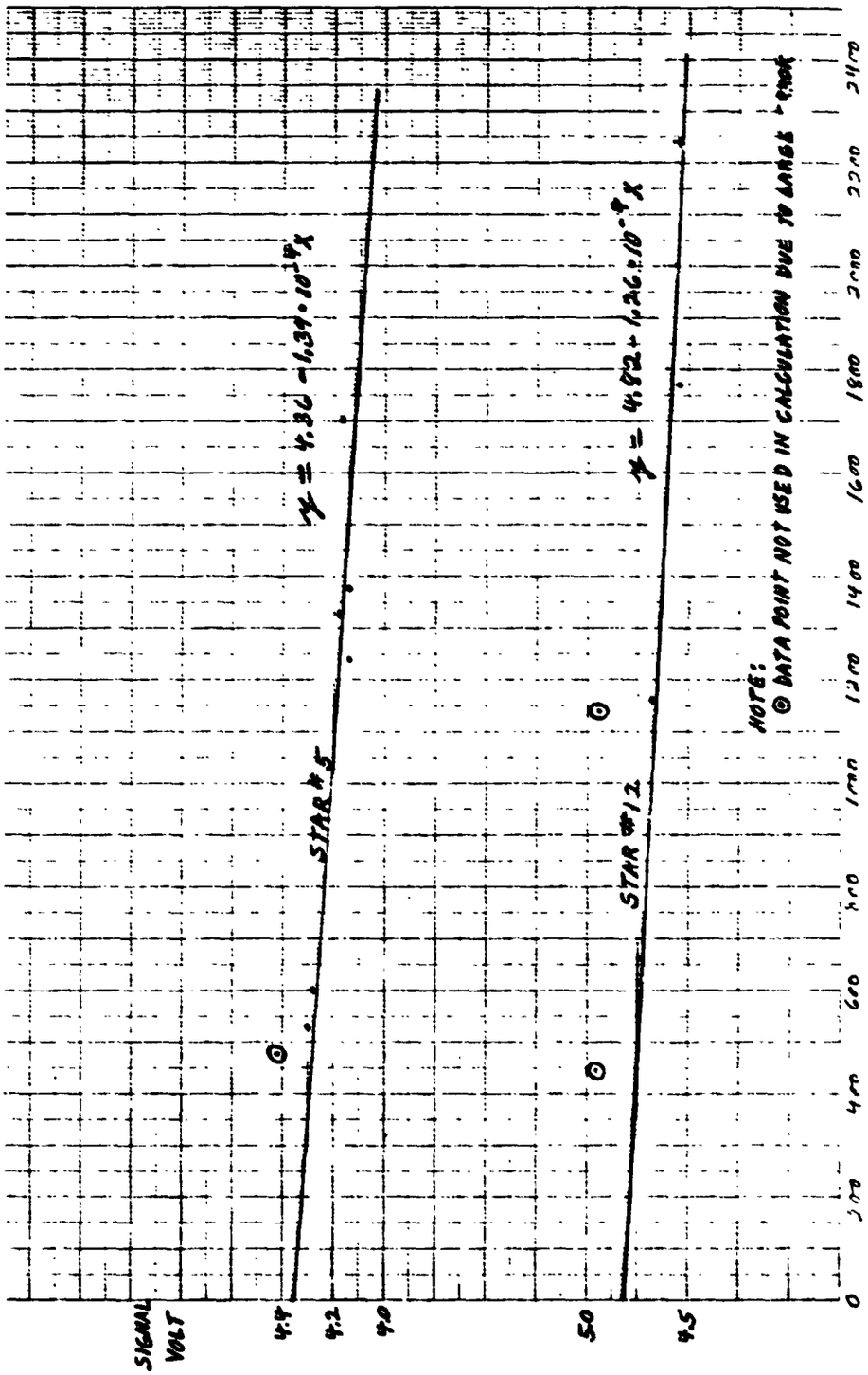

Figure 6-5. OAO-3 Star Tracker No. 3 Sensitivity.

TABLE 6-2
STAR TRACKER #4

Star	True Mag.	Meas. Mag.	Signal Volt.	Days
5	.35	1.11	4.42	474
"	.35	.85	4.30	523
"	.35	.89	4.28	601
"	.35	.54	4.14	1241
"	.35	.59	4.18	1326
"	.35	.50	4.14	1375
"	.35	.54	4.16	1702
12	1.25	2.33	4.96	445
"	1.25	1.81	4.74	659
"	1.25	2.24	4.94	1142
"	1.25	1.72	4.68	1160
"	1.25	1.37	4.54	1768
"	1.25	1.37	4.54	2234
"	1.25	1.42	4.56	2235

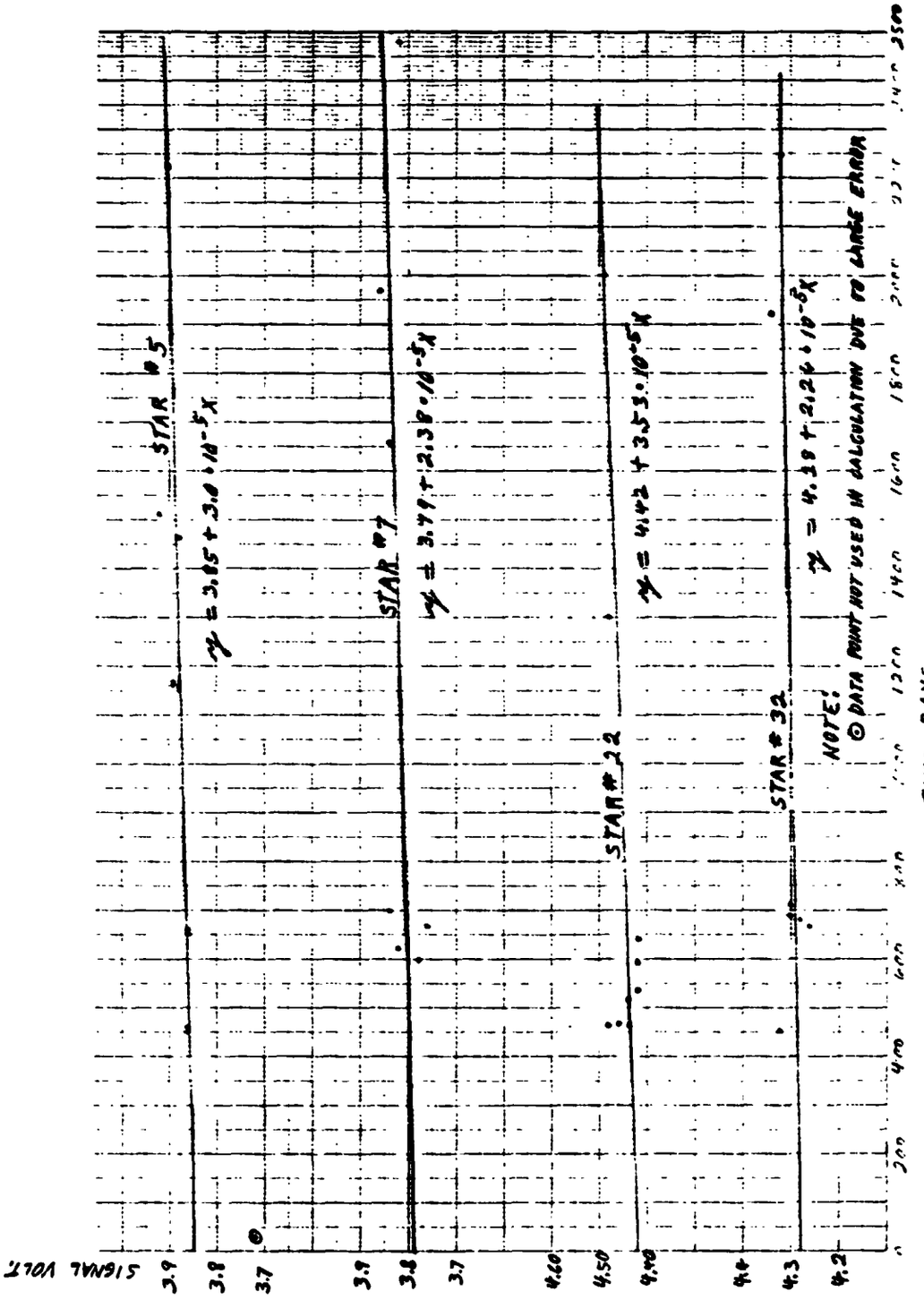

Figure 6-6. OAO-3 Star Tracker No. 4 Sensitivity.

Only two stars were available for this star tracker having a minimum of 7 data points. Parameter b in the regression line equations in Figure 6-6 indicates the linear sensitivity curves have a very small negative slope. This result is insufficient to conclude that a change occurred in the No. 4 star tracker's sensitivity.

The sensitivity characteristic curves for star tracker No. 5 were determined from data shown in Table 6-3 for guide stars No. 8, 22 and 32 and are presented in Figure 6-7. Similar linear characteristic curves and their associated regression line equations were derived for this sensor as was done for Nos. 3 and 4. This graph shows that the equations for two of the curves have a very small positive slope while the third has a very small negative slope. With such results a conclusion cannot be established that a change occurred in the No. 5 star tracker's sensitivity.

6.6 CONCLUSIONS

The telemetry data, provided by the three star trackers, resulted in both positive and negative slopes for the sensor sensitivity curves as shown in Figures 6-5, 6-6 and 6-7. Furthermore, all of the linear curves presented on the graphs have slopes that are very small.

There are essentially two primary factors that contributed to the inaccuracy of the sensor sensitivity curves for each guide star. One factor was the large data errors that resulted from the coarse resolution and the inherit noise in the telemetry subsystem. The second factor was the lack of more data points over the long span of time. Optimum accuracy in the sensor's sensitivity characteristic curves was achieved by using the method of least squares to obtain the best linear fit to the erratic telemetry data. Greater accuracy would have been achieved if more data points were provided for each star tracker and its corresponding guide stars. In addition, further improvement would have resulted if the data points were selected at uniform intervals across the full time span.

Because of the errors contributed by the above two factors, any variation in the star tracker sensitivity over the eight year life of the mission was masked by the noise of the above two factors. It appears that there was no significant change in the star tracker sensitivities.

TABLE 6-3
STAR TRACKER #5

Star	True Mag.	Meas. Mag.	Signal Volt.	Days
8	.60	.71	3.90	445
"	.60	.86	3.96	457
"	.60	.71	3.90	480
"	.60	.86	3.94	511
"	.60	.81	3.94	1219
"	.60	.81	3.94	1968
"	.60	.91	3.98	2246
22	1.75	2.08	4.44	565
"	1.75	2.03	4.42	649
"	1.75	2.03	4.42	665
"	1.75	2.08	4.44	1239
"	1.75	1.98	4.40	1320
"	1.75	2.03	4.42	1378
"	1.75	1.93	4.38	1658
"	1.75	2.03	4.42	2694
"	1.75	2.03	4.40	2738
32	1.2	1.58	4.24	462
"	1.2	2.03	4.84	475
"	1.2	1.58	4.22	694
"	1.2	2.20	4.92	714
"	1.2	1.52	4.22	1148
"	1.2	1.47	4.24	1157
"	1.2	1.52	4.20	1198
"	1.2	1.52	4.22	2198
"	1.2	1.58	4.24	2612

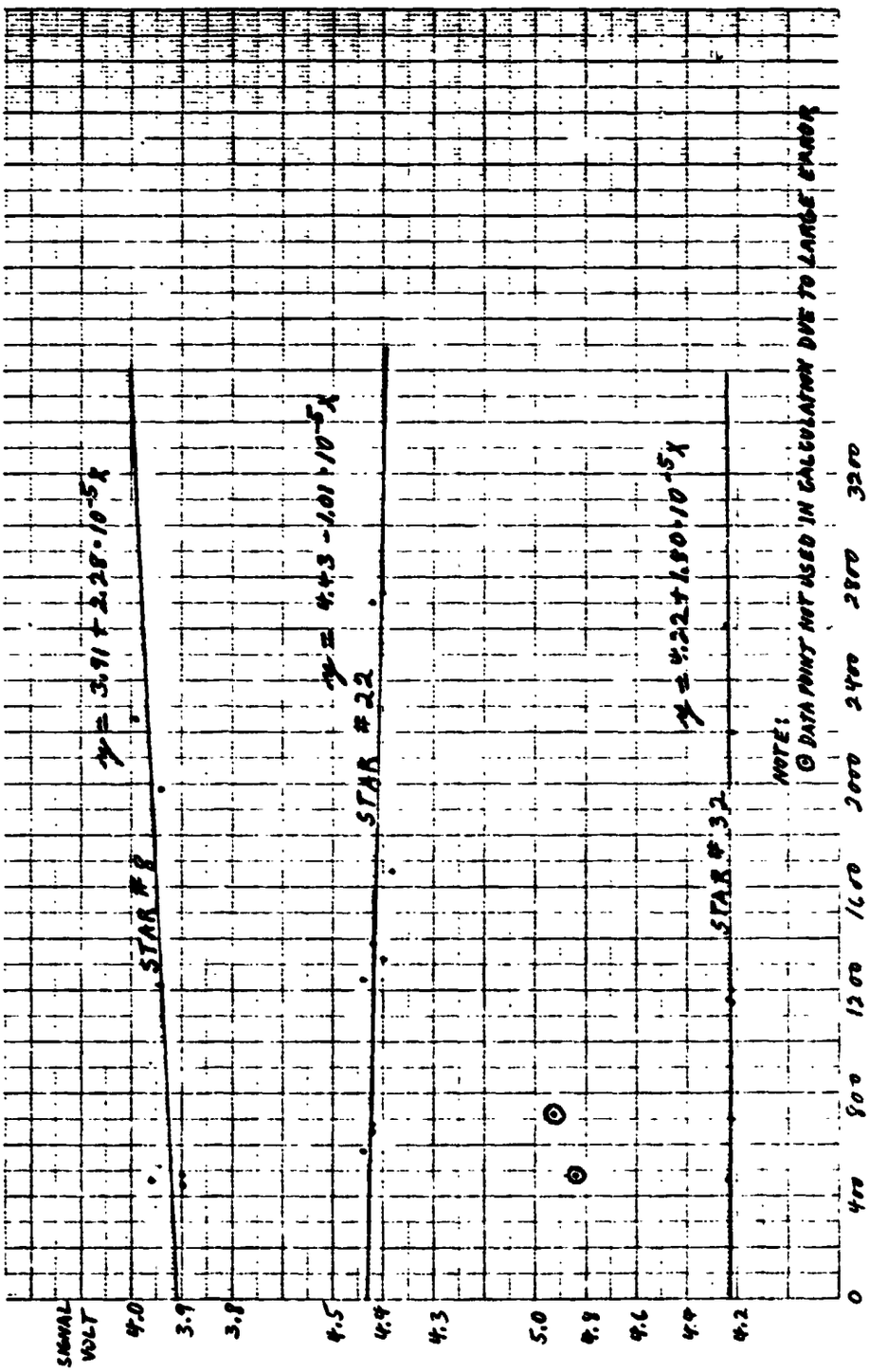

Figure 6-7. OAO-3 Star Tracker No. 5 Sensitivity.

REFERENCES

1. R.S. Burington, D.C. May, "Handbook of Probability and Statistics with Tables," Handbook Publishers Inc.

GLITCH TESTING OF PRINCETON EXPERIMENTAL PACKAGE (PEP)

by

Dr. R.S. Polidan
Princeton University Observatory
August 5, 1981

TABLE OF CONTENTS

SECTION 7
GLITCH TESTING OF PRINCETON EXPERIMENTAL PACKAGE (PEP)

7.1 SUMMARY

Unscheduled high voltage shutdowns (glitches) in the PEP were investigated in order to identify their cause. Detailed analysis failed to identify a unique cause of the glitches. Interaction between the spacecraft electronics and the environment is the most probable cause.

7.2 INTRODUCTION

In the Princeton Experiment Package (PEP) voltages are supplied to the phototubes (5100 and 3200 volts for the U (open) and V (windowed) tubes respectively) via three vented Data high Voltage Power Supplies (DHVPS). Each DHVPS actuates a different combination of the six PEP phototubes. Any two DHVPS will power all six phototubes. Normal operating procedure for most of the mission was to have two DHVPS on line continuously. Beginning shortly after launch (Orbit 131) the PEP began experiencing unscheduled DHVPS shutdowns ("GLITCHES"). During the first five years of the mission glitch events were rare (a few per year) and seemed to occur randomly. In late 1977 the incidence of glitches increased until they were almost a weekly occurrence. A major effort was made to discover the cause of glitches and stop their occurrence. By the spring of 1979 (after more than 150 glitches) the cause was still unknown but a technique has been developed to avoid their occurrance.

7.3 OBJECTIVE

The purpose of this test was to obtain additional high voltage shutdown (glitches) data in order to better establish their causes.

7.4 METHOD OF TEST

It was found that most glitches occurred when the spacecraft was pointing in the plane of the orbit ($\pm 30°$) near the point in the spacecraft's orbit where it

is approaching the target at maximum velocity. Spacecraft operations were modified to turn off the DHVPS when the spacecraft was in the "GLITCH" portion of its orbit. Immediately, all glitches stopped. Subsequent analysis of the glitch data produced some questions about the glitch avoidance procedure and still failed to isolate a cause of the phenomenon. Further testing could not be done during the scientific portion of the mission because of the danger to the spacecraft and the heavy observing schedule.

7.5 RESULTS AND ANALYSIS

During the testing period twenty-eight (28) glitches were produced in the PEP. All the glitches conformed to the predictions of the flight theory developed in 1979. Glitches were found to occur in the plane of the orbit (+20) near the point where the spacecraft is approaching the target at maximum velocity. This location in the orbit is the point where the ram pressure is maximized and, hence, the ambient air density in the spacecraft is at its highest value. Figures 7-1 and 7-2 illustrate these relationships.

A detailed study of the forced (EOM) glitches did not reveal a unique source of the shutdowns. The high voltage power supplies must be on line to produce a glitch, but they may simply be the most visible effect rather than the cause of the glitch. Analysis suggests the cause is global, i.e., affecting many spacecraft systems. Arcing of electrical devices/systems is strongly suggested by the orbital location of the glitches. Unfortunately, no evidence of arcing could be found in the data.

7.6 CONCLUSIONS

Analysis of all the glitch data did produce some important conclusions. While no evidence could be found for acring, the increase in glitches in late 1977 and subsequent years and the orbital location (Figures 7-1 and 7-2) of the glitch zone strongly argues that the increase in atmospheric density produced by solar maximum plays a fundamental role in the glitch phenomenon. The open (i.e., to the environment) nature of the DHVPS and the U phototubes must also be a major factor. No single source of the glitches could, however, be found. Nor could any events be found that directly point to an interaction between the spacecraft systems and their environment (e.g., arching). Without these sources of information no specific recommendations can be made.

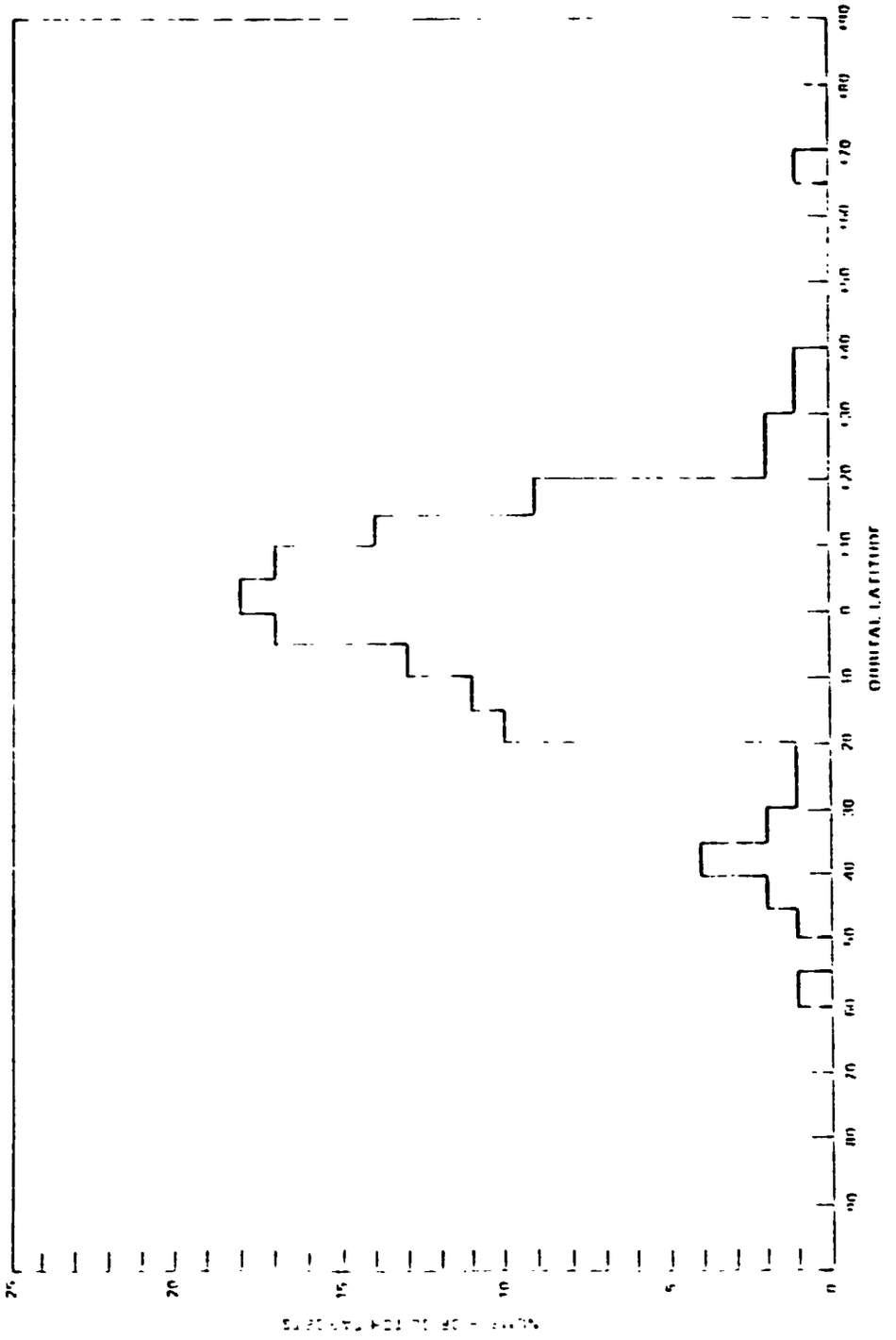

Figure 7-1. Distribution of All Glitches Versus Orbital Latitude

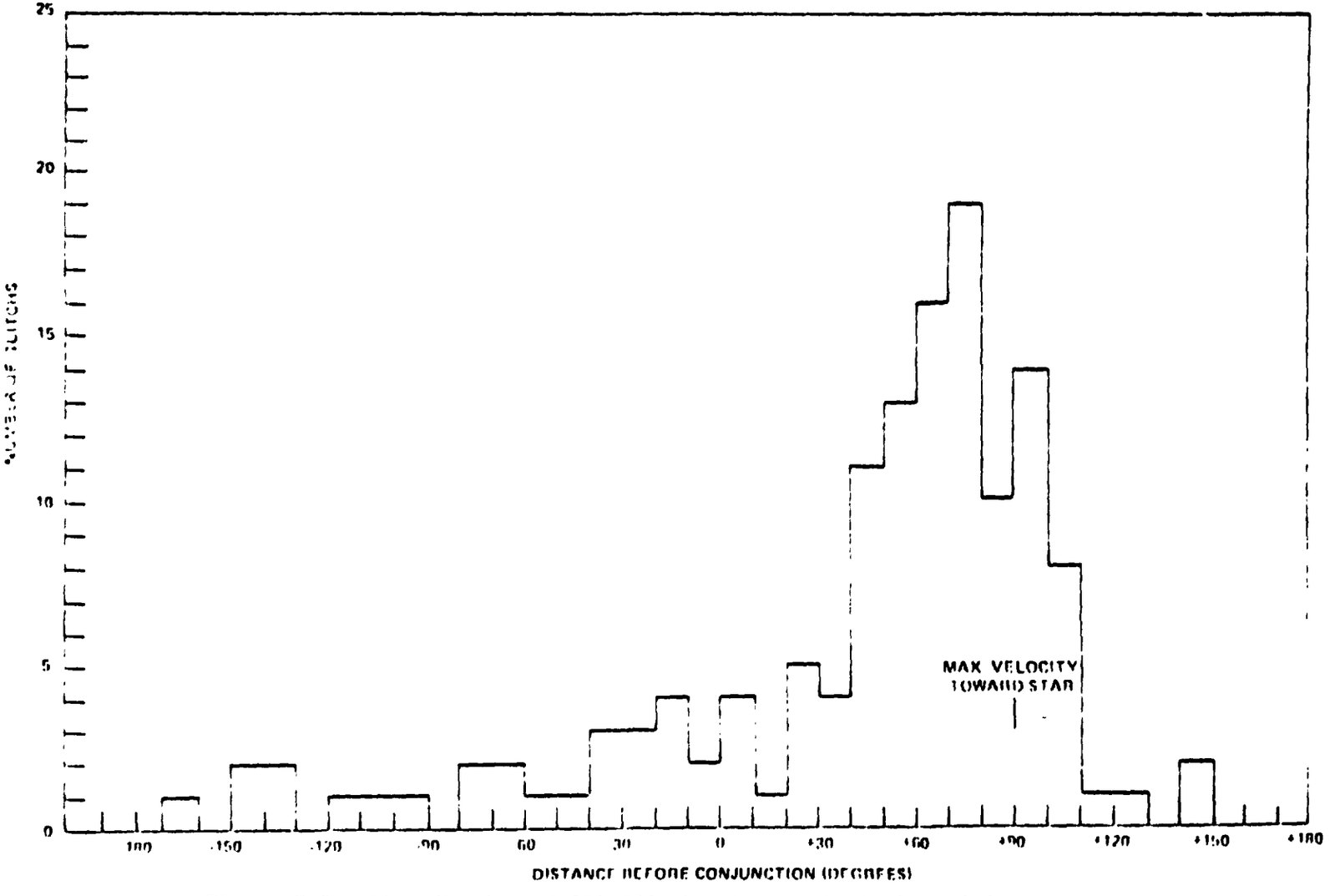

Figure 7-2. Distribution of All Glitches Versus Orbital Position (Conjunction = Spacecraft and Target have the same right ascension)

FINAL SENSITIVITY MEASUREMENTS OF PEP

by
Dr. R.S. Polidan
Princeton Unviersity Observatory

August 5, 1981

TABLE OF CONTENTS

SECTION 8
FINAL SENSITIVITY MEASUREMENTS OF PEP

8.1 SUMMARY

Final sensitivity measurements were made to document the sensitivity decline and obtain the final instrument calibration. Results are graphically presented.

8.2 INTRODUCTION

Throughout the OAO-3 mission observations were made of standard stars (stars of known characteristics) in order to calibrate the PEP spectrometer. The final set of sensitivity observations were done during the EON period.

8.3 OBJECTIVES

The purpose of the test was to complete documentation of instrument degradation and to perform the final instrument calibration.

8.4 RESULTS AND ANALYSIS

The tests were performed without problems. Figure 8-1 presents the history of sensitivity of U1, the principal phototube. U2 displayed a similar but slightly worse decline, where as V1 and V2 were relatively unaffected, retaining 60% of their launch sensitivity. Details of this decline in sensitivity can be found in the Final Operations Report.

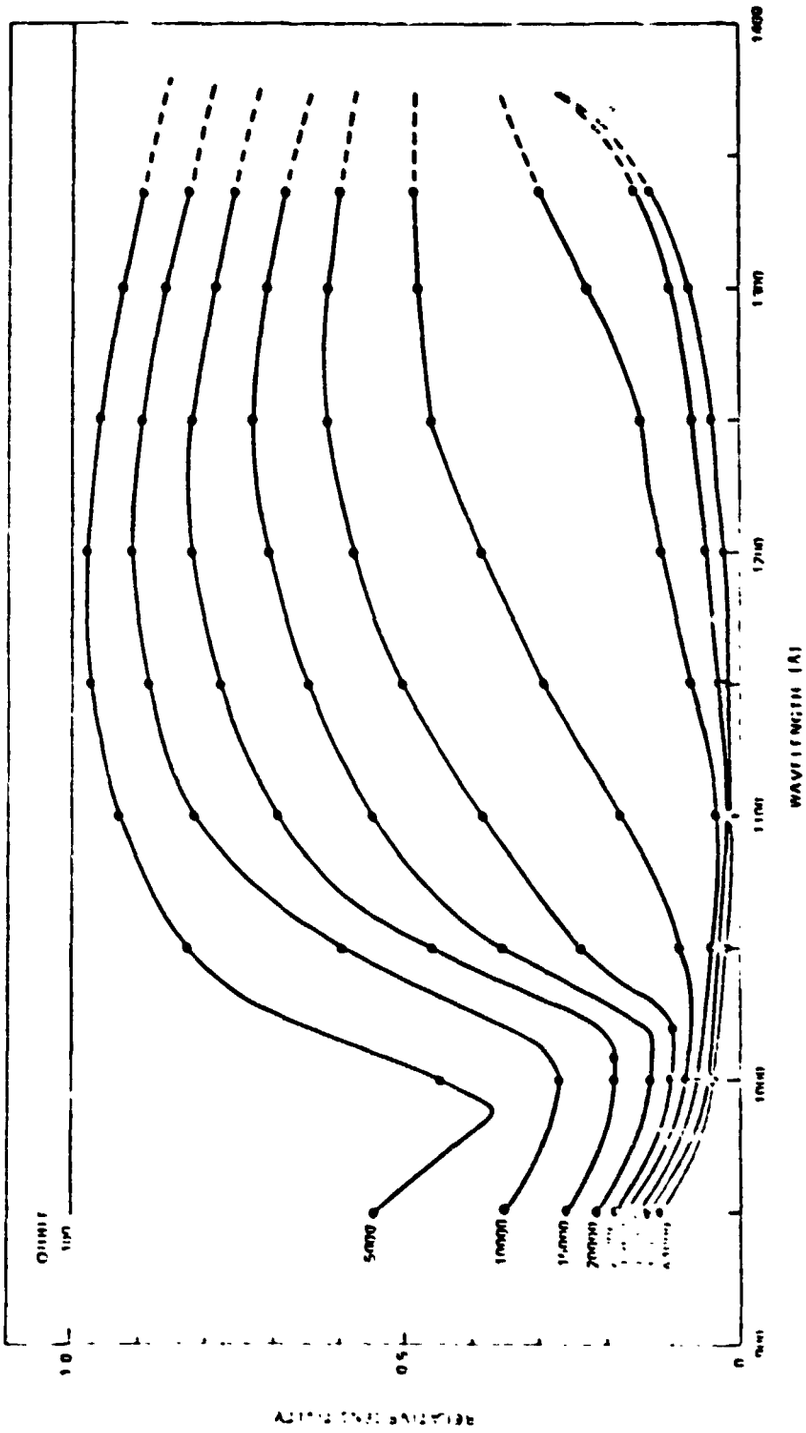

Figure 8-1. UI Relative Sensitivity

SENSITIVITY DEGRADATION OF THE PEP SPECTROMETER

by

Dr. R.S. Polidan
Princeton University Observatory
August 5, 1981

TABLE OF CONTENTS

SECTION 9
SENSITIVITY DEGRADATION OF THE PEP SPECTROMETER

9.1 SUMMARY

Efforts to isolate the cause of the decline in the PEP spectrometer sensitivity did not completely succeed. Insufficient information was obtained to fully identify the cause of the rapid decline in sensitivity. The available data does, however, suggest that the mechanism identified by TIROS and Nimbus as causing their loss of sensitivity is responsible for the loss in OAO-3. This mechanism should be considered when future spacecraft are designed, particularly the Space Telescope.

9.2 INTRODUCTION

Throughout the lifetime of OAO-3 the PEP spectrometer has declined in sensitivity which was not unexpected. Contamination of critical surfaces, decay of electronic components, and other effects act to slowly reduce instrument sensitivity. For the first five years (27,000 orbits) of the mission decline in sensitivity was slow and not unexpected. By the end of the sixth year of operation it was noted that the spectrometer (specifically the far-UV phototubes) had dramatically increased their rate of decline. Four possible causes of this rapid decline were considered likely:

1. Failure of electronic units (e.g., high voltage);
2. Failure in the dynode chain in the phototubes;
3. Image focus; and
4. Severe contamination of the critical surfaces.

The first possible cause (unit failure) was checked in late 1978 and found not to be the cause of the problem. Failure in the dynode chain of the phototubes was not testable but it was considered unlikely because of the long term similar behavior of the two rapidly decaying phototubes (U1 and U2). Instrument focus was tested in 1978 and appeared to absolve it as the cause of the loss in sensitivity, although the results were confusing. The final, and most likely possible cause (contamination) could not be adequately tested until the EOM period.

9.3 OBJECTIVES

The purpose of this test was to isolate the cause and the rapid sensitivity loss. Three separate tests were performed to resolve the above problems.

9.4 RESULTS AND ANALYSIS

Analysis of the results obtained from the three tests that were performed consisted of the following:

a. Contamination of the slit jaws - If the cause of the sensitivity loss was blockage of the entrance slit jaws by outgassed materials then it would be expected that the narrow slit (24 micron separation) would be more blocked than the wide slit (96 micron separation). Observations taken in the early part of the mission established "launch" values for the ratio of light passing through the two slits. These observations were repeated on January 12-14, 1981. Table 9-1 gives these results and the launch values.

   Significant contamination of the narrow slit relative to wide would have produced an increasee in the wide/narrow ratio. A small (10-20%) increase is seen in the ratio for U1 and U2 but it is insufficient to explain the large drop in instrument sensitivity. The only other possibility is that the slit jaws are equally contaminated; this is unlikely. Slit jaw contamination does not appear to be the cause of the instrument degradation.

b. Alteration of the image size and/or shape - The light entering the PEP could be reduced if the focused stellar image were altered (e.g., greatly enlarged or distorted). A measurement of the image size and shape was done on January 31, 1981. Unfortunately the data was improperly recorded in house and discarded at the remote site before a retransmission could be requested.

   Data from the fine error sensor suggest that the image has not greatly changed since launch. This argues that image distortion is not the cause of the sensitivity loss.

TABLE 9-1

RELATIVE SIGNAL STRENGTH - 24 and 96 MICRON SLITS

Tube	Wide/Narrow Ratio (Launch)	Wide/Narrow Ratio (1981)
V2	2.2	2.1
U1	1.7	1.9
U2	1.9	2.3

c. Contamination of the optical surfaces of the PEP - At the same time OAO-3 was experiencing its rapid decline in sensitivity TIROS and Nimbus satellites were experiencing similar declines in some sensors (Reference 1). Their analysis suggested that the cause was contamination by outgassed material polymerized by atmospheric oxygen. They were able to recover full sensitivity by heating their optical surfaces. Unfortunately, OAO-3 does not have heaters appropriately placed to heat the optical package. It can, however, be heated by an external source - the Sun. On February 9, 1981 OAO-3 was pointed at the sun for approximately six (6) minutes. The solar disk was imaged directly on the spectrometer. Temperature rises were noted in all sensors; they were, however, small. The largest rise occurred in the mid-telescope thermistor: 27°C (from -19°C to +8°C). Most sensors showed rises of 5 to 10°C.

Calibration scans were done before and after the sun pointing. They showed that the signal dropped by a factor of seven (7) at short wavelengths and almost three (3) at long wavelengths.

This result was quite unexpected. Tests were quickly done to check this result. A series of guidance offset tests revealed that the image size and/or shape had been greatly altered. Further tests

could not be done to explore this problem due to time constraints. It does, however, appear that the stellar image was greatly altered by the Sun pointing and that this alteration is the principal cause of the decline in sensitivity after the Sun pointing. No information could be obtained on the evaporation of contaminants in the PEP.

9.5 CONCLUSION

The exact cause of the rapid decline in instrument sensitivity in the PEP could not be isolated. However, all available data suggest contamination of critical surfaces as the most probable cause of the decline. The data also suggest that the rapid decline began in late 1977 or early 1978. This corresponds to the time TIROS and Nimbus observed a rapid decline in the sensitivity of their earth sensors (Reference 1). This correspondence and the observed increase in the local (i.e., at the OAO-3 altitude) oxygen abundance strongly suggest that the TIROS mechanism or something closely related is responsible for the OAO-3 sensitivity loss. Unfortunately, OAO-3 was unable to heat its critical surfaces to the high temperature required to evaporate the contamination.

It should be noted that the next major astronomical satellite, Space Telescope, is expected to be operating during the next solar maximum.

REFERENCES

1. Memo to TIROS Project (Code 480) from MC and A Branch (Code 313) dated October 12, 1979.

FINE ERROR SENSOR (FES) FINAL EVALUATION

by

Dr. R.S. Polidan
Princeton University Observatory
August 5, 1981

TABLE OF CONTENTS

SECTION 10
FINE ERROR SENSOR (FES) FINAL EVALUATION

10.1 SUMMARY

Final evaluation of the Fine Error Sensor (FES) showed no anomalies. Guidance channel A was found to be fully operative. The earlier apparent failure was due to an improper turn-on sequence.

10.2 INTRODUCTION

The Fine Error Sensor (FES) is the principal guidance device of the PEP. The performance of the FES was periodically evaluated throughout the mission.

10.3 OBJECTIVE

The purpose of this test was a final evaluation of the FES.

10.4 RESULTS AND ANALYSIS

The only major anomaly during the mission was the apparent failure of one of the guidance channels (channel A). This failure was never confirmed.

10.5 CONCLUSION

Tests conducted throughout the engineering test period showed that the FES continued to operate at or above prelaunch specification. Guidance channel A, thought to have failed in 1978, was found to be fully functional. The apparent failure was traced to an improper turn-on sequence.

FAILED UNIT TEST

by

Dr. R.S. Polidan
Princeton University Obsrvatory
August 5, 1981

TABLE OF CONTENTS

SECTION 11
FAILED UNITS TEST

11.1 SUMMARY

Investigation of the status of the five PEP failed untis showed that four did indeed fail and one (guidance channel A) was fully operative.

11.2 INTRODUCTION

During the 8 1/2 years of OAO-3 operation five electronic units gave indications of partial or total failure.

11.3 OBJECTIVE

The purpose of this test was to thoroughly check the status of the five failed untis in the PEP: focus drive (failed at launch), calibration lamps (failed), sequence controller A (dual mode, stuck in fast mode), sequence controller B (failed), and guidance channel A (failed).

11.4 RESULTS AND ANALYSIS

Attempts to turn on the focus drive, calibration lamps and sequence controller B confirmed that the units had failed. Attempts to move sequence controller A out of the fast mode also failed. However, the attempt to turn on guidance channel A worked. The unit functioned perfectly during the last few days of the mission. The earlier apparent failure was due to an improper turn-on sequence. Thus, after 8 1/2 years of operation only four (4) out of more than sixty (60) separate units failed.

CHECK OF REDUNDANT UNITS

by

Dr. R.S. Polidan
Princeton university Observatory
August 5, 1981

TABLE OF CONTENTS

SECTION 12
CHECK OF REDUNDANT UNITS

12.1 SUMMARY

Unfortunately this test was cancelled in order to further test the results of the Sun pointing.

12.2 OBJECTIVE

The purpose of this test was to evaluate the performance of the least used units.

12.3 CONCLUSION

Almost all electronic units in the PEP were triply redundant. During the mission most of these units were at one time turned on. During the switch to guidance channel A all A units were put on line for the first time in three years. All worked to expectations. The spacecraft was left in this mode.

OAO-3 SPACECRAFT

PERFORMANCE OF INERTIAL REFERENCE UNIT (IRU)

by

Jerry Kull
NASA/Goddard Space Flight Center

May 20, 1981

TABLE OF CONTENTS

SECTION 13
PERFORMANCE OF INERTIAL REFERENCE UNIT (IRU)

13.1 INTRODUCTION

The high performance Inertial Reference Unit (IRU) utilized on the OAO-3 Spacecraft was developed under Contract NAS5-11002 by the MIT Instrumentation Laboratory (later designated as the Charles Stark Draper Laboratory). The contract provided for the delivery of one engineering system and three flight systems. The IRU utilized three single degree of freedom floated rate integrating gyros designated as the 2FBG-6F-OAO. These gyros were custom built by the MIT Instrumentation Laboratory for the OAO program. The gyro design utilized magnetic suspension for the float assembly and ball bearings for the rotor. The signal and torque generator functions were provided by ducosyn units (dual co-planar microsyns). The torque to balance loop used in the IRU design was a two state digital system, with three selectable quantization levels (one for each of the available rate ranges). The IRU was operated primarily in the low rate-high performance mode for approximately the first year of in-orbit operation, with the exception of those periods when the spacecraft was being slewed between target stars. For the balance of the mission, the IRU was maintained in the slew rate-medium performance mode to eliminate the need for mode changes between observation and slew activities. This was possible due to the small reduction in performance characteristics incurred in the slew rate mode.

13.2 PURPOSE

The purpose of this report is to summarize the performance characteristics of the IRU for the OAO-3 mission. The two key performance characteristics addressed are the bias drift stability and scale factor stability. the bias drift stability will be addressed quantitatively; however, due to the lack of available data, the scale factor stability must be addressed on a qualitative basis.

13.3 RESULTS

The IRU met or exceeded all of the established goals relative to performance and reliability in the OAO-3 application. All three channels of the IRU (Roll, Pitch and Yaw) operated within specification limits related to bias drift for the entire 100+ months of in-orbit operations. The specification required that the in-orbit calibrated (compensated) bias drift rate not exceed 10.8 seconds of arc per hour and that the bias drift rate be stable within ±10 seconds of arc per hour per month. Due to test facility limitations, the drift rate stability was not verified during ground test. Figure 13-1 illustrates the stability of the bias drift during the last seven years of operation in the slew rate-medium performance mode. Figure 13-1 is a plot of the bias drift compensation levels (which can be set by ground command) that were in effect during the seven year period. It can be noted that the average variation in bias drift rate is within the specification limit by, at least, an order of magnitude. Table 13-1 provides a listing of the bias drift calibration results which reflect the residual bias drift errors relative to the compensated reference. It should be noted that the average error approached zero. The standard deviation of these calibration errors were less than 3.5 seconds of arc per hour. Taking into account the rebalance loop pulse quantization level of 2.4 seconds of arc and other errors, the most predominant being velocity aberration effects on the reference sensor during calibration activities, the anticipated calibration uncertainties are consistent with the 3.5 second of arc per hour variation. In addition, the bias drift calibration results indicate that the maximum calibrated bias drift rate was consistently less than the specified 10 seconds of arc per hour. Data is not available to quantitatively define the scale factor stability. The performance related to scale factor stability can be best characterized by the large magnitude multi-axis slews that could be accommodated and still allow the spacecraft to acquire specified target stars within the 4x4 minute of arc field-of-view of the payload sensor. Unfortunately, a scheduled end-of-mission test to verify the capability of restarting the gyros after being turned off was not conducted due to schedule conflicts. This test could have demonstrated one of the major advantages of ball bearing gyros over the various gas bearing designs utilized in the majority of current high performance inertial reference systems.

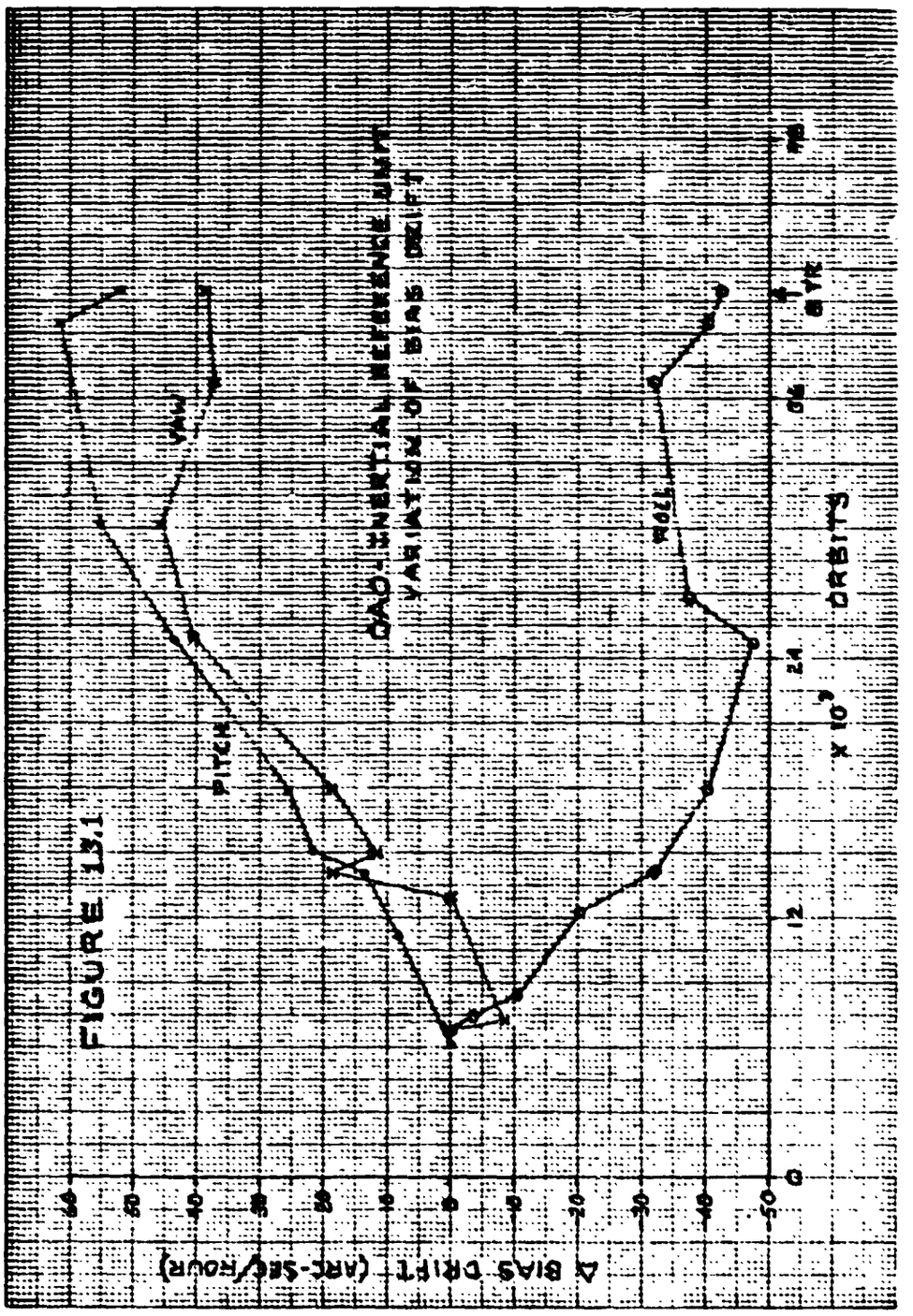

Figure 13-1. OAO - Inertial Reference Unit Variation of Bias Drift.

TABLE 13.1
BIAS DRIFT CALIBRATION RESULTS

ORBIT	DRIFT (ARC SEC/HOUR)		
	PITCH	YAW	ROLL
13690	-5.37	-0.29	
13703			3.24
13934	-6.68	-2.38	-0.64
14509	-2.35	-2.05	-2.98
14991	6.67		0.0
15355	-2.73	3.41	-3.74
16352	4.39	4.74	-3.67
16827	1.46	2.85	-2.80
17801	3.48	6.24	
18103	4.39	-3.92	5.12
18912		-2.97	2.18
19064	2.88	-5.12	-4.21
22171	1.39	1.36	0.72
24302			-6.30
24661	3.88		-4.54
24678	-1.97	1.94	-7.45
24842			-2.70
25716	0.42	2.01	-1.48
27597	2.67	0.01	2.84
30132		5.12	1.14
30176	-1.40	2.14	1.81
32450	-3.23	-0.49	3.17
33189	-2.54	-0.51	3.31
34685	-1.66	-3.04	-1.05
35300	-1.53	-5.25	0.73
35530	0.08		
36674	0.41	1.83	-2.19

TABLE 13.1

BIAS DRIFT CALIBRATION RESULTS (Continued)

ORBIT	DRIFT (ARC SEC/HOUR)		
	PITCH	YAW	ROLL
37339			-1.78
39444	5.86	-4.08	-8.98
39488	-1.28	-2.94	0.88
40967		2.28	-1.98
41108	-0.93	0.48	4.06
42619	-4.40	1.93	1.58
	3.5	3.2	3.5

13.4 CONCLUSIONS

The IRU developed by the MIT Instrumentation Laboratory for OAO-3 operated flawlessly and met all operational performance requirements for a period in excess of 100 months. This has demonstrated that with proper design and quality control procedures, ball bearing gyros can meet stringent performance requirements for long life mission applications.